Graduate Theses and Dissertations   Graduate School

September 2015

Optimization and Control for Microgrid and Power Electronic Converters

Vahid Rasouli Disfani
University of South Florida, vahid@mail.usf.edu

Optimization and Control for Microgrid and Power Electronic Converters

by

Vahid Rasouli Disfani

A dissertation submitted in partial fulfillment
of the requirements for the degree of
Doctor of Philosophy
Department of Electrical Engineering
College of Engineering
University of South Florida

Major Professor: Lingling Fan, Ph.D.
Andrew M. Hoff, Ph.D.
Rajesh Kavasseri, Ph.D.
Selcuk Kose, Ph.D.
Zhixin Miao, Ph.D.
Bo Zeng, Ph.D.

Date of Approval:
July 3, 2015

Keywords: Decision Making Paradigm, Distributed Algorithms, Model Predictive Control,
Multi-Agent, Smart Grid

DEDICATION

To my lovely wife and supportive parents

TABLE OF CONTENTS

LIST OF TABLES

LIST OF FIGURES

ABSTRACT

The proposed dissertation research investigates Optimization and Control for Microgrid and Power Electronic Converters. The research has two major parts.

  i Microgrid Operation and Control

 ii Power Electronic Converter Control and Optimization

In the first part, three focuses are investigated. First, a completely distributed algorithm is developed for dc optimal power flow problem for power distribution systems as one of the necessary functions considered in unit-commitment problem in day-ahead markets. This method is derived based upon the partial primal-dual representation of the economic dispatch problem, which is finally translated to DC-OPF problem. Second, the optimal interaction between the utility and communities will be studied, due to its improtance in real-time markets. The objective of this section will be to develop an iterative agent-based algorithm for optimal utility-community control. The algorithm will consider the AC power system constraints to maintain power system stability. In this algorithm, a simplified model of microgrid is considered. In the third focus, a comprehensive model of microgrid is taken into account. The optimal operation of the microgrid considering energy storage systems and renewable energy resources is investigated. The interaction of such microgrids with the main grid to define the optimal operation of the entire embedded system is studied through two iterative methods. In the microgrid's internal problem, a moving-horizon algorithm is considered to define the optimal dispatch of all distributed energy resources while considering the time-correlated constraints of energy storage systems. A thorough analysis of the effects of the size of storage systems on energy and reserve market parameters are also performed.

In the second part, the focus of research is to develop optimal control strategies for Power Electronic Converters. A Model Predictive Control (MPC) switching method is proposed for Modular Multilevel Converters (MMC). The optimal solution of MPC problem is then represented as

an optimization problem. Due to lack of efficient algorithms to seek the optimal solution, a fast algorithm will be proposed in this research. The method proposed reduces the number of possible solutions and computation efforts dramatically.

CHAPTER 1

INTRODUCTION

1.1 Background

The international concerns about the environmental pollution has encouraged governments to promote electricity generation from renewable energy resources by introducing renewable energy credit and implementing carbon tax, which defines the trend to future power grids. The capability of renewable resources to be used for distributed power generation and to be operated by the private parties introduced the concept of microgrid, a small-scale electrical power grid. Microgrids may consist of renewable energy resources, energy storage systems, plug-in electric vehicles, and conventional distributed generations. According to their control systems, microgrids may be capable to work in grid-connected and/or stand-alone (autonomous, islanding, off-grid) operation modes.

Although the microgrids and the main grid are electrically connected together, they are managed by different agents (communities and the utility). Unlike the conventional structure of the power system, the new structure includes different aspects and must be considered from power exchange, information flow, and monetary points of view. Design and operation of such a structure requires the combination of a broad range of science such as power, communication, control, IT, management, and economics. This structure enables the agents (the utility and the communities) to optimize their own objectives in real-time with effective communications with other agents, which turns the conventional power grid to Smart Grid.

1.1.1 Microgrid Structure

A microgrid is an electric power grid consisting of different types of Distributed Energy Resources (DER) which is supervised by the microgrid control center (MGCC). Different types of

Distributed Energy Resources are renewable energy resources, energy storage systems (ESS), plug-in electric vehicles (PHEV), conventional distributed generations (DG), and Demand Response (DR). Fig. 1.1 illustrates a standard scheme of a microgrid.
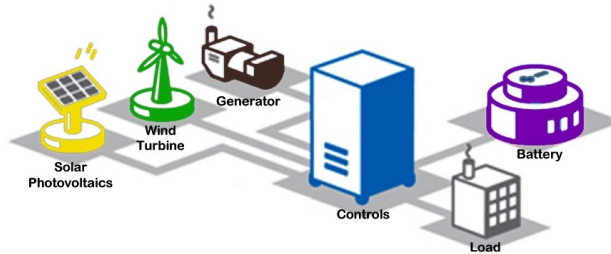
Figure 1.1. Microgrid structure.

Renewable energy resources such as wind, solar and fuel cell require advanced integration technologies. Unlike traditional energy resources such as gas, coal and oil, the output of renewable energies depends on various factors including wind speed, sunlight irradiance and temperature. Hence, power generated from renewable energies is has some level of uncertainty and varies from time to time, which is one of the challenging aspects from the MGCC point of view. MGCC needs to have a prediction from the generation level of the renewable energy resources to control and operate the microgrid most efficiently.

The most of the renewable energy resources and energy storage systems have DC output. Also, the voltage and frequency of the other components with AC output are not necessarily synchronized with those of the entire microgrid. Therefore, the microgrid must be equipped with power electronic converters to integrate all distributed energy resources to the microgrid. Thanks to the development of power electronics technology, it is now a preferred solution to utilize VSC to integrate those renewable energies into power system. Due to high freedom control capabilities of VSC, wind, solar, fuel cell, and battery systems could be integrated into power system via proper back to back, or dc/ac converters.

1.1.2 Utility-Community Interaction Optimization and Control

Microgrids are typically operated and managed by private agents (communities) and their main objectives are to maximize their profit subject to some constraints announced by the utility. MGCC

is responsible for optimal control and operation of all the components of the microgrid to fulfill the objectives desired by the community. Both centralized and decentralized control structures are possible for MGCC to operate the system. In centralized control system, all measurements and data of the entire microgrid are sent to the MGCC and it defines and sends the control signals back to the components. As the computing effort for centralized MGCC are too high and most portion of data and measurements have local usage, decentralized control structure has been proposed in the literature [1, 2, 3, 4]. In decentralized control structure each component has its own local control center and the MGCC makes coordination between the local centers. Decentralized control centers need smart systems with effective communication and IT management systems to operate the power system efficiently. A typical structure for utility-community data interaction is illustrated in Fig. 1.2. The figure shows how the communities and utility communicate with each other through an interaction coordinator.
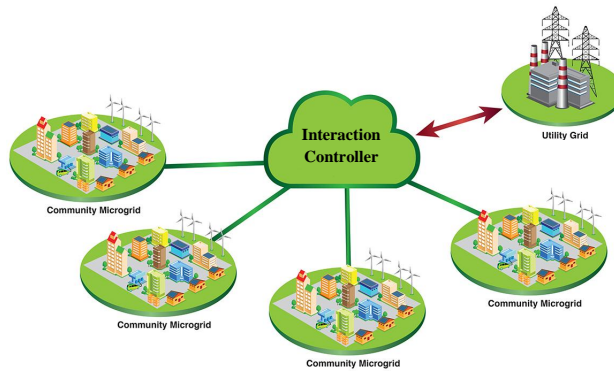
Figure 1.2. Utility-community data interaction structure.

Energy storage systems enable the community to consider them in its optimization problem to increase its profits. The utility is able to save energy whenever there is excess power supply (lower energy price) in the microgrid and use the saved energy when the there is excess demand (higher energy price), which remarkably reduces the microgrid operation cost. As energy storage systems have limited energy capacity, optimal dispatch of the energy storage systems are normally sought in a horizon of time. Hence, the multi-horizon optimization is the best solutions for such dispatch problems.

3

According to the uncertainty of the renewable energy resources and demand forecast versus real-time outputs, however, solving the multi-horizon problem for the day-ahead likely leads to inaccurate results. It is obvious that the inaccuracy of the predictions about one incident at a specific time reduces by the time passes. Thus, the solution to address such discrepancies is to solve the multi-horizon problems in shorter steps, which upgrades the algorithm to a moving-horizon solution. At each time step, a multi-horizon problem is solved for the next time horizon (next 24 hours, for example) and the very first results are used until the next time step. At the next time step, a new multi-horizon problem will be solved using the updated predictions of demand and renewable resources.

1.1.3 Decision Making Timeline for Utility-Microgrid Interaction

In a power market infra structure, where private agents participate in decision making procedure, there are different schedules for various decision making problems such as unit commitment, dc/ac optimal power flow, and DER internal control. There are normally two types of decision making schedules practiced in the power markets, day-ahead market as a long-term and real-time as short-term problems.

The day-ahead market determines hourly market-clearing prices and unit commitments through a mixed-integer optimization problem with the objective function of minimizing the total operation cost for the next day subject to meeting reliability needs. The day-ahead market simultaneously optimizes the energy and ancillary services market to define the transmission capacity required (congestion management) and confirm the reserves needed to balance supply and demand based on supply and demand bids. It guarantees generation plus imports equals load, exports, and transmission losses, and that all final schedules are feasible with respect to the constraints enforced in the full network model as well as 100 percent of the ancillary services requirement. In order to ensure the reliability and fully meeting ancillary services, the network constraints such as line congestion, voltage limits and unit reactive power must be considered in unit commitment problem. Although taking the voltage limits and reactive power into account in unit commitment problem urges a comprehensive ac model of the network, it is avoided from being combined with the unit commitment

problem which has mixed integer feature, due to the inherent complexity (non-convexity) of the ac model of the power network. Instead, dc optimal power flow as an approximation to the ac optimal power flow is practiced for the reliability evaluation of the unit commitment results.

The unit commitment problem is normally solved once in the middle of each day for the entire next day after collecting all the bidding information from generation units and/or price-responsive demands. In California ISO, for example, the market opens seven days prior to the trade date and closes the day before the trade date, and the results are published at 1:00 p.m.[5] on the same day. Fig. 1.3 shows a sample of schedule for different decision making procedures. In addition to the inherent complexity of ac power flow model, the other justification for using the approximate dc power flow model combined with unit commitment is the time difference between clearing the market and trade date. due to less complexity of dc power flow model and the fact that such hour-scale time difference in day-ahead markets already includes significant levels of uncertainty about demand and output of renewable energy resources, dc power flow model of the network is still a reasonable model to be considered in unit commitment model, although it is not so accurate as ac optimal power flow. The optimization algorithms used to solve day-ahead market are expected to solve the problem in less than one hour to enable the market operator to have enough time for final tests before publishing the market clearing results. The results sought by day-ahead market procedure are the base solutions for commitment of the generation units for the day ahead and are valid until the realtime market opens.

Once the results of the day-ahead market is published, other type of markets called realtime market is opened. The realtime market is a spot market to procure energy/reserve and manage congestion in the real-time after all the other processes have been performed. This type of markets produces energy to fulfill instantaneous demand, reduce supply if demand disconnected, offer ancillary services as required and curtail demand in extreme conditions. In California ISO, this market opens at 1:00 p.m. prior to the trading day and closes 75 minutes prior to the start of the trading hour. The results are published about 45 minutes before the trading hour starts. Please see [6] for more details. Since the realtime market for each hour is run separately from the others, it is obvious that the number of switching on/off events in realtime markets is much less than that

in day-ahead market, which results in a smaller size for realtime markets. Such properties allows the market operator to practice comprehensive ac optimal power flow for more accurate reliability evaluation of the solutions.
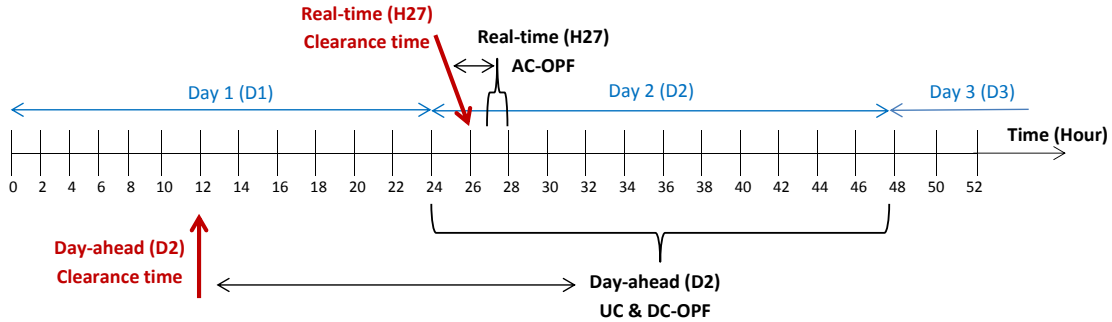
Figure 1.3. Timeline for day-ahead and realtime markets.

Due to integration of renewable energy resources to the power market and their inherent uncertainties, independent system operators (ISO) recently started to practice shorter-term types of power markets. These markets are designed to be run in 15-minute or 5-minute intervals to mitigate the effect of stochastic behavior of renewable resources. As an instance, California ISO launched the western Energy Imbalance Market (EIM), the ISO enhanced real-time market, on November 1, 2014 to create significant renewable integration and reliability benefits for consumers by dispatching a broad array of resources economically [7]. Figure 1.4 shows the timeline for CAISO EIM. The nature of such markets and the optimization problem to be solved for it is exactly the same as those of realtime markets. Therefore, a light unit commitment problem with ac optimal power flow is expected to be solved to run these markets. By emerging these extra short-term markets, the algorithms practiced to solve such AC OPF problems must be capable of seeking the optimal solutions in less than five minutes.

1.2 Statement of Problems

1.2.1 Privacy-Preserving Day-Ahead Markets

The future microgrids which are expected to be run by private agents will likely very reluctant about sharing their private information due to economical and security concerns. This situation

6
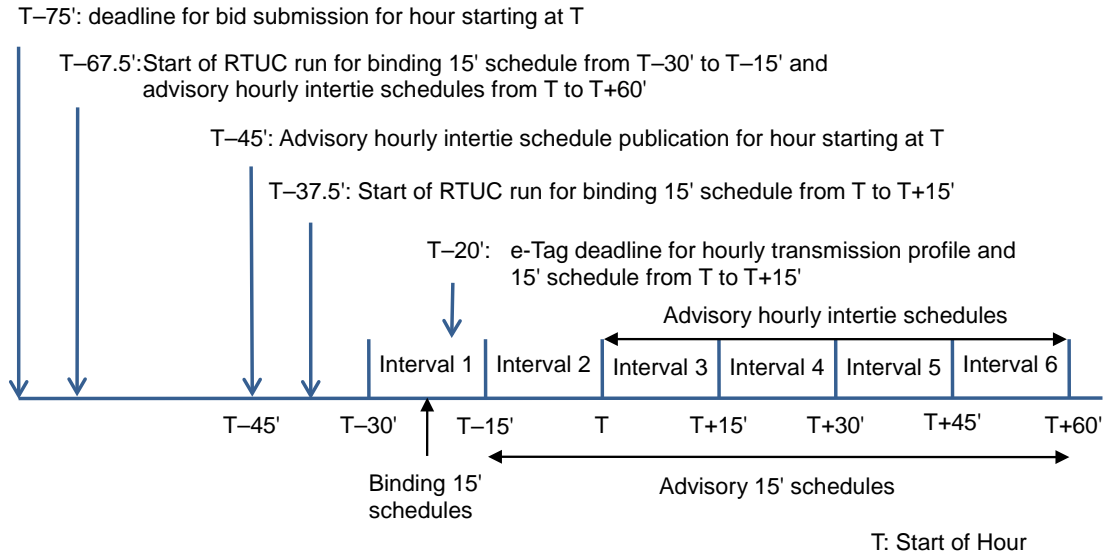
Figure 1.4. Timeline for energy impulse market (EIM) in California ISO.

will likely be significant challenges for power markets to solve their optimization problems such as unit commitment and dc/ac optimal power flow. Thus multi-agent or distributed platforms are needed to be designated to solve such problem while preserving the privacy of microgrids.

Necessity for reduction of the size and costs of communication infrastructure for smart grid has raised the concept of distributed algorithms for power system control and optimization. These algorithms create an infrastructure for the entire grid to converge to the optimal solution with minimum information exchange between the agents. Having such structures completely complies with the fact that the agents do not like to reveal their financial and private information to the upper-level control or operator, which make them interested to participate in such procedures. These algorithms lets each microgrid communicate with a limited number of other microgrids based upon a cooperative strategy. Knowledge of development of such distributed optimization algorithms could be used toward the development of distributed control methods which seek the optimal solutions.

As mentioned above, a day-ahead network-constrained unit commitment (normally modeled with dc approximation of power flow) takes care of the network constraints while minimizing the total system cost on the entire next day. Two problems are identified here. First, for the day-

7

ahead market in presence of microgrids, a multi-agent platform is needed to solve unit commitment problem while preserving the agents' privacy concerns, which is addressed in several research works in the literature [8, 9, 10, 11]. Second, after the solution of unit commitment is sought, a distributed optimal power flow solution is desired to define how much power we expect from each microgrid to exchange with the main grid. Typically due to its simplicity against ac optimal power flow, in power markets, dc optimal power flow is the most common model to to define a rough estimation about the generation level of each committed generator at each hour in order to evaluate the other security constraints such as contingency analysis. In this dissertation, the solution for the distributed unit commitment problem is taken as granted and the focus is on the development of fully distributed structure to solve dc optimal power flow problem.

According to the timeline of different power markets, one of the important concerns about distributed algorithm is their solution time due to their iterative structures. It is vital to confirm that these algorithms will converge in a reasonable time for that particular type of markets.

1.2.2 Co-optimization of Utility-Community Interaction

In a realtime market which is mostly based on solving AC OPF problem, more detailed power flow models are expected to appear in the optimization problem. Compared to the day-ahead market problem, this problem is more complicated from the network modeling point of view but less complex due to its lack of integer decision variables. As the realtime market is very close to the trade time, more detailed models of microgrids including various types of distributed energy resources are needed to be considered, where makes the problem more complex. For example, considering these resources in an optimization problem makes the problem be determined in a horizon of time instead of one single snapshot, due to their time-correlated energy constraints. In addition, renewable energy resources have their own uncertainty which makes the problem be modeled as an stochastic optimization problem or necessitates reliable short-term prediction models. The other resources introducing complexity to the problem are energy storage systems.

The second concern with such problem is again the privacy-preserving requirement of the algorithm. Therefore, multi-agent algorithms are expected to be developed for such purposes. It is

obvious that the concerns with the solution time for these algorithms are more critical than with the day-ahead market problem, due to less time difference from market settlement and trade times.

1.2.3   Fast Switching Converters Control

Focusing inside the microgrid, most of distributed energy resources must be equipped with a reliable converter to follow the reference points obtained from the optimization problem. Among all of the converter topologies, the MMC is the most promising topology due to its inherent salient features of modularity and scalability. However, there are some issues associated with MMC which do no exist in two-level converters where each bridge is connected to a common dc link. In MMC, there are several submodules with their own capacitors. These capacitors may have different voltages due to the operation scheme. Such difference in capacitor voltages also introduces different voltages on upper-arms and lower-arms of the converter and cause circulating current, which gets into neither ac system nor dc system.

Although Pulse Width Modulation (PWM) is the most common switching method proposed for MMC, its shortcoming about the capacitor voltage regulation and circulating current have led the scientist to seek other control methods for switching like Model Predictive Control (MPC). In MPC method, the optimal sequence of the power electronic switches are selected for the next switching period regarding the instant measurements. The redundancy of the switches provides high number of options for the MPC algorithm to optimize its problem, but it increases the complexity of optimization problem. In the literature, the brute search algorithm has been proposed to the problem. However, its computing effort prevents the problem to be solved for high switching frequencies. Finding more efficient with less computing effort needs more research and investigations.

1.3   Approach

1.3.1   A Review on Decomposition Techniques

Regarding the nature of the problems identified in the previous section which are mainly concerning about preserving agents' privacy, the main approach of this dissertation is to develop distributed algorithms via decomposition of optimization problems. As the objective function of

all these problems is the total generation cost and generation cost of each generator does not have any dependence to the other generators' parameters, the objective function in these problems is inherently decomposable. However, there are some coupling constraints in the problem such as total/nodal power balance which necessitate decomposition techniques to be applied. There are different methods proposed in the literature on optimization problems decomposition such as dual, primal, ADMM, primal-dual, and Benders decomposition.

Dual decomposition [12, 13], which is the most widely used technique to develop multi-agent algorithms, is based on applying Lagrange relaxation on both equality and inequality constraints by considering a distinct Lagrange multiplier for each constraint. The new objective function including the relaxed constraints is ready to be decomposed into different subproblems for the agents. Please see [13] for more details. Several iterative methods have been proposed in the literature to solve the dual-decomposition based distributed problems. Subgradient method [14] is widely practiced for this purpose and shows a convergence convergence rate from the order of $O(1/\sqrt{k})$, *i.e.*, $O(1/\epsilon^2)$ iteration is needed to guarantee $f(x_{best}^k) - f(x^*) < \epsilon$ [14]. In this method, at each iteration, each agent solves its own sub-problem and shares the parameters involved in the relaxed constraints. The Lagrange multipliers are updated based on the parameters announced by the agents and are sent back to the agents for next iteration. LUBS method is the other the other method to solve this problem in an iterative fashion, which is proposed in [15, 16]. In this iterative method, one of the agents solves its subproblem to define its own decision variables while the other agent updates the dual variable (Lagrange multiplier) based on the value announced by the first agent. The updated dual variable is then sent to the first agent for the next iteration, and the procedure continues until convergence is met. This method also shows a convergence rate similar to that in subgradient method and converges in $O(1/\epsilon^2)$ iterations.

Primal decomposition is the other decomposition method [12, 13] which is widely used in the optimization problems with decomposable constraints. In this method, the constraints is separated between the agents by considering auxiliary primal variables. Each agent solves its own subproblem at each iteration, and the auxiliary variables are updated based on the agents' parameters for the next iteration. Please see [13] for more details. The main issue with the primal decomposition is

that the subproblems must be feasible at each iteration or the algorithm fails. Subgradient method is also the iterative method widely used to solve primal decomposed method which converges in $O(1/\epsilon^2)$ iterations, as stated above.

As stated before, dual decomposition is founded based on applying Lagrange multipliers to the coupling constraints which may be involved with the decision variables from three or more agents. In the relaxed problem, there is now several Lagrange multipliers (dual variables) involved which are coupled between several agents. Introducing separate dual variables for each agents mandates the problem to have some equality constraints over these dual variables to reflect the fact that they are expected to be same at optimal solution. Relaxing such coupling constraints using Lagrange relaxation leads to another decomposition method called "primal-dual". In this method, a central unit to update the dual variables is no longer needed. In fact, the agents are not only responsible to solve their own subproblem, but also in charge of updating both dual and primal-dual variables. Please see [17, 18] for more details. Interior point method (IPM) [19, 20] is the iterative method typically adopted to solve primal-dual algorithms. The method is founded based on iteratively updating the primal, dual, and primal-dual variables toward the projection of the optimal solution at each iteration. Interior point method is proved to converge in a polynomial time $O(p(n))$ for convex optimization problems [21].

Alternative direction method of multipliers (ADMM) [22] is the other decomposition method to establish distributed optimization platforms. This method is basically the dual decomposition with an additional quadratic term in dual variable updating equation. ADMM is also capable of being adopted to develop distributed optimization platforms. The only difference between dual decomposition and ADMM appears in the dual variable updating process. For some applications in power systems [23], applying ADMM needs indirect data communication between the agents for their updating process which introduces some inappropriate coupling equations for distributed structures. This method is claimed to converge in $O(1/\epsilon)$ iteration to assure $f(x_{best}^k) - f(x^*) < \epsilon$ [22], which is faster than subgradient and LUBS method because of its extra quadratic term.

Another decomposition method in practice is Benders decomposition [24, 25]. This algorithm, which is also applied to power system optimization problems [26, 27], is mainly adopted for mixed

integer programming (MIP) problems and is based on the fact that fixing the the complicating variables values reduces the problem to an ordinary linear program, parameterized by the value of the complicating variables vector. To apply Benders decomposition, the original problem is decomposed into several subproblems and a master problem such that the master program be an integer problem and subproblems be linear programs. The lowerbound solution for master problem normally involves fewer constraints. Then, the solution of the master problem is examined by the subproblems if it satisfies the other constraints. If the subproblems are feasible, the original problem upperbound solution is calculated, and a new objective function for the master-problem solution is formed for further optimization. In case of infeasibility of any subproblem, an infeasibility cut is introduced to the master problem to reflect the least satisfying constraint. Thee iterations continues until final solution is achieved. Since the upprbound and lowerbound of the original problem is calculated during the iterations, the duality gap can be examined frequently. The final solution is achieved when the duality gap is less than a predefined threshold value. Benders decomposition is typically used for MIP problems, and its convergence rate highly depends on the nature of the original problem.

1.3.2 Distributed DC Optimal Power Flow

To address the problems identified for day-ahead market problem, a privacy-preserving unit commitment algorithm is proposed in [8]. The algorithm is developed based on Lagrange relaxation of the unit commitment problem by assigning a Lagrange multiplier (dual variable) indicating the energy price on each node of the network. The price information is exchanged to the microgrids to run their own profit-based single-agent unit commitment and define the level of power exporting to main grid. Then, the utility is then responsible to update the Lagrange multiplier of line congestion inequality constraints, update the nodal energy prices based on supply/demand power imbalance and to announce the nodal prices back to the utilities for next iteration.

After the units to be committed are determined, a dc optimal power flow problem must be solved to define the generation level of each microgrid. According to the recent interest in fully distributed structures for energy management problems including dc optimal power flow, a fully distributed

platform is proposed in this dissertation which considers each bus as one distinct agent. Such fully distributed algorithms are the keys to create distributed control structures which are recently developed based on fully distributed methods for economic dispatch problem. The algorithm adopted in this dissertation is partial primal-dual algorithm, which guarantees the convergence rate toward globally optimal solution for uniformly convex problems and has several advantageous features for radial networks. Compared to dual decomposition based algorithms, where sub-optimization problems are solved given Lagrange multipliers, in a primal-dual algorithm, there is no optimization carried out for sub-problems. Instead, an updating procedure is adopted to update the control variables. Compared to center-free algorithm, the update process in the proposed algorithm has physical meaning of price updating and is able to address the nodal price differences due to network constraints. It is also faster than the other algorithms taking care of the network constraints which are already proposed in the literature due to less volume of updating processes, especially on the Lagrange multipliers of inequality constraints. The development process starts from economic dispatch problem and applies dual decomposition techniques to extract a distributed economic dispatch. After applying primal decomposition technique to the distributed economic dispatch problem, we further develop a distributed DC-OPF algorithm. The solution sought by the algorithm is proved to be optimal since it satisfies the necessary and satisfactory KKT conditions of the DC-OPF problem for radial networks.

1.3.2.1 Importance of Distributed DC OPF Algorithms

As stated before, dc optimal power flow is an approximation to the AC optimal power flow problem,which simplifies the model of the network and neglects the network power loss, reactive power limits, and voltage constraints. The major focus of DC-OPF is on the network congestions. The DC power flow application performed in DC-OPF problem, however, does not show enough accuracy when it is practiced in distribution systems where the R/X ratio is significant. Since the focus of this dissertation is on distribution networks, application of such techniques seems not reasonable. However, there are several justifications on the reasons of modeling fully distributed DC-OPF problem in this dissertation.

First, one of the main optimization problems, which is involved with the decision about on/off status of the generators is the unit commitment problem. This problem is inherently a mixed integer programming (MIP) problem, and mixing it with AC-OPF problem with inherent non-convexity makes the problem extremely hard to be solved. Therefore, in the real-world practices in power markets, the most developed algorithms combined with unit commitment problem is still DC-OPF problem. Big power software companies are still developing unit commitment solutions just by considering DC-OPF problem even for distribution network applications.

Second, by integration of the microgrids to the main power system and their privacy concerns and private interests, there is a growing attraction toward conducting research on multi-agent or distributed algorithms for power system optimization and control problems. There are several distributed methods developed for unit commitment problem without considering network constraints [8, 10, 11]. There is an appealing research path toward distributed method solving unit commitment problem while considering the network congestion constraints (DC-OPF) which is started to be discovered by researchers from Carnegie Mellon University [9]. However, there is still a long way toward fully distributed unit commitment algorithms while considering network constraints with minimum communication and data management efforts. This path needs more comprehensive knowledge about distributed DC-OPF problem to be combined with simple unit commitment problem at the first stage. The distributed DC-OPF problem proposed in this dissertation is one of the two fully distributed algorithms proposed in the literature [17, 28].

Third, one of the significant application of the distributed optimization methods is to develop distributed control algorithms via emulating the optimization updating rules with controller designs. One of the research groups working on this topic is from Lehigh University. In their recent work, they have developed a distributed control algorithm with minimum communication needs to catch the point of economically optimal operation [29]. This algorithm follows the updating rules of distributed economic dispatch problem. There is still lack of research on distributed network-constrained optimal generation control which requires a completely distributed DC-OPF platform as the basis.

1.3.3 Utility-Community Decision Making Paradigm

As articulated before, since the microgrids may have different types of distributed energy resources, the optimization problems of the microgrids must be basically multi-horizon ones. On the other hand, the utility may also have some energy storage systems in its grid which changes its problem to multi-horizon. Further, the utility is responsible to take care of the AC security constraints of the entire grid to maintain the reliability of the system, which is a nonlinear non-convex problem itself. Looking at the entire problem in one optimization structure, the problem is multi-horizon, nonlinear and non-convex. These characteristics make the problem really difficult to be solved. The entire problem then must be decomposed to different subproblems to seek the final solutions through an iterative process.

The key point of the decomposition of the problem is to avoid any mixture of OPF problem and multi-horizon problems. Therefore, the strategy of decomposition is as follows:

i The subproblems associated with each microgrid is allocated to the corresponding community, which removes the multi-horizon nature of microgrids' subproblems from utility's problem.

ii If the utility has any components in its grid which determines the multi-horizon nature to the utility's problem, those components are considered as some fake agents communicating with the utility.

iii The rest of the problem is completely separable across the horizons, and the utility actually solves 24 OPF problems without any mutual coupling constraints.

Fig. 1.5 shows how the entire problem is decomposed to several multi-horizon problems associated with the private agents and several subproblems (OPF) for utility without any time correlation.

Two steps are taken in this dissertation to address these problems. In the first step, the focus is on the optimal interaction of the communities and utilities, assuming that the community's microgrid is consisting just one simple generator. To solve this problem, a multi-agent platform is developed which basically solves the AC OPF problem for one single snapshot. The problem is, in fact, decomposed using dual decomposition and is solved through two different iterative algorithms. The dual decomposition is performed by applying Lagrange relaxation on the active/reactive power
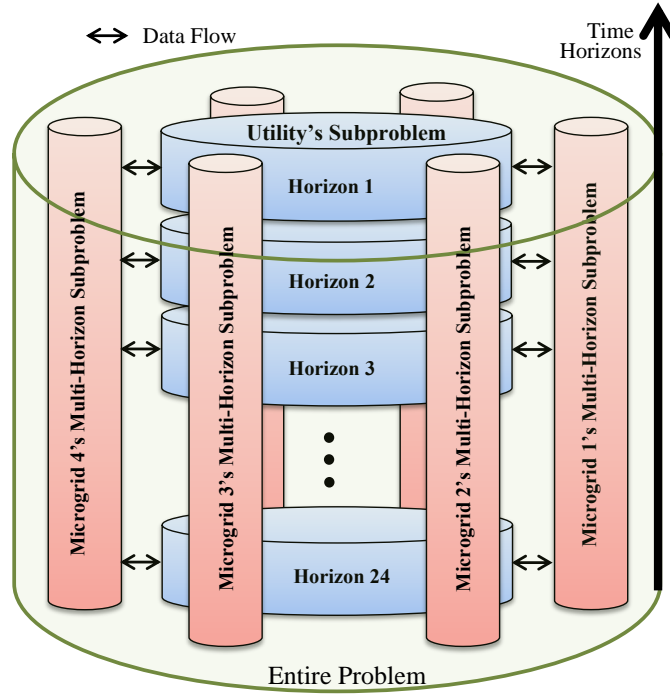
Figure 1.5. Decomposition of the entire multi-horizon optimal power flow problem.

balance constraints on the PCC of the microgrids. Having the problem decomposed between the communities and the utility, in one of the iterative algorithms (subgradient method), communities easily calculate their own desired level of power exchange and the utility solves a simpler OPF problem and determine the level of power exchange with communities. Wisely updating the nodal prices according to the levels of active/reactive power pushes the solution to the optimal solution of the entire problem. In the other iterative process which is called Lower-Upper-Bound-Switching (LUBS) in this dissertation, the community receives power information about the power level requested by utility to determine the marginal price of that value of power. Exchanging such information with utility, enables it to update its desired power level. The procedure converges to the optimal solution in an iterative fashion.

In the second step, detailed model of microgrids are considered in the problem. As mentioned before, according to the time-correlated energy constraints associated with the energy storage systems, the microgrid's optimization problem must be determined in a horizon of time due to

the energy constraints of the battery. In such a problem, the power output of renewable energy resources and microgrid internal demand must be predicted and considered in the problem. The accuracy of these prediction are inherently functions of time difference between the simulation time and the actual time incident is going to happen happen. Therefore, the approach in this problem to decrease the effect of prediction error is to update the problem to a moving-horizon scheme, where the problem is solved every time step for the next horizon of time considering all constraints. After the solution is sought the most immediate results are applied and the algorithm waits until the next time step arrives. Fig. 1.6 depicts the time schedule for the moving-horizon problems to be solved by the time passes. As shown in this figure, every hour a new multi-horizon problem is being solved, that is, the time step in 1 hour. Each multi-horizon problem is defined on a 24-hour time span with 24 horizons. As time passes, the demand and renewable output prediction gets updated, the problem is formulated and solved. The results associated to the first horizon of the problem is applied until the next multi-horizon problem is formed at the next time step.
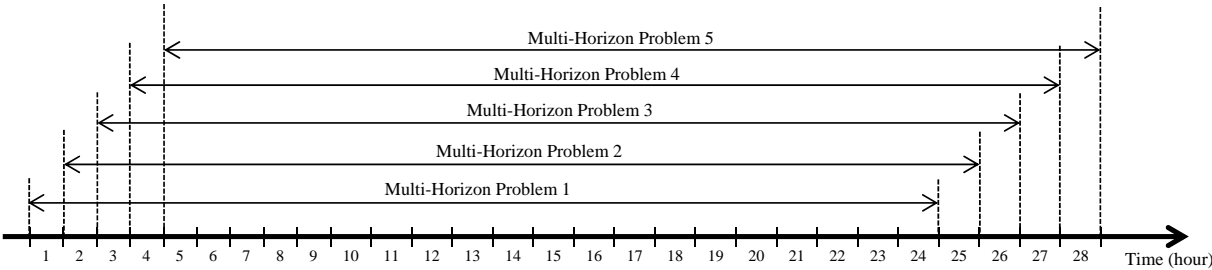
Figure 1.6. Time schedule for moving-horizon problems solving.

In this work, two iterative distributed algorithms are developed for reserve-constrained MHOPF problem. Having identified the private agents as communities and main grid operator as utility, the entire problem is decomposed between utility and communities. Consequently, the entire multi-horizon nonconvex problem is decomposed into several single-horizon nonconvex subproblems for utility and several multi-horizon convex problems for communities along with an update process to make the algorithm iteratively converge to the global optimal solution. The proposed information flow structure completely addresses the economical and privacy-related concerns of the private

agents. In this work, a novel analysis on sensitivity of power generation, reserve availability, and price of energy and reserve versus size of energy storage systems is also represented.

1.3.4 Fast Model Predictive Control for Fast-Switching MMC

The method proposed in the literature to solve model predictive control for MMC compares all possible switching combinations for the MMC switches in one bridge for their predicted performance one step ahead. This method requires significant computing effort. At each time step with the step size defined by the switching frequency, e.g. 100 μs for 10 kHz, the solution must be sought. For a 5-level MMC, there are 8 submodules in each bridge. Among the eight submodules, four submodules should be turned on to keep the dc-link voltage constant. Therefore, the number of the combination is $C_8^4 = 70$. The algorithm needs to check 70 possible on/off sequences and find the best one. For a 13-level MMC, C_{24}^{12}, or 2.7 million combinations should be checked. For a 16-level MMC, 155 million combinations should be checked.

In this dissertation, the mathematical model of MPC-based (n-1)-level MMC, which has n submodules at each arm, is proposed in order to track ac reference current, mitigate circulating current and to keep capacitor voltage nominal subject to selection of exactly n submodules to be trigged at each arm. The multi-objective optimization problem is then reformulated to a new model and the weighting sum method is employed to merge the objectives. To solve such problem, two algorithms are represented to seek the optimal solution for switching pattern. The first search algorithm design remarkably reduces the size of feasible solution to n instead of C_{2n}^n, but the simulation results shows that it has serious drawbacks in satisfying the objectives of MPC, which has led the authors to an alternative algorithm for better performance while maintaining the computation advantages. The second algorithm is developed by applying a relaxation on the constraint of number of switched-on submodules and increases the size of the feasible set to n^2, which introduces additional computation burden compared the first algorithm especially for high values of n. However, it is proved in this dissertation that this size can be cut down to 4 if appropriate weighting factors are selected and checking just 4 of the solutions is enough to find the optimal solution.

1.4 Outline of the Dissertation

The structure of the dissertation is organized as follows.

Chapter 1 gives a brief introduction of the research issues including background information, statement of problem, and approach adopted in this dissertation.

Chapter 2 presents a detailed literature survey on the various problems tackled in this dissertation.

In Chapter 3, a distributed method is presented to solve DC Optimal Power Flow (DC-OPF) for radial networks based on partial Primal-Dual algorithm.

Chapter 4 presents the design of multi-agent based method to solve AC optimal power flow problem while considering each microgrids as one simple generator.

Chapter 5 develops two algorithms to expand the algorithms proposed in Chapter 5 in order to solve the multi-horizon ac optimal power flow problem while considering more comprehensive model for microgrids.

In Chapter 6, a binary integer programming based MPC with minimum computing effort has been proposed to control the ac currents, keep the capacitor voltages nominal, and mitigate the circulating currents.

Chapter 7 summarizes the research conclusions of this dissertation and proposes some suggestions for the future work.

CHAPTER 2

LITERATURE REVIEW

2.1 Partial Primal Dual Algorithm for Distributed DC Optimal Power Flow

Optimal power flow (OPF, AC-OPF), which determines the most economic schedule to operate generation units and controllable demands in a power network, has always been a challenging problem in power system operation due to its inherent nonlinearity and nonconvexity. Several works are reported in the literature to tackle the OPF problem in a distributed fashion [30, 31, 23, 32, 15]. All of these algorithms separate the entire network into several sub-networks, each of which solves its own OPF problem at each iteration mostly using interior point method. These algorithms then develop an information flow scheme and an update process to push the solution toward the optimal solution. In [30], coarse-grained distributed implementation is used to parallelize the OPF problem, which is extended in [31] and compared to some other distributed approaches. Alternative-Direction Method of Multipliers (ADMM) is employed in [23] to develop distributed OPF solution. The same method (ADMM) is used in [32] to determine a distributed method for semi-definite program-based (SDP-based) formulation of OPF problem, which is first proposed in [33]. A modified subgradient-based method along with Lower-Upper-Bound-Switching (LUBS) method is presented in [15] for distributed AC-OPF problem. In the LUBS method, the microgrids update their desired prices based of which the main grid iteratively defines its optimal power export/import level from each microgrid. The main grid also compares the upperbound and lowerbound of the optimal solution to guarantee zero duality gap of the final solution.

Several distributed algorithms have been presented for economic dispatch and DC-OPF problems, as it is the mainly used technique to define the generation level of the committed generators after the unit commitment results are determined. Different methods have been deployed in the

literature for such purposes. A gradient-based approach along with consensus-based update process using center-free algorithms [34] is employed in [29] to develop a distributed platform for online optimal generation control or economic dispatch. In fact, the gradient-based method guarantees the power balance in the entire network using local frequency signal while the consensus-based process unifies all the locational marginal prices (LMP) on their unique final values. The center-free algorithms have fast convergence speed but are not appropriate for DC-OPF problems because they cannot address the difference between nodal prices due to line constraints. Thus, a subgradient method is employed to develop the consensus-based update process for distributed DC-OPF problems in [35, 36, 37]. The idea of separating the entire network into some sub-networks, which is widely used to develop distributed AC-OPF solutions, is also practiced for distributed DC-OPF problems in the aforementioned references. At each iteration, each sub-network (agent) solves its own DC-OPF problem locally; then, a pricing mechanism employing subgradient method updates the price using the information gathered from the neighbors, and iterations continues until convergence is met. The most distributed way to define these sub-networks is to consider each bus of the system as a distinct agent, which is proposed in [28]. In this algorithm, which is developed based on subgradient method, each bus defines its optimal power generation level and updates its own multipliers, shares some data with its neighbors, and continues to iterate until global convergence is reached.

Primal-dual interior point method is a well-studied solution to tackle the convex optimization problems[19]. The partial primal-dual algorithm is used in cases where the Lagrange multipliers of the main problem has physical meanings in the subject, but they are constrained by some equality constraints in the dual problem. To address such constraints of the dual problem, one possible solution is applying the Lagrange multiplier another time, the results of which is called primal-dual formulation of the original problem. The problems gets more interesting when the Lagrange multipliers of the dual problem are also constrained, which might prevent the final solution to satisfy the dual problem equality constraints. This method is widely used to solve the optimization problems, and its convergence is proved in the literature. It has been also employed in [38, 39] to explain that the droop control is aligned with a primal-dual process. In [17], a distributed DC

OPF problem is developed using partial primal-dual algorithm. Since the Lagrange multipliers in economic dispatch problem has the physical meaning of the energy price and it can be demonstrated that the Lagrange multiplier which measures the price mismatch on two neighboring nodes has the meaning of power flow of the line between them, it can be mapped to a real-world problem. Considering the power network constraints which limits the power flow on the line, the DC optimal power flow problem is modeled in [17].

2.2 Optimal Utility-Microgrid Interaction

AC optimal power flow problem is the other problem which is highly challenging when private microgrids are considered. To solve such problem, a multi-agent based optimization platform is desired. According to inherent nonlinearity and nonconvexity of OPF problem, it has always been a complicated problem to handle in power system operation. Its complexity even increases when some private microgrids are connected to the grid and conduct power transaction with the main grid, where the OPF problem must be tackled in a distributed fashion. In the literature, there are several works developing distributed algorithm for both AC-OPF [30, 31, 23, 32, 15] and DC-OPF problems [35, 36, 37, 17]. All of these algorithms decompose the problem to smaller subproblems and design an iterative process to seek the optimal solution, where one agent is responsible to each one of these subproblems. After the agents solve their own OPF problem mostly using interior point method, these algorithms performs an update process to push the solution toward the optimal solution, following an information flow scheme which needs the agents to share as minimum as possible amount of private data. Coarse-grained distributed implementation is proposed to parallelize the OPF problem in [30], followed by its extension and comparison versus some other distributed approaches in [31]. The other algorithm used to develop distributed solution for OPF problem is Alternative-Direction Method of Multipliers (ADMM) which is employed in [23]. This algorithm first modifies the updating process of Lagrange multipliers to increase the robustness of the solution with a slight change compared to subgradient method [32]. ADMM is also employed in [32] to develop a distributed solution for semi-definite program-based (SDP-based) OPF problem, which is first presented in [33]. A modified subgradient-based method is proposed in [15], where the

22

microgrids and utility name their desired level of power transactions and a price updating trajects the solution toward the optimal solution. The other method proposed in [15] is named Lower-Upper-Bound-Switching (LUBS), where the microgrids update their desired prices based of which the main grid iteratively defines its optimal power export/import level from each microgrid. To guarantee the optimality of the final solution, the main grid checks the duality gap by comparing the upperbound and lowerbound at each iteration as the most significant signal of convergence.

Multi-agent control has been also applied in microgrid or demand side interactions with utility [40, 41, 42, 43]. Microgrids or demand side make their own decisions while exchanging limited information with the grid. For example, in [40], an optimal demand response is designed for the demand sides to bid the amount of load shedding as a a supply function of price. The utility collects the bids from all demand sides and update the price. In [41], the demand sides send the utility the information on their demands, and the utility sets the prices. The demand sides update their demand requests upon receiving the price.

In all above mentioned references, distribution networks are either represented in a simplified way or not represented at all. In this work multi-agent control of demand sides and utility while considering ac network constraints including line flow limits and bus voltage limits is developed.

Implementing multi-agent control requires distributed algorithms. For optimization problems, there are ways to decompose and construct distributed optimization algorithms [12]. In the field of communication layering problems, primal decomposition, dual decomposition, and primal-dual decomposition can be applied in different scenarios [44]. In power systems optimization problems, due to the decoupled cost function structure and coupled constraints, Lagrangian relaxation based dual decomposition is commonly used. Example applications can be found in aggregated PHEV control considering global constraint [45], and distributed voltage control [46].

In optimization decomposition, an original problem is separated into a master problem along with many subproblems with small size. After each subproblem makes decision, the main problem is solved adopting iterative methods such as subgradient update. Subgradient algorithm which is based on Lagrangian relaxation has been applied by Luh *et al* for manufacturing job scheduling [47]. Zero or small duality gap can prove that the solution is optimal or very close to optimal. In

game theory, iteration means each agent in the system is exchanging information and learning to reach a Nash equilibrium.

Not all distributed algorithms have the information exchange structure suitable for game theory based multi-agent control [48]. In this dissertation, two distributed algorithms and learning methods are developed which are suitable for multi-agent based microgrid and utility interaction while considering ac power system constraints.

2.3 Comprehensive Model for Utility-Community Optimal Control

The distributed AC-OPF problem gets much challenging when a thorough model of microgrid is taken into account. The microgrids may be equipped with different distributed energy resources such as energy storage systems, renewable energy resources and demand response. Among these resources, energy storage systems brings more complexity into the problem due to their time-correlated energy constraints. To handle the time-correlated constraints of ESS, OPF must be considered in a horizon of time instead of just one snapshot. Several approaches has been addressed in the literature to tackle Multi-Horizon Optimal Power Flow (MHOPF) problem. A Benders decomposition method is developed in [27] to tackle energy constraints of hydroelectric plants integrated in irrigation systems. Another thread of research [49, 50] develops a KKT-based solution for MHOPF considering battery storage systems. An optimization model is also proposed in [51] for MHOPF embedded with wind generation and battery storage.

The other constraints normally addressed in energy management problems is reserve adequacy, which is considered not only in unit commitment problem [52] but also in OPF problem [53, 54]. A reserve-constrained OPF problem is developed in [53] to incorporate the expected security costs in the system using reserve marginal value (reserve price) which indicates how much cost is imposed to the system operation if one more unit of reserve is needed. The extension of MATPOWER 4.1 which solves OPF with co-optimization of energy and reserve is proposed in [54], and its capability is employed later in this dissertation to solve reserve-constrained OPF problems. In some other research works, the capability of ESS to provide ancillary services such as reserve is also taken into

24

account to tackle reserve constraints in OPF problem without considering their time-correlated constraints [55, 56].

2.4   Model Predictive Control of Modular Multilevel Converters

Modular Multilevel Converter (MMC) is reported in the literature as the most promising topology proposed for Voltage Source Converters (VSC) due to its salient characteristics such as scalability and modularity [57, 58, 59, 60, 61, 62, 63].

Several switching methods have been proposed for MMC. The popularly used schemes are based on Sinusoidal Pulse Width Modulation (SPWM) which defines the number of switches that must be trigged in the lower arm and the upper arm of all phases by comparing the sinusoidal reference waveforms with a set of high-frequency carrier waveforms with different dc off shifts [64, 65, 66, 67]. SPWM is popular for its simplicity of implementation. However it cannot handle the circulating currents in the converter bridges.

In a two-level VSC, the switching scheme is the output of PWM which is directly applied to the gates of IGBTs. However, in MMC, higher number of submodules on each arm makes the switching algorithm more complicated. PWM is the most widely used method for MMC as well. The main objective in MMC's PWM switching is to define the number of submodules to be turned-on on each arm at switching time using higher number of carriers instead of just one. Having the number of submodules known, the capacitor voltages and the direction of current on each arm define the arrangement of the submodules to be on or off.

In SPWM switching method, the comparison of the sinusoidal reference waveforms with the multi-carrier triangular waveforms defines how many submodules are required to be switched on on each arm. Then, the switching algorithm sorts the submodules based on their capacitor voltages, either in ascending or descending order according to the direction of the corresponding arm. Since, the total voltage of submodules selected are not necessarily equal for all bridges, the currents flowing through the bridges is prone to have some unbalanced components. This unbalanced component, which is address as circulating current, increases the converter loss and mandates higher ratings

for power electronic switches [68, 69, 57, 70]. Therefore, mitigation of circulating current is highly desired in MMC switching and control design.

Although SPWM switching method can be simply implemented for MMC applications, it cannot address the issue of circulating current. Therefore, several PWM-based algorithms are introduced in the literature. The main idea of all these algorithms is to appropriately change either the sinusoidal reference waveforms or multi-carrier triangular waveforms. Phase-shifted Carrier PWM (PSPWM) is the method widely used for circulating current mitigation, which shifts the phase of the sinusoidal reference waveforms to regulate the capacitor voltages and to mitigate the circulating current simultaneously [71, 72, 73]. This switching scheme changes the the upper and lower arms' modulation signals to obtain the capability of dynamically adjusting the capacitor voltages. However, the method causes more harmonics in the arm current, changes the characteristics of circulating current, and may get unstable. Therefore, it is valid only to a limited extent [74]. The other method which is proposed for circulating current mitigation is Phase-disposition PWM (PDPWM) [74]. This method, instead of changing the reference waveform, makes changes to the carrier waveforms to increase the stability of the control method while mitigating the circulating current and capacitor voltage deviation [74]. Several other works have been also proposed in the literature to address the circulating current issue by adding additional components to the current reference waveforms. It has been shown in the literature that circulating current has has a dc component and a second-order frequency component at steady state [75, 76]. Eliminating the second-order component needs a proportional-resonance (PR) controller. A strategy for MMC circulating current suppression using PR controller has been presented in [69]. In [68], a control strategy has been developed to convert the ac component of circulating current into dc signal through acb/dq transform to mitigate the circulating current. Recently, an integrated MMC control is proposed in [70], which includes the conventional vector control (outer PQ control, inner line current control), circulating current mitigation control, phase-shifted PWM scheme, and submodule voltage balancing block.

Along with the research works on improving MMC switching control using PWM technique, there is another thread of research focusing on model predictive control as a solution to this problem [57, 77]. In these research works, the MMC switching problem is modeled as an optimization

problem with specific objective functions such as following the reference ac current, circulating current suppression, and capacitor voltage regulation. The decision variables in MPC control method are the binary variables indicating the status of each submodules at each switching time step. Simultaneous regulation of submodule capacitor voltages and elemination/minimization of the circulating current flowing through three phases of the converter is still one of the technical challenges associated with MMC application due to their mutual effects. Circulating current, in fact, not only is a function of the capacitor voltages of the submodules turned on at each time step, but also determines how the capacitor voltages of the same submodules change until the next switching time step arrives, which may lower the efficiency of the converter and cause more ripples in the capacitor voltages if it is not well suppressed. However, it should be noted that the circulating current is a useful mean to balance the energies between all six arms in situations where some energy unbalance are caused by asymmetric operations and fault situations and tolerances of the components [78].

The method proposed in [57] compares all possible switching combinations for the MMC switches in one bridge for their predicted performance one step ahead. This method requires significant computing effort. At each time step with the step size defined by the switching frequency, e.g. 100 μs for 10 kHz, the solution must be sought. For a 5-level MMC, there are 8 submodules in each bridge. Among the eight submodules, four submodules should be turned on to keep the dc-link voltage constant. Therefore, the number of the combination is $C_8^4 = 70$. The algorithm needs to check 70 possible on/off sequences and find the best one. For a 13-level MMC, C_{24}^{12}, or 2.7 million combinations should be checked. For a 16-level MMC, 155 million combinations should be checked.

In [77], a one-step model predictive control has been proposed. The proposed method aims to track the ac reference currents and eliminate the circulating currents. Based on the two objectives, the optimal upper-arm voltage and lower-arm voltage for a MMC bridge can be found. Based on the desired voltage level, capacitor voltages are sorted in order. When the arm current is positive, the capacitors with lowest voltages will be switched on to get charged. When the arm current is negative, the capacitors with the highest voltages will be switched off to get discharged. This

Table 2.1. MMC sizings proposed in the recent literature for particular applications.

Reference	Number of Levels	DC Link Voltage (kV)	Capacity (MW)	Application
[81]	401	640	1000	HVDC (France-Spain)
[82]	401	640	1000	HVDC
[83]	201	400	400	HVDC
[84]	121	180	180	HVDC
[85]	21	300	300	HVDC
[86]	9	150	300	HVDC
[57]	9	60	50	HVDC
[87]	9	5	1.5	HVDC (small scale)

method requires only sorting algorithms, which makes it efficient for MMCs with a large number of submodules.

The disadvantage of the above algorithm is its omission of the dc-voltage constraint. The number of submodules to be switched on is required to be fixed in PWM scheme and the MPC scheme proposed in [57]. In order to take this constraint into account, a mathematical programming problem is formulated and solved using heuristic way. In many papers, commercial solvers such as CPLEX are employed to solve MIP problems [79, 80]. However, for this power electronics application, it is not feasible to employ a commercial solver. Firstly, the switching scheme will be programmed in a chip. It is not possible to have a commercial solver on a chip. Secondly, commercial solvers use general methods to solve optimization problems. In many cases, CPLEX has convergence issues due to its adoption of enumeration. For special optimization problems, a specific solving method will achieve much faster solving speed than a commercial solver.

From application point of view, MMC has been proposed in the literature mostly for HVDC applications. Table 2.1 summarizes the MMC sizings proposed in the literature for particular applications in the recent literature.

2.5 Summary

The dissertation has an opportunity to conduct research on the following issues since they have not been investigated in the literature:

i fully distributed platform to solve DC Optimal Power Flow problem for radial networks,

28

ii optimal interactions between utility and communities equipped with energy storage systems while preserving the privacy of the communities, and

iii fast, optimal control of fast-switching power electronic converters.

CHAPTER 3

DISTRIBUTED DC OPTIMAL POWER FLOW

3.1 Introduction

Significant increase in amount of private distributed energy resources such as renewable energy resources, energy storage systems, distributed generations, and price-responsive demands is expected in the future smart grid. Not only will it lead to a competitive environment in power system, but also it will introduce a huge volume of control variables in the entire power network. Further, private agents are generally not willing to reveal their own control variables and economical data due to either privacy or economical reasons. These two facts have motivated the recent interest in distributed methods in power systems.

Optimal power flow (OPF, AC-OPF), which determines the most economic schedule to operate generation units and controllable demands in a power network, has always been a challenging problem in power system operation due to its inherent nonlinearity and nonconvexity. Several works are reported in the literature to tackle the OPF problem in a distributed fashion [30, 31, 23, 32, 15]. All of these algorithms separate the entire network into several sub-networks, each of which solves its own OPF problem at each iteration mostly using interior point method. These algorithms then develop an information flow scheme and an update process to push the solution toward the optimal solution. In [30], coarse-grained distributed implementation is used to parallelize the OPF problem, which is extended in [31] and compared to some other distributed approaches. Alternative-Direction Method of Multipliers (ADMM) is employed in [23] to develop distributed OPF solution. The same method (ADMM) is used in [32] to determine a distributed method for semi-definite program-based (SDP-based) formulation of OPF problem, which is first proposed in [33]. A modified subgradient-based method along with Lower-Upper-Bound-Switching (LUBS) method is presented in [15] for

distributed AC-OPF problem. In the LUBS method, the microgrids update their desired prices based of which the main grid iteratively defines its optimal power export/import level from each microgrid. The main grid also compares the upperbound and lowerbound of the optimal solution to guarantee zero duality gap of the final solution.

Several distributed algorithms have been presented for economic dispatch and DC-OPF problems. A gradient-based approach along with consensus-based update process using center-free algorithms [34] is employed in [29] to develop a distributed platform for online optimal generation control or economic dispatch. In fact, the gradient-based method guarantees the power balance in the entire network using local frequency signal while the consensus-based process unifies all the locational marginal prices (LMP) on their unique final values. The center-free algorithms have fast convergence speed but are not appropriate for DC-OPF problems because they cannot address the difference between nodal prices due to line constraints. Thus, a subgradient method is employed to develop the consensus-based update process for distributed DC-OPF problems in [35, 36, 37]. The idea of separating the entire network into some sub-networks, which is widely used to develop distributed AC-OPF solutions, is also practiced for distributed DC-OPF problems in the aforementioned references. At each iteration, each sub-network (agent) solves its own DC-OPF problem locally; then, a pricing mechanism employing subgradient method updates the price using the information gathered from the neighbors, and iterations continues until convergence is met. The most distributed way to define these sub-networks is to consider each bus of the system as a distinct agent, which is proposed in [28]. In this algorithm, which is developed based on subgradient method, each bus defines its optimal power generation level and updates its own multipliers, shares some data with its neighbors, and continues to iterate until global convergence is reached.

In this chapter, a distributed algorithm considering each bus as a distinct agent is proposed to solve DC-OPF problem for radial networks. The algorithm adopted in this chapter is partial primal-dual algorithm, which guarantees the convergence rate toward globally optimal solution for uniformly convex problems [88] and has several advantageous features for radial networks. Compared to dual decomposition based algorithms, where sub-optimization problems are solved given Lagrange multipliers, in a primal-dual algorithm, there is no optimization carried out for sub-

problems. Instead, an updating procedure is adopted to update the control variables. Compared to center-free algorithm, the update process in the proposed algorithm has physical meaning of price updating and is able to address the nodal price differences due to network constraints. It is also faster than the algorithm proposed in [28] due to less volume of updating processes, especially on the Lagrange multipliers of inequality constraints.

The partial primal-dual algorithm has been employed in [38, 39] to explain that the droop control is aligned with a primal-dual process. Our development process starts from economic dispatch problem and applies dual decomposition techniques to extract a distributed economic dispatch. After applying primal decomposition technique to the distributed economic dispatch problem, we further develop a distributed DC-OPF algorithm. The solution sought by the algorithm is proved to be optimal since it satisfies the necessary and satisfactory KKT conditions of the DC-OPF problem for radial networks. In order to demonstrate its efficiency, the algorithm is tested on a radial power network (a modified version of IEEE 9-bus test system).

3.2 DC-OPF and KKT Conditions

Consider a power network containing several generators and controllable loads. The network has finite numbers of buses belonging to $\mathcal{N}$ and finite numbers of branches (edges) belonging to $\mathcal{E}$. The numbers of nodes and branches are then $|\mathcal{N}|$ and $|\mathcal{E}|$ respectively. Generation, demand, and voltage angle on bus $i \in \mathcal{N}$ are denoted by P_{gi}, P_{di}, and θ_i, whereas the power flow on line $(i,j) \in \mathcal{E}$ from node i to j is called P_{ij}.

A typical formulation of DC Optimal Power Flow problem is presented below.

$$\text{maximize } W(\mathbf{P_g}, \mathbf{P_d}) = \sum_{i \in \mathcal{N}} U_i(P_{di}) - C_i(P_{gi}) \tag{3.1a}$$

$$\text{over: } \mathbf{P_g}, \mathbf{P_d}, \mathbf{P_L}, \theta$$

$$\text{subject to: } \sum_{i \in \mathcal{N}} P_{gi} = \sum_{i \in \mathcal{N}} P_{di} \tag{3.1b}$$

$$P_{gi} - P_{di} = \sum_{j:(i,j) \in \mathcal{E}} P_{ij} \tag{3.1c}$$

$$\underline{P_{gi}} \leq P_{gi} \leq \overline{P_{gi}} \qquad \forall i \in \mathcal{N} \qquad\qquad (3.1\text{d})$$

$$\underline{P_{di}} \leq P_{di} \leq \overline{P_{di}} \qquad \forall i \in \mathcal{N} \qquad\qquad (3.1\text{e})$$

$$P_{ij} + P_{ji} = 0 \qquad \forall (i,j) \in \mathcal{E} \qquad\qquad (3.1\text{f})$$

$$-\overline{P_{ij}} \leq P_{ij} \leq \overline{P_{ij}} \qquad \forall (i,j) \in \mathcal{E} \qquad\qquad (3.1\text{g})$$

$$P_{i,j} = \frac{\theta_i - \theta_j}{x_{ij}} \qquad \forall (i,j) \in \mathcal{E} \qquad\qquad (3.1\text{h})$$

$$\theta_0 = 0 \qquad\qquad (3.1\text{i})$$

where

$$\mathbf{P_g} = \{P_{gi} : i \in \mathcal{N}\}$$

$$\mathbf{P_d} = \{P_{di} : i \in \mathcal{N}\}$$

$$\mathbf{P_L} = \{P_{ij} : i \in \mathcal{E}\}$$

$$\theta = \{\theta_i : i \in \mathcal{N}\}$$

Besides, (3.1a) describes the objective function so as to maximize the welfare in the entire network, (3.1b)- (3.1c) denote total and nodal power balance, and (3.1d)-(3.1e) explain the inequality constraints on power generation and demand. (3.1f) guarantees the network to be lossless, and line capacity limits are also explained by (3.1g). (3.1h) describes the line power in terms of the voltage angles of the buses across each line. (3.1i) fixes the voltage angle of the slack bus on zero.

Although the constraint (3.1b) holds if the constraints (3.1c) and (3.1f) satisfied, it is mentioned here to make emphasis of total power balance. Likewise, (3.1f) is mentioned to be emphasized though it is explicitly guaranteed by the constraint (3.1h).

As the equality constraints are affine functions and the inequality constraints are continuously differentiable convex functions in the optimization problem (3.1), the feasible solution set is a convex set.

Assuming that the generation cost function $C_i(P_{gi})$ and the demand utility function $U_i(P_{di})$ are respectively strictly convex and strictly concave for any $i \in \mathcal{N}$, the welfare function is strictly concave. Therefore, the problem (3.1) is a convex optimization problem.

If DC-OPF is defined over a radial power network, any vector P_L can be mapped on a unique vector θ where $\theta_0 = 0$. Therefore, removing the constraints (3.1h)-(3.1i) does not affect the optimal solution of the DC-OPF problem described in (3.1) for a radial power network, so the constraints (3.1h)-(3.1i) are neglected in the DC-OPF problem, hereafter.

According to Karush-Kuhn-Tucker (KKT) conditions, if the solution $(\mathbf{P_g^*}, \mathbf{P_d^*}, \mathbf{P_L^*})$ is a local optimum of (3.1), it necessarily satisfies the following regulatory conditions,

$$\sum_{i \in \mathcal{N}} \left\{ \frac{\partial C_i}{\partial P_{gi}}(P_{gi}^*) - (\lambda_i - \overline{\mu_{gi}} + \underline{\mu_{gi}}) \right\} = 0 \tag{3.2a}$$

$$\sum_{i \in \mathcal{N}} \left\{ \frac{\partial U_i}{\partial P_{di}}(P_{di}^*) - (\lambda_i + \overline{\mu_{di}} - \underline{\mu_{di}}) \right\} = 0 \tag{3.2b}$$

$$\overline{\mu_{gi}}(\overline{P_{gi}} - P_{gi}) = \underline{\mu_{gi}}(P_{gi} - \underline{P_{gi}}) = 0 \quad \forall i \in \mathcal{N} \tag{3.2c}$$

$$\overline{\mu_{di}}(\overline{P_{di}} - P_{di}) = \underline{\mu_{di}}(P_{di} - \underline{P_{di}}) = 0 \quad \forall i \in \mathcal{N} \tag{3.2d}$$

$$\min\{\overline{\mu_{gi}}, \underline{\mu_{gi}}, \overline{\mu_{di}}, \underline{\mu_{di}}\} \geq 0 \quad \forall i \in \mathcal{N} \tag{3.2e}$$

$$(3.1c) - (3.1g) \tag{3.2f}$$

where the vector $\lambda \in \mathbb{R}^{|\mathcal{N}|}$ denotes the Lagrange multipliers corresponding to the equality constraint (3.1c), and the vectors $\underline{\mu} \in \mathbb{R}^{|\mathcal{N}|}$ and $\overline{\mu} \in \mathbb{R}^{|\mathcal{N}|}$ are Lagrange multipliers of the inequality constraints (3.1d)-(3.1e).

Due to the convexity of the original problem (3.1), the KKT necessary conditions described in (3.2) are also sufficient for optimality of $(\mathbf{P_g^*}, \mathbf{P_d^*}, \mathbf{P_L^*})$.

3.3 Design of Distributed DC-OPF

Consider a new optimization problem which is defined same as the optimization problem (3.1) if the constraints corresponding to the lines i.e. (3.1c),(3.1f)-(3.1i) are neglected. The new opti-

mization problem is exactly the problem of Economic Dispatch as defined below.

$$\text{minimize} \sum_{i \in \mathcal{N}} C_i(P_{gi}) - U_i(P_{di}) \tag{3.3a}$$

$$\text{over: } \mathbf{P_g}, \mathbf{P_d}$$

$$\text{subject to: } \sum_{i \in \mathcal{N}} P_{gi} = \sum_{i \in \mathcal{N}} P_{di} \tag{3.3b}$$

$$\underline{P_{gi}} \leq P_{gi} \leq \overline{P_{gi}} \quad \forall i \in \mathcal{N} \tag{3.3c}$$

$$\underline{P_{di}} \leq P_{di} \leq \overline{P_{di}} \quad \forall i \in \mathcal{N} \tag{3.3d}$$

Note that (3.3b) does not require the nodal power balance of generation and demand, but only balance across the entire network. If the the objective function (3.3a) is strictly convex, the optimization problem (3.3) is also convex.

The dual representation of (3.3) is

$$\max_{\lambda} \sum_{i \in \mathcal{N}} \underbrace{\left\{ \begin{array}{c} \min\limits_{P_{gi},P_{di}} C_i(P_{gi}) - U_i(P_{di}) + \lambda(P_{di} - P_{gi}) \\[2mm] \text{s.t. } \underline{P_{gi}} \leq P_{gi} \leq \overline{P_{gi}} \\[2mm] \underline{P_{di}} \leq P_{di} \leq \overline{P_{di}} \end{array} \right\}}_{\Phi_i^{\dagger}(\lambda)}$$

where the optimal solution of the minimization problem can be explicitly defined as

$$\Phi_i^{\dagger}(\lambda) := C_i(P_{gi}^{\dagger}) - U_i(P_{di}^{\dagger}) \tag{3.4}$$

with

$$P_{gi}^{\dagger}(\lambda) := \left[MC_i^{-1}(\lambda) \right]_{\underline{P_{gi}}}^{\overline{P_{gi}}} \tag{3.5}$$

$$P_{di}^{\dagger}(\lambda) := \left[MU_i^{-1}(\lambda) \right]_{\underline{P_{di}}}^{\overline{P_{di}}} \tag{3.6}$$

where $MC_i(P_{gi}) = \frac{\partial C_i}{\partial P_{gi}}$ and $MU_i(P_{di}) = \frac{\partial U_i}{\partial P_{di}}$ are the marginal cost and marginal utility corresponding to bus i, and $[\cdot]_a^b$ denotes $\max\{\min\{\cdot, b\}, a\}$ for $a, b \in \mathbb{R}$, $a \leq b$.

3.3.1 Distributed Economic Dispatch

The objective function $\Phi_i^\dagger(\lambda)$ is not separable across buses $i \in \mathcal{N}$ since it has a scalar variable λ which is common between all $i \in \mathcal{N}$. The following *distributed* version of the dual problem is proposed in this chapter by introducing the vector $\lambda := (\lambda_i, i \in \mathcal{N})$. The variables λ_i are constrained to be equal for all $i \in \mathcal{N}$ at optimality i.e. $\lambda_i = \lambda_j \ \forall i, j \in \mathcal{N}$.

$$\max_{\lambda} \quad \Phi(\lambda) := \sum_{i \in \mathcal{N}} \Phi_i^\dagger(\lambda_i) \tag{3.7a}$$

$$\text{s.t.} \quad \lambda_i = \lambda_j \qquad \forall(i, j) \in \mathcal{E} \tag{3.7b}$$

Since the power network is assumed to be a connected grid, it is enough to define the constraints (3.7b) across the lines.

The following two results suggest solving the distributed optimization problem (3.7) rather than ED. The unique optimal point (P_g^*, P_d^*) will be then recovered from the unique dual optimal λ^*. A proof has been provided in Appendix B of [39] for these results.

i The objective function Φ of DED is strictly concave over $\mathbb{R}^{|\mathcal{N}|}$.

ii DED has a unique optimal point (λ^*) with $\lambda_i^* = \lambda_j^* = \lambda^*$ for all $(i, j) \in \mathcal{E}$

iii ED has a unique optimal point (P_g^*, P_d^*) where $P_{gi}^* = P_{gi}^\dagger(\lambda^*)$ and $P_{di}^* = P_{di}^\dagger(\lambda^*)$.

Applying the Lagrange relaxation upon the equality constraints leads to the following Lagrange function of DED which will be employed to derive a distributed solution.

$$L(\lambda, \pi) := \sum_{i \in \mathcal{N}} \Phi_i^\dagger(\lambda_i) - \sum_{(i,j) \in \mathcal{E}} \pi_{ij}(\lambda_j - \lambda_i) \tag{3.8}$$

36

where $\pi \in \mathbb{R}^{|\mathcal{E}|}$ is the vector of lagrange multipliers for the equality constraints (3.7b). In fact, any multiplier π_{ij} measures the cost of mismatch between λ_i and λ_j across the line $(i, j) \in \mathcal{E}$. A partial primal-dual algorithm for DED takes the form below for (3.7) and (3.8):

$$\lambda_i(k+1) = \lambda_i(k) + \gamma_i \frac{\partial L}{\partial \lambda_i}(\lambda(k), \pi(k)) = \lambda_i(k)+$$

$$\gamma_i \left(P_{di}^\dagger(\lambda_i(k)) - P_{gi}^\dagger(\lambda_i(k)) + \sum_{j:(i,j)\in\mathcal{E}} \pi_{ij}(k) \right) \tag{3.9}$$

$$\pi_{ij}(k+1) = \pi_{ij}(k) - \xi_{ij} \frac{\partial L}{\partial \pi_{ij}}(\lambda(k+1), \pi(k))$$

$$= \pi_{ij}(k) + \xi_{ij}(\lambda_j(k+1) - \lambda_i(k+1)) \tag{3.10}$$

where γ_i and ξ_{ij} are positive real numbers.

3.3.2 Distributed DC Optimal Power Flow

It is implied from the stationary point of (3.9) that $P_{di}^* - P_{gi}^* - \sum_{j:(i,j)\in\mathcal{E}} \pi_{ij}^* = 0$ for any $i \in \mathcal{N}$, which is identical to the constraint (3.1c) if the π is identified by $\mathbf{P_L}$. Therefore, the DC-OPF problem (3.1) can be recovered from distributed economic dispatch by adding the following two constraints:

$$\pi_{ij} + \pi_{ji} = 0 \quad \forall(i, j) \in \mathcal{E} \tag{3.11}$$

$$-\overline{P_{ij}} \leq \pi_{ij} \leq \overline{P_{ij}} \quad \forall(i, j) \in \mathcal{E} \tag{3.12}$$

where (3.11) and (3.12) are identical to the constraints (3.1f) and (3.1g), respectively. With these definitions, the parameters λ_i and π_{ij} have the physical meanings of locational marginal price on bus $i \in \mathcal{N}$ and power flow on line $(i, j) \in \mathcal{E}$, which exclude any information of the agents' cost functions and maintain their privacy.

Although the agents are required to follow specific instructions securing convergence, there is no need for them to adopt same updating rules with same coefficients in a cooperative algorithm. However, some parameters must be meaningful before being fed back into the algorithm at the

37

next iteration. For example, the constraint (3.11) is automatically satisfied if $\pi_{ij} = -\pi_{ji}$ for any $(i,j) \in \mathcal{E}$ at initial point and the corresponding update coefficients are equal in the entire process *i.e.* $\xi_{ij} = \xi_{ji}$ for all $(i,j) \in \mathcal{E}$. Since it is not guaranteed by the agent to start from an ideal π or to keep their own coefficients exactly equal to the neighbors' parameters, the solution proposed in this chapter to secure the constraint (3.11) is applying a center-free-based update over π_{ij} and $-\pi_{ji}$ at each iteration *i.e.*

$$\pi_{ij} = \frac{\pi_{ij} - \pi_{ji}}{2} \quad \forall (i,j) \in \mathcal{E} \tag{3.13}$$

which are carried out by the agent i after receiving ξ_{ji} from its neighboring agents $j : (i,j) \in \mathcal{E}$. The center-free-based update method causes a coefficient equal to $(\xi_{ij} + \xi_{ji})/2$ to be applied to update both π_{ij} and π_{ji} at each iteration before updating λ.

Replacing (3.10) which describes the update process of π with the equation below would also satisfy (3.12).

$$\pi_{ij}(k+1) = [\pi_{ij}(k) + \xi_{ij}(\lambda_j - \lambda_i)]_{-\overline{P_{ij}}}^{\overline{P_{ij}}} \tag{3.14}$$

All the necessary and sufficient conditions for the optimality of (P_g^*, P_d^*, P_L^*) described in (3.2a)-(3.2f) are satisfied by the proposed partial primal-dual algorithm. The conditions (3.2a)-(3.2b) as well as the constraints (3.1d)-(3.1e) are satisfied by (3.5)-(3.6) with the definitions below,

$$\underline{\mu_{gi}} := \max\left\{0, MC^{-1}(P_{gi}) - \lambda_i\right\} \tag{3.15}$$

$$\overline{\mu_{gi}} := \max\left\{0, \lambda_i - MC^{-1}(P_{gi})\right\} \tag{3.16}$$

$$\underline{\mu_{di}} := \max\left\{0, MU^{-1}(P_{di}) - \lambda_i\right\} \tag{3.17}$$

$$\overline{\mu_{di}} := \max\left\{0, \lambda_i - MU^{-1}(P_{di})\right\} \tag{3.18}$$

There is no need to change the communication network to tackle the generation/demand capacity constraints although some reconfigurations are introduced in [29] as required actions for such a purpose. The dual feasibility and complementary slackness conditions (3.2c)-(3.2e) are also

satisfied by (3.15)-(3.18). The equality constraints (3.1c) and (3.1f) are satisfied by the stationary points of (3.9) and (3.13), respectively.

To summarize, the partial primal-dual algorithm described by (3.9) and (3.13)-(3.14) solves the optimization below, which is called *Distributed* DC-OPF due to its distributed properties.

$$\min_{\pi} \quad \max_{\lambda} \quad \sum_{i \in \mathcal{N}} \left(\Phi_i^{\dagger}(\lambda_i) - \sum_{j:(i,j) \in \mathcal{E}} \pi_{ij}(\lambda_j - \lambda_i) \right) \tag{3.19}$$

$$\text{s.t.} \quad -\overline{P_{ij}} \leq \pi_{ij} = -\pi_{ji} \leq \overline{P_{ij}}$$

Algorithm 1 illustrates a distributed algorithm to solve the DDC-OPF problem (3.19) through an iterative process.

Algorithm 1 Distributed Algorithms for DC Optimal Power Flow
---
  initialize vectors λ and π
  while Convergence is not met **do**
    for all $i \in \mathcal{N}$ **do**
      for all $j : (i,j) \in \mathcal{E}$ **do**
        Receive λ_j from the neighboring agent j
        Update π_{ji} using (3.14)
        Send π_{ij} to the neighboring agent j
      end for
    end for
    for all $i \in \mathcal{N}$ **do**
      for all $j : (i,j) \in \mathcal{E}$ **do**
        Receive π_{ji} from the neighboring agent j
        Update π_{ij} using (3.13)
      end for
      Calculate P_{g_i} using (3.5)
      Calculate P_{d_i} using (3.6)
      Update λ_i using (3.9)
      Send λ_i to the neighboring buses $j : (i,j) \in \mathcal{E}$.
    end for
    Check Convergence
  end while

3.4 Simulation Results

In order to demonstrate the efficiency of the algorithm proposed in the chapter, it is tested against a modified version of IEEE 9-bus test system, including three generators on buses 1-3. This test system is a meshed network including only one loop. In this study, the line between buses 4 and 9 is removed to create a radial test system, as shown in Fig. 3.1. The details of the cost functions and limits of generation units are provided in Table 4.1.
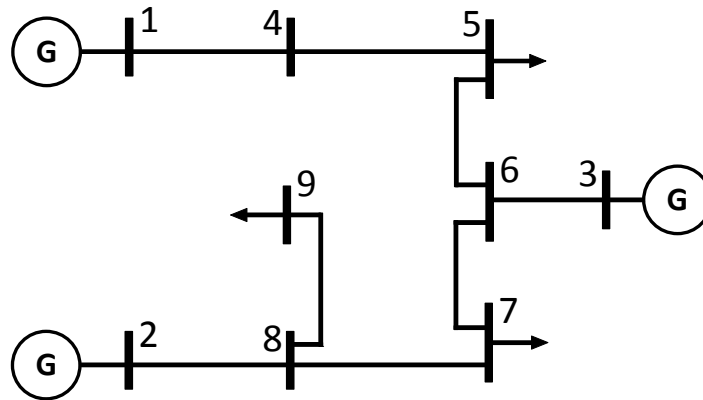
Figure 3.1. Modified IEEE 9-bus test system.

Table 3.1. Details of generators in IEEE 9-bus test system. $C(P_g) = aP_g^2 + bP_g + c$

Gen #	Bus #	$\underline{P_g}$	$\overline{P_g}$	a	b	c
1	1	10	50	0.11	5	150
2	2	10	300	.085	1.2	600
3	3	10	270	.1225	1	335

The coefficients used for updating process are selected as γ_i for any $i \in \mathcal{N}$ and $\xi_{ij} = 8$ for any $(i, j) \in \mathcal{E}$. The algorithm starts the iteration from the initial values of $\lambda_i = 0$ for any $i \in \mathcal{N}$ and $\pi_{ij} = 0$ for any $(i, j) \in \mathcal{E}$.

3.4.1 Case 1: Without Line Congestion

This case is studied against the modified IEEE 9-bus test system with the above-mentioned modifications. Fig. 3.2 depicts the simulation results corresponding to this case study. The

algorithm converges to the optimal solution, which is benchmarked against the results obtained by MATPOWER 4.1 [89], in 200 iterations. As none of the network lines is congested in this case, all locational marginal prices λ converge to a unique price ($\lambda_i = 27.71 \frac{\$}{\text{MWhr}}$ $\forall i \in \mathcal{N}$), as illustrated in Fig. 3.2-a. According to Fig. 3.2-b, The generator 1 provides its maximum power output ($P_{g1} = 50$ MW) to the system while the other two generators are operated at $P_{g2} = 156$ MW and $P_{g3} = 109$ MW. Total power generation supplies the total power demand with a cost equal to \$5430.18. The power flow on the lines are also provided in Fig. 3.2-c, where the line power P_{ij} and P_{ji} are shown by solid and dashed lines but in the same color.

3.4.2   Case 2: With Line Congestion

In order to investigate the algorithm in congested networks, the maximum power flow on the line between buses 7 and 8 (L_{78}) is assumed to be 10 MW. The algorithm proposed converges to the same solution as MATPOWER suggests in 300 iterations. Fig. 3.3 illustrates the simulation results for this case study. Unlike Case study 1, locational marginal prices at different nodes are different due to line congestion. Locational marginal prices of Buses 2, 8, ad 9 are equal to $24.15 \frac{\$}{\text{MWhr}}$ while this parameter on the other buses of the network is $32.85 \frac{\$}{\text{MWhr}}$, as shown in Fig. 3.3-a. In this case, generator 3 has to provide more power compared to the previous case since generator 2 cannot transfer more power to supply the load on bus 7 due to line congestion of L_{78}. Therefore, power generations of generators 2 is diminished to 135 MW while that of the generator 3 is boosted upto 130 MW, as illustrated in Fig. 3.3-b. The power on the lines are also shown in Fig. 3.3-c, which obviously depicts that the power flow on the line L_{78} is obviously restricted to its maximum power limit on both sides ($P_{87} = -P_{78} = 10$ MW). As expected, such binding of the line constraint causes an increases in the total cost of the network compared to the case 1, which is \$5521.38 (1.7% higher).
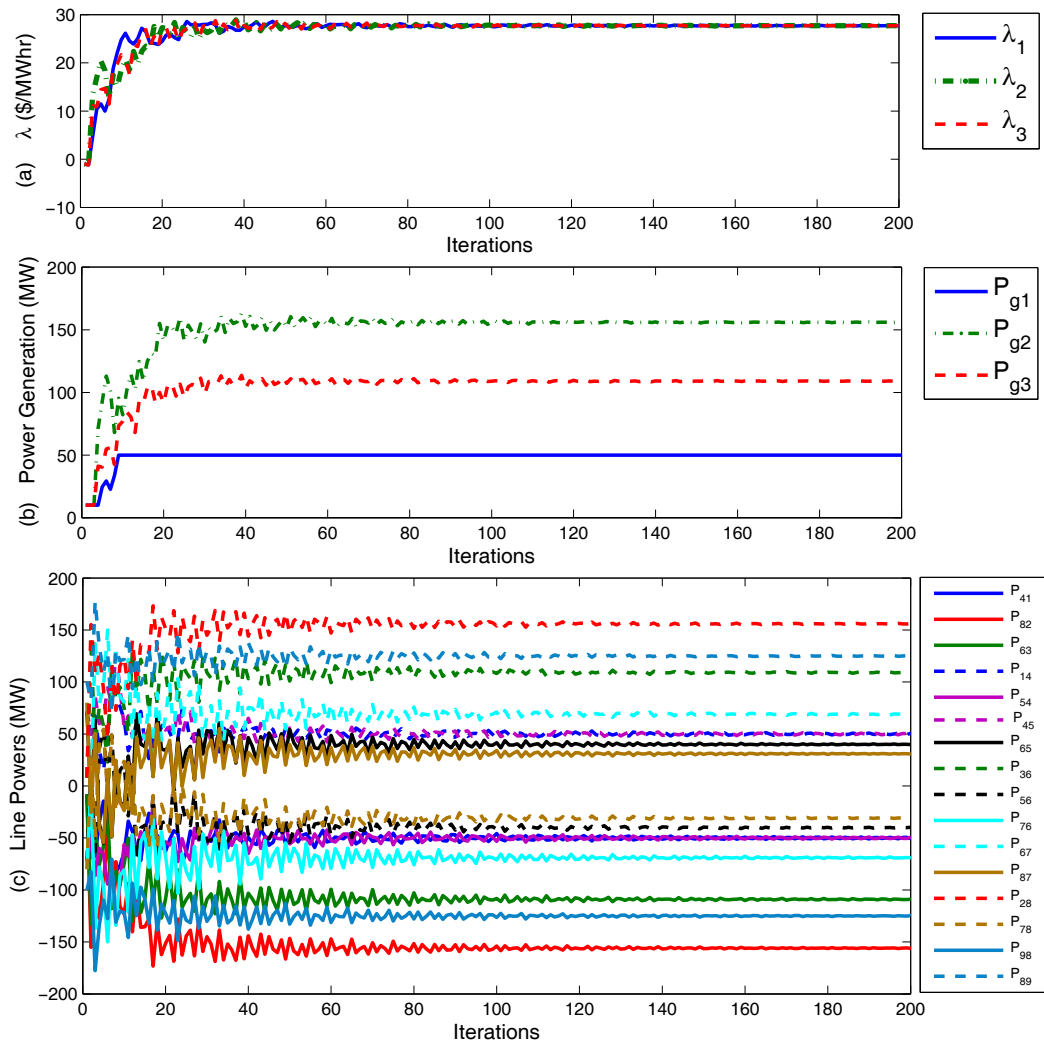
Figure 3.2. Simulation results of case 1. a) Locational Marginal Price (LMP, λ), b) active power output of generators, c) power flow on the lines.
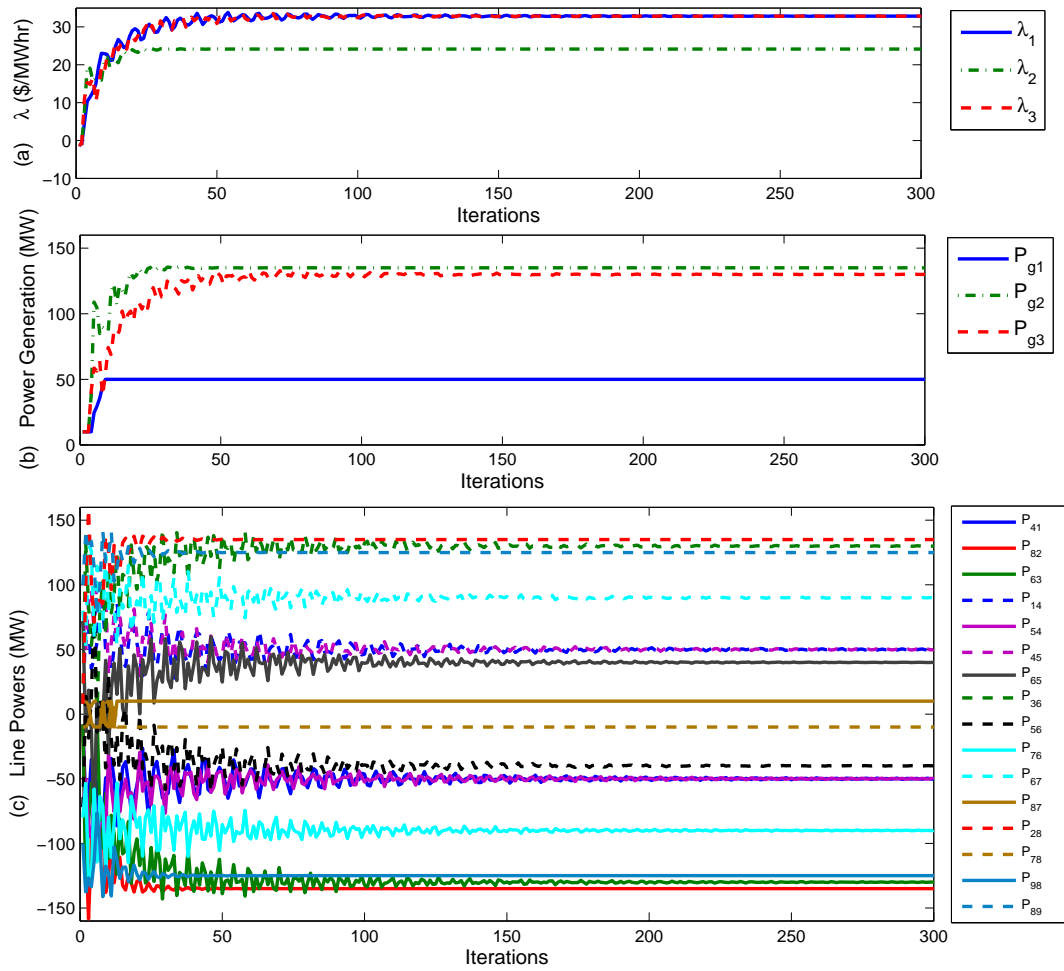
Figure 3.3. Simulation results of case 2. a) Locational Marginal Price (LMP, λ), b) active power output of generators, c) power flow on the lines.

CHAPTER 4

MULTI-AGENT UTILITY-COMMUNITY INTERACTION CONTROL

4.1 Introduction

Multi-agent control has been applied in microgrid or demand side interactions with utility [40, 41, 42, 43]. Microgrids or demand side make their own decisions while exchanging limited information with the grid. For example, in [40], an optimal demand response is designed for the demand sides to bid the amount of load shedding as a a supply function of price. The utility collects the bids from all demand sides and update the price. In [41], the demand sides send the utility the information on their demands, and the utility sets the prices. The demand sides update their demand requests upon receiving the price.

In all references working on this problem, distribution networks are either represented in a simplified way or not represented at all. The objective of this chapter is to implement multi-agent control of demand sides and utility while considering ac network constraints including line flow limits and bus voltage limits.

Implementing of multi-agent control requires distributed algorithms. For optimization problems, there are ways to decompose and construct distributed optimization algorithms [12]. In the field of communication layering problems, primal decomposition, dual decomposition, and primal-dual decomposition can be applied in different scenarios [44]. In power systems optimization problems, due to the decoupled cost function structure and coupled constraints, Lagrangian relaxation based dual decomposition is commonly used. Example applications can be found in aggregated PHEV control considering global constraint [45], and distributed voltage control [46].

This chapter was published in Electric Power System Research in 2014 [15]. Permission is included in Appendix B.

In optimization decomposition, an original problem is separated into a master problem along with many subproblems with small size. After each subproblem makes decision, the main problem is solved adopting iterative methods such as subgradient update. Subgradient algorithm which is based on Lagrangian relaxation has been applied by Luh *et al* for manufacturing job scheduling [47]. Zero or small duality gap can prove that the solution is optimal or very close to optimal. In game theory, iteration means each agent in the system is exchanging information and learning to reach a Nash equilibrium.

Not all distributed algorithms have the information exchange structure suitable for game theory based multi-agent control [48]. In this research, distributed algorithm and learning methods suitable for multi-agent based microgrid and utility interaction will be examined.

Subgradient update based distributed algorithms are popular as seen in the literature. One shortcoming of subgradient method is its slow convergence speed. Scaling factors of Lagrangian multipliers need to be updated to enhance convergence. The update is dependent on specific problems. An improved Lagrangian multiplier or price update scheme is presented to improve convergence. In addition, this chapter proposes an alternative algorithm based on lower bound and upper bound switching to have a faster convergence speed. The philosophy of the bound switching algorithm is similar as the philosophy of Bender's decomposition where lower bound and upper bound are computed. Details and refinement of the bound switching algorithm and the requirement of information exchange structure for demand response program are represented. Both algorithms are tested against multiple case studies, a radial network IEEE 399 system and two meshed networks (IEEE 30-bus system and IEEE 300-bus system), to demonstrate their accuracy, convergence speed, and scalability.

4.2 Lagrangian Relaxation Based Dual Decomposition

4.2.1 Lagrangian Relaxation

An optimization problem is generally defined as

$$f_0^* = f_0(\mathbf{x}^*) = \min_{\mathbf{x}} \quad f_0(\mathbf{x})$$

$$\text{s.t.} \quad f_i(\mathbf{x}) \le 0 \quad 1 \le i \le m$$

$$h_j(\mathbf{x}) = 0 \quad 1 \le j \le p \tag{4.1}$$

where $\mathbf{x}^*$ is its optimal solution.

Lagrangian relaxation technique relaxes the minimization problem by transferring constraints to objective function in the form of weighted sum as shown in (4.2).

$$L(\mathbf{x}; \lambda, \mu) = f_0(\mathbf{x}) + \sum_{i=1}^{m} \mu_i f_i(\mathbf{x}) + \sum_{j=1}^{p} \lambda_i h_j(\mathbf{x}) \tag{4.2}$$

Considering the Langrange dual function, $g(\lambda, \mu)$, as the greatest lower bound of $L(\mathbf{x}; \lambda, \mu)$, the Lagrange dual problem is defined as (4.3).

$$g^* = \max_{\{\lambda, \mu\}} \ g(\lambda, \mu) = \max_{\{\lambda, \mu\}} \ \{\inf_{\mathbf{x}} \ L(\mathbf{x}; \lambda, \mu)\} \tag{4.3}$$

According to weak duality theorem, for any feasible solution (λ, μ) for dual problem (4.3) and any feasible solution $\mathbf{x}$ of the original problem (4.1),

$$g(\lambda, \mu) \le g^* \le f_0(\mathbf{x}^*) \le f_0(\mathbf{x}) \quad \forall \mu \in \mathbb{R}_+^m, \lambda \in \mathbb{R}^p \tag{4.4}$$

Therefore, any feasible solution of the dual problem can be considered as a lower bound of the optimal value of (4.1).

4.2.2 Lower Bound, Upper Bound, and Gap

The definition of upperbound (UB) and lowerbound (LB) must guarantee that $UB \ge f_0^*$ and $LB \le f_0^*$, respectively. Indicated from the previous subsection, the cost corresponding to any feasible solution for dual problem (4.3) is a *Lower Bound*. On the other hand, since the optimal solution $\mathbf{x}^*$ for original problem (4.1) leads to the minimum cost, the resulting cost of any feasible solution $\mathbf{x}$ is an *Upper Bound*. The difference between an upper bound and a lower bound which indicates the efficiency of the solution sought is called *Duality Gap* or *Gap*. (*Gap=UB-LB*).

4.3 System Model and Algorithms

Consider a power network consisting of a set N of buses and a set B of branches. The utility is responsible to operate the power grid, its generation units and transactions with transmission systems. Some community microgrids are connected to the network and behave as autonomous agents. The connected buses belong to a set A.

The communities share with the utility only limited information, which implies the following situations:

i Due to privacy issues, a community does not fully share information to the grid.

ii Due to computing burden, the energy management center of a utility has no ability to collect every piece of information from customers. Instead, it is more feasible to have aggregated loads.

iii The utility, the communities all behave as autonomous agents.

4.3.1 Lagrange Relaxation and Dual Decomposition of AC-OPF Problem

Optimal Power Flow (OPF), the most well-known problem in power system operation, is defined as (4.5). It is obvious that an AC OPF takes care of not only active and reactive power balance constraints but also the other constraints such as voltage constraints, power line capacities, maximum and minimum limits of generators, etc.

$$\min \ \sum_{i \in N} C_i(P_{g_i})$$

$$\text{s.t.} \ \ \forall i \in N, \ \forall_{j \in B}$$

$$P_{g_i} - P_{L_i} - P_i(V, \theta) = 0$$

$$Q_{g_i} - Q_{L_i} - Q_i(V, \theta) = 0$$

$$V_i^m \leq V_i \leq V_i^M$$

$$P_{g_i}^m \leq P_{g_i} \leq P_{g_i}^M$$

$$Q_{g_i}^m \leq Q_{g_i} \leq Q_{g_i}^M$$

$$S_j(V, \theta) - S_j^M \leq 0 \qquad (4.5)$$

where $C(\cdot)$ is the cost function, superscripts M and m denote upper and low bounds, subscript i refers to the variables corresponding to bus i, P_g, Q_g, P_L and Q_L are the vectors of bus active/reactive power injection and active/reactive loads, $P(V, \theta)$ and $Q(V, \theta)$ are the power injection expressions in terms of bus voltage magnitude and phase angles, and $S(V, \theta)$ is the vector of line complex power flow.

Let us define two subscripts $(\cdot)_{imp_i}$ and $(\cdot)_{exp_i}$ which are used in Fig. 5.2. The subscript $(\cdot)_{imp_i}$ denote the utility's power import from community connected to bus i while $(\cdot)_{exp_i}$ denotes the same community's power export to utility. Hereafter, the community connected to bus i will be called community i for simplicity. In order to meet the power balance constraint, (5.11) must be fulfilled for all $i \in A$.

$$
\begin{aligned}
P_{imp_i} &= P_{exp_i} \\
Q_{imp_i} &= Q_{exp_i}
\end{aligned}
\qquad (4.6)
$$

In order to decompose the OPF problem between utility and communities, joint constraint can be relaxed using Lagrange relaxation. Apply Lagrangian relaxation to (4.5) while considering constraints in (5.11):

$$\min \ \sum_{i \in A} C_i(P_{g_i}) + \sum_{i \in N-A} C_i(P_{g_i}) + \sum_{i \in A} \lambda_i^p (P_{imp_i} - P_{exp_i}) + \sum_{i \in A} \lambda_i^q (Q_{imp_i} - Q_{exp_i})$$
$$\text{s.t. Constraints of (4.5)} \qquad (4.7)$$

where λ_i^p and λ_i^q are lagrangian multipliers which also determine the marginal prices for active and reactive power exchange between the utility and community i.

The decomposition is illustrated in Fig. 5.2 and explained as follows,

Decomposition of (4.7) creates agent-based optimization problems. In these agent-based subprograms, the Lagrangian multipliers λ_i^p and λ_i^q are given. The utility level decides utility generator active and reactive power outputs (P_{g_i}, Q_{g_i}) and power import levels (P_{imp_i}, Q_{imp_i}). The problem
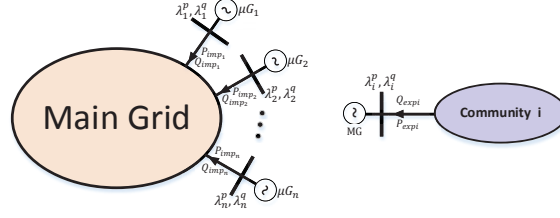
Figure 4.1. Power networks in utility and community optimization problems.

is formulated as below,

$$\min \quad \sum_{i \in N-A} C_i(P_{g_i}) + \sum_{i \in A} [\lambda_i^p P_{imp_i} + \lambda_i^q Q_{imp_i}]$$

$$\text{s.t.} \quad \text{Constraints in (4.5)}$$

$$P_{imp_i}^m \leq P_{imp_i} \leq P_{imp_i}^M \quad \forall_{i \in A}$$

$$Q_{imp_i}^m \leq Q_{imp_i} \leq Q_{imp_i}^M \quad \forall_{i \in A} \tag{4.8}$$

Each community will solve an optimization problem (4.9), where the power prices are given and the decision variables are the community system generator output power levels (P_{g_i} and Q_{g_i}). It is assumed in this chapter that each community has only a generator and a defined power load. Thus, no AC network constraints appear in community optimization problem (4.9).

$$\min \quad C_i(P_{g_i}) - \lambda_i^p P_{exp_i} - \lambda_i^q Q_{exp_i}$$

$$\text{s.t.} \quad P_{g_i} - P_{L_i} - P_{exp_i} = 0$$

$$Q_{g_i} - Q_{L_i} - P_{exp_i} = 0$$

$$P_{g_i}^m \leq P_{g_i} \leq P_{g_i}^M$$

$$Q_{g_i}^m \leq Q_{g_i} \leq Q_{g_i}^M \tag{4.9}$$

In both utility's and communities' optimization problems, constraints (5.11) are not considered explicitly, but rather are used as terminating conditions.

4.3.2 Subgradient Algorithm

The subgradient method is an iterative method in which active and reactive power price signals are first specified by the Price Update Center (PUC) as illustrated in Fig. 5.3. The price signals are used by the utility and communities to define their power import and export levels. Any mismatch between corresponding power import and export levels is then used to update the price values for the next iteration. Fig. 5.3 also depicts the information flow between these three blocks through the algorithm. The utility is assumed to know the maximum and minimum power export level of each community and they are kept constant during the iterations.
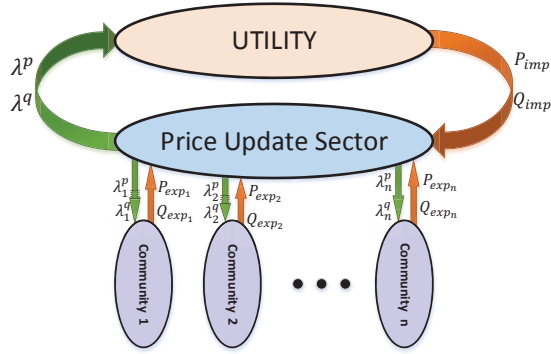
Figure 4.2. Information flow of subgradient algorithm.

4.3.2.1 Price Updating

The Price Update Center is responsible for updating the electricity price at each bus in the power grid through comparing the power import and export levels announced by the utility and communities, respectively. The update procedure agrees the well-known economic rule: the excess demand always leads to increase the price while excess supply causes to reduce it.

Subgradient method based price update is given as follows.

$$\lambda_i^p(k+1) = \lambda_i^p(k) + \alpha_i^p(k) \cdot (P_{imp_i} - P_{exp_i})$$

$$\lambda_i^q(k+1) = \lambda_i^q(k) + \alpha_i^q(k) \cdot (Q_{imp_i} - Q_{exp_i}) \tag{4.10}$$

where k is the index of step, $\alpha_i^p(k)$ and $\alpha_i^q(k)$ denote the step sizes to update active and reactive power prices of bus i at k-th iteration. The values $P_{imp_i} - P_{exp_i}$ and $Q_{imp_i} - Q_{exp_i}$ are the gradients.

The α values are required to get updated (reduced) during the algorithm run to prevent the algorithm to fluctuate over the final solution. It is reported in the literature that the convergence of algorithm to the optimal solution is guaranteed for a decreasing step-size rule $\alpha_i(k) = (1+m)/(k+m)$ and $m \geq 0$, if the gradient/subgradient $P_{err_i} = (P_{imp_i} - P_{exp_i})$ and $Q_{err_i} = Q_{imp_i} - Q_{exp_i}$ are bounded [44].

A shortcoming of subgradient method is its slow convergence rate. The conventional update algorithm reduces the convergence speed and needs to be modified for two reasons.

i It updates all alpha values even if any update is not needed, which make the algorithm meet $P_{err_i} = 0$ and $Q_{err_i} = 0$ in more iterations.

ii Its effectiveness in updating α, which can be indicated by its derivative $d\alpha_i(k)/dk = -(1+m)/(k+m)^2$, decreases significantly for big number of iterations.

Therefore the modified algorithm (4.11) is proposed to update α values at each iteration k.

$$\alpha_i^p(k+1) = \begin{cases} \frac{\alpha_i^p(k)}{2} & \text{if } P_{err_i}(k) \cdot P_{err_i}(k-1) \leq 0 \\ \alpha_i^p(k) & \text{otherwise} \end{cases}$$

$$\alpha_i^q(k+1) = \begin{cases} \frac{\alpha_i^q(k)}{2} & \text{if } Q_{err_i}(k) \cdot Q_{err_i}(k-1) \leq 0 \\ \alpha_i^q(k) & \text{otherwise} \end{cases} \tag{4.11}$$

The two major changes in the modified algorithm compared to the conventional method are:

i Instead of updating all α values at each iteration, only those α values which require updating will change.

ii The method proposed reduces α values only when the sign of their corresponding gradients changes. Otherwise, there is no change.

4.3.2.2 Utility Optimization

After utility receives the price profile from PUC, it runs OPF assuming that the communities are traders selling their power with a linear cost function or a fixed price equal to the updated price. The OPF determines how much active and reactive power the utility is willing to purchase or import from each community. These values create the power import vector P_{imp} and Q_{imp}, which can be either positive or negative. The utility announces P_{imp} and Q_{imp} to the PUC. MATPOWER 4.1 [89] is employed to solve the utility optimization problem.

4.3.2.3 Community Optimization

In order to define its power export level, each community must perform its optimization based on the given price from the PUC. It is assumed, in this chapter, that each community has only a generator and a defined power load. The optimization problem corresponding to the community connected to bus $i \in A$ is presented in (4.9).

The community receives the updated price, solves its own subproblem (4.9) and determines the amount of active and reactive power to sell or to export to the main grid (P_{exp_i} and Q_{exp_i}) as shown in Fig. 5.3. Then the values of P_{exp_i}, Q_{exp_i} are announced to PUC. Algorithm 2 presents the subgradient method based algorithm.

Algorithm 2 Subgradient Method

---
  initialize vectors λ^p and λ^q
  while Convergence is not met **do**
    Solve (4.8) given (λ^p, λ^q) to define (P_{imp}, Q_{imp})
    for all $i \in A$ **do**
      Solve (4.9) given (λ_i^p, λ_i^q) to define (P_{exp_i}, Q_{exp_i})
    end for
    Check Convergence
    Update vectors α^p and α^q using (4.11)
    Update vectors λ^p and λ^q for the next step using (5.15)
  end while

4.3.3 Lower-Upper-Bound Switching (LUBS) Algorithm

Algorithms such as Branch-and-Bound and Bender's decomposition rely on finding lower bound and upper bound iteratively [90]. Once lower and upper bounds converge, the optimal solution is found.

We apply this philosophy in developing a new algorithm. Here the information flow between the utility and communities are shown in Fig. 5.4: the communities send the bid prices to the utility; the utility determines how much power to import from each community based on the bid price; and the communities update the bid price according to the utility decision.
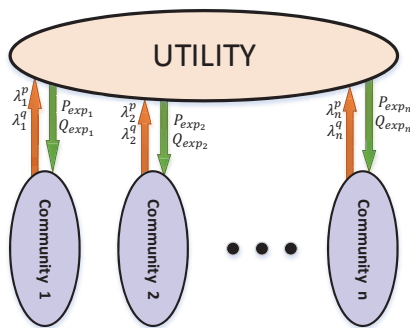
Figure 4.3. Information flow of LUBS algorithm.

The utility's role is exactly the same as that in the subgradient algorithm. However, there is no Price Update Center to update the power price vectors. In this structure, communities are responsible to determine the price vectors. The utility is assumed to know the maximum and minimum power export level of each community and they are kept constant during the iterations.

Mathematically speaking, when the communities announce prices and the utility determines power import level considering the prices, there is one common price vector shared by the communities and the utilities. As the the solution found is a feasible one for the dual problem (4.7), aggregating the costs of all communities and utility leads to a *lower bound*.

On the other hand, when the utility announces power import levels and the communities determine prices based on the power import levels, the coupling constraints (5.11) are met. As the decision variables are in the feasible region of the master optimization problem (4.5), aggregating the costs leads to an *upper bound*.

The algorithm relies on iteration and the converging of the lower and upper bounds.

4.3.3.1   Utility Optimization

At iteration k, the utility solves (4.8) given price vectors $(\lambda_i^p(k), \lambda_i^q(k))$ at the first iteration or updated price vectors at the next iterations to determine the power import vector (P_{imp}, Q_{imp}). Then, the vectors P_{imp} and Q_{imp} are announced to the communities. The procedure to solve utility OPF problem is the same as that in the subgradient method. The utility also computes the utility cost $C_u(k)$ at k-th iteration.

4.3.3.2   Community Optimization and Price Updating

Once the communities receive the utility's power import vector, they must determine their local generator outputs and announce their price signals back to the utility.

As general, the community connected to the bus $i \in A$ seeks the Lagrangian multipliers related to the equality constraints $(\lambda_i^{p^*}, \lambda_i^{q^*})$ in (5.16). When the limits are not binding, the prices are same as the marginal prices of the generators.

$$\min \quad C_i(P_{g_i}) \tag{4.12}$$

$$\text{s.t.} \quad P_{g_i} - P_{L_i} = P_{imp_i}$$

$$Q_{g_i} - Q_{L_i} = Q_{imp_i}$$

$$P_{g_i}^m \le P_{g_i} \le P_{g_i}^M$$

$$Q_{g_i}^m \le Q_{g_i} \le Q_{g_i}^M \tag{4.13}$$

In a special case where the communities only have generation units and fixed loads, $(\lambda_i^{p^*}, \lambda_i^{q^*})$ are their marginal costs corresponding to $(P_{imp,i}, Q_{imp,i})$. For example, if the cost function of a generation unit is quadratic $C_i(P_{g_i}) = 0.5a_i P_{g_i}^2 + bi P_{g_i} + c_i$, the active power price is equal to $\lambda_i^{p^*} = a_i(P_{imp,i} + P_{L_i}) + b_i$.

The cost of the community i at k-th iteration, denoted as $C_{ci}(k)$, is computed by the community and announced to the utility.

4.3.3.3 Lower and Upper Bound Computation

The lower bound can be found when the utility and the communities share the same price vector.

$$LB = C_u(k) + \sum C_{ci}(k-1) \tag{4.14}$$

The upper bound can found when the utility and the communities share the same power exchange.

$$UB = C_u(k) + \sum C_{ci}(k) \tag{4.15}$$

Duality gap is then calculated to decide whether to stop the iterations or continue.

In some cases, especially for meshed power networks, prices shuffle and have difficulty to converge. A modified LUBS algorithm is proposed here. A parameter σ is introduced to smoothly update the prices using (4.16). This technique can prevent the instability of the algorithm although it may slightly decrease the convergence speed.

$$\lambda_i^p(k+1) = \sigma \cdot \lambda_i^{p^*}(k) + (1-\sigma) \cdot \lambda_i^p(k)$$
$$\lambda_i^q(k+1) = \sigma \cdot \lambda_i^{q^*}(k) + (1-\sigma) \cdot \lambda_i^q(k) \tag{4.16}$$

After the price vector is updated, the communities compute their generation cost considering the updated price in lower bound computation.

Algorithm 3 illustrates how LUBS method works.

4.4 Convergence Analysis

4.4.1 Subgradient Method

In this method, the price λ^k is announced to both utility and community at iteration k, then they decide how much power they would like to exchange with each other. Regarding the power level of both sides, the price update sector updates the price for the next iteration. If the slopes of

Algorithm 3 LUBS Method
```
initialize vectors λᵖ and λ�q
while Convergence is not met do
    Solve (4.8) given (λᵖ, λq) to determine (P_imp, Q_imp, C_u)
    Compute C_u
    for all i ∈ A  do
        find (λᵢᵖ*, λᵢq*) by solving optimization problem (5.16)
        Update vectors λᵖ and λq using (4.16)
        Compute C_ci
    end for
    Compute lower bound using (4.14)
    Compute upper bound using (4.15)
    Check Convergence
end while
```

marginal cost functions corresponding to utility and microgrid are respectively $a_1 > 0$ and $a_2 > 0$, assuming that:

$$P_{imp}^k = P_{imp}^0 - a_1\lambda^k \tag{4.17}$$

$$P_{exp}^k = P_{exp}^0 + a_2\lambda^k \tag{4.18}$$

Then,

$$\lambda^{k+1} = [1 - \alpha(a_1 + a_2)]\lambda^k + \alpha(P_{imp}^0 - P_{exp}^0) \tag{4.19}$$

The iteration problems can be viewed as discrete domain dynamic problems. Hence, the convergence of the algorithm is the same as the stability of corresponding discrete problem which is examined by checking whether $\left|\frac{\lambda^{k+1}}{\lambda^k}\right|$ lies inside the unit circle or not. It is obvious that $\left|\frac{\lambda^{k+1}}{\lambda^k}\right| = 0$ defines the critical value of α which is called α_{cr} here. Through a straightforward calculation, α_{cr} can be derived as $\frac{2}{a_1+a_2}$. When $\alpha < \alpha_{cr}$, subgradient always converges. If When $\alpha > \alpha_{cr}$, the algorithm will not converge. For an α equal to critical value, the iterations will circulate in a loop. Fig. 4.4 illustrates shows the possible regions for λ^{k+1} in a case where $P_{imp}^k > P_{exp}^k$ which is divided by the line $\lambda^{k+1} = \lambda^k + \alpha_c r(P_{imp}^k - P_{exp}^k)$ to converging and diverging areas.
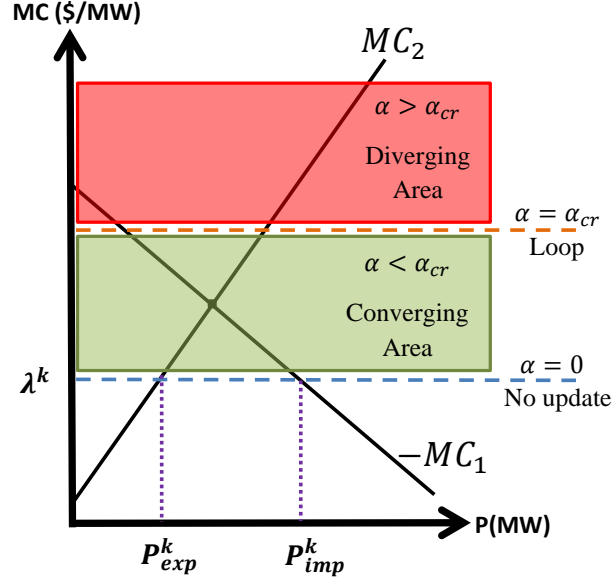
Figure 4.4. Graphical presentation of subgradient method convergence for various values of α. The algorithm converges if $\alpha < \alpha_{cr}$, diverges if $\alpha > \alpha_{cr}$, and circulate in a loop if $\alpha = \alpha_{cr}$.

4.4.2 LUBS Method

In this method, microgrid sets its power export level on the latest level of power demanded by utility at each iteration $k + 1$, *i.e.*, $P_{exp}^{k+1} = P_{imp}^k$ and updates its own price λ^{k+1}. Consequently, utility defines its P_{imp}^{k+1} based on the updated price. Therefore,

$$P_{imp}^k = P_{imp}^0 - a_1 \lambda^k \tag{4.20}$$

$$P_{exp}^k = P_{exp}^0 - a_2 \lambda^{k+1} \tag{4.21}$$

which lead to the following equation regarding the fact that $P_{exp}^{k+1} = P_{imp}^k$ in LUBS method,

$$\lambda^{k+1} = \frac{P_{imp}^0 - P_{exp}^0}{a_2} - \frac{a_1}{a_2} \lambda^k \tag{4.22}$$

Applying the σ modification proposed in [15], the updated price value is derived as:

$$\lambda^{k+1} = (1 - \sigma)\lambda^k + \sigma \left(\frac{P_{imp}^0 - P_{exp}^0}{a_2} - \frac{a_1}{a_2} \lambda^k \right) \tag{4.23}$$

$$\lambda^{k+1} = \left(1 - \sigma \frac{a_1 + a_2}{a_2}\right) \lambda^k + \frac{\sigma}{a_2}(P_{imp}^0 - P_{exp}^0) \tag{4.24}$$

The convergence criteria is then identified as whether $\left|1 - \frac{a_1+a_2}{a_2}\right| < 1$ or not. The critical value of σ can be explicitly derived as $\sigma_{cr} = \frac{2a_2}{a_2+a_1}$. LUBS algorithm converges if $\sigma < \sigma_{cr}$, it diverges when $\sigma > \sigma_{cr}$, and it is trapped in a loop if $\sigma = \sigma_{cr}$. It is obvious that for $\sigma = 1$, the convergence of the algorithm depends on the relation between the slopes of utility's and community's marginal cost functions, where the marginal cost of microgrid must have lower slope than that of main grid to guarantee convergence. This fact is shown graphically in Fig. 4.5 where LUBS diverges when utility has more convex generation cost than microgrid does, $i.e.$, $a_1 > a_2$ (Fig 4.5-a) and it converges otherwise when $a_1 < a_2$ (Fig 4.5-a). The case of $a_1 = a_2$ is also considered as non-converging situation since the solutions will be trapped in a loop.
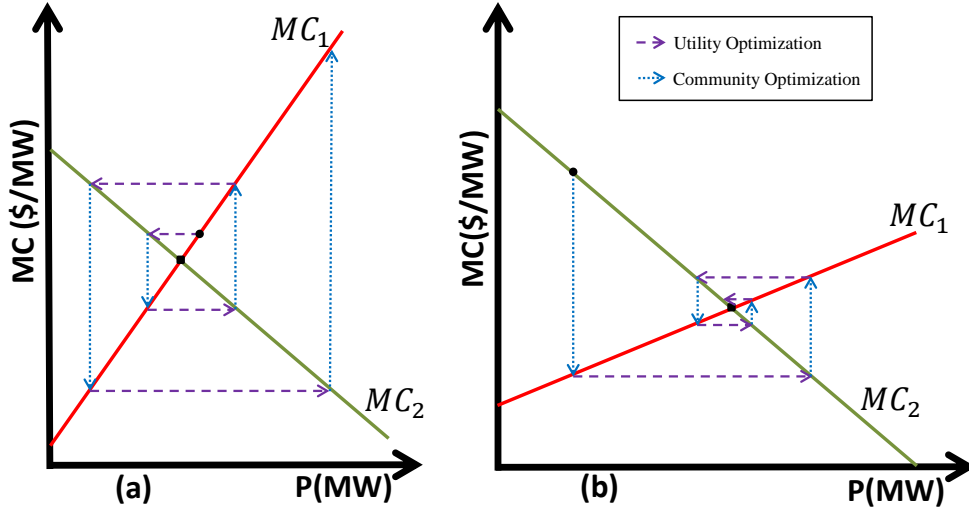
Figure 4.5. Graphical presentation of LUBS convergence for different cases. a) LUBS diverges when agent 1's generation cost is less convex than generator 2's, b) LUBS converges if agent 1's generation cost is more convex than generator 2's.

Fig. 4.6 also shows how applying σ modification makes the algorithm converge to the optimal point for the case where $a_1 < a_2$ (Fig 4.5-a).
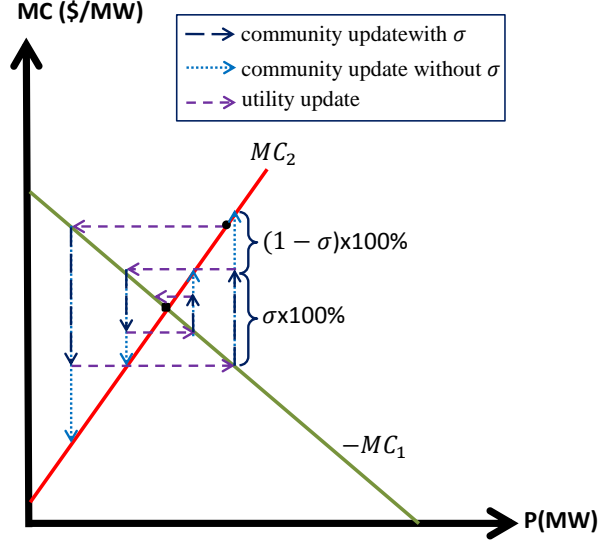
Figure 4.6. Graphical presentation of convergence of LUBS method by applying σ.

4.4.3 Global Solution Search Capability

Subgradient method is guaranteed to converge in just convex optimization problems [91, 14]. Although it is not assured to converge in non-convex problems, there is an α parameter in subgradient structure which may be used to scape from a locally optimal solution. Adjusting these parameters on higher values enables the optimization algorithm to search a larger space for the global solution. One of the concerns about LUBS method is whether this method has the same capability or it will always stuck in one locally optimal solution and cannot lead to the global solution.

It is claimed here that the σ parameter in LUBS method shares the same capability that α shows in subgradient method. Consider Figs. 4.4 and 4.6 for discussion here about subgradient and LUBS methods, respectively. It is stated above that, in both methods, the value of price at iteration $k + 1$ can be denoted as a function of the price at iteration k as below:

$$\text{For subgradient method: } \lambda^{k+1} = \left[1 - \alpha^k(a_1 + a_2)\right]\lambda^k + \alpha^k(P_{imp}^0 - P_{exp}^0) \qquad (4.25)$$

$$\text{For LUBS method: } \lambda^{k+1} = \left(1 - \sigma^k\frac{a_1 + a_2}{a_2}\right)\lambda^k + \frac{\sigma^k}{a_2}(P_{imp}^0 - P_{exp}^0) \qquad (4.26)$$

where both α and σ values are assumed to be controlled at each iteration. A quick comparison of the equations above (4.25)-(4.26) demonstrates that α^k and σ^k/a_2 resemble one another. That is, both methods has their own parameters which may be modified, if required, to change the λ value from its value at each iteration to another specific value at the next iteration. As the σ^k value is a direct function of α^k, LUBS method is proved to have the same capability of not getting trapped in local optimal solution as subgradient method demonstrates.

4.4.4   On Algorithm Complexity

It has been mentioned in the literature that the only OPF algorithms which solves the problem in a polynomial time are SDP and SOCP, both of with are based semidefinite programming formulation of power flow [92, 93]. No prior solutions for OPF problem including interior point method, which is highly adopted to solve optimal power flow problem, are not guaranteed to find the globally optimal solution in a polynomial time. Although the utility's subproblem (an OPF problem with simpler cost model for microgrids' generators) are solved in this dissertation using interior point method, it is beneficial to show that solving the problem in a multi-agent fashion maintains at most the same complexity order that solving the main problem offers.

Assume that the main OPF problem is solved in $O(g(n))$ order of time. When it is decomposed between the communities and the utility, the utility's subproblem is involved with a complexity from at most the same order of complexity $O(g(n))$ and each community's subproblem is a convex optimization problem. The communities' subproblems can be solved in polynomial time, e.g. $O(p(n))$, due to their convexity [91]. It is also shown in [14] that subgradient method has a convergence rate of $O(1/\sqrt{k})$, i.e., $O(1/\epsilon^2)$ iteration is needed to get to get $f(x_{best}^k) - f(x^*) < \epsilon$.

Therefore, the total complexity of the distributed algorithm is the product of iteration number required for subgradient method and the complexity of utility's and communities's subproblems at each iteration, that is, $O(1/\epsilon^2) \times [O(g(n)) + O(p(n))]$. In general, the complexity order of the entire problem is $O[(1/\epsilon^2) \times [g(n) + p(n)]$. However, as $O(g(n)) >> O(p(n))$ and $O(1/\epsilon^2) >> O(p(n))$ for large values of n, it is true to say the entire complexity is still from the order of $O(g(n))$ when n

goes to infinity, and the multi-agent algorithm has a similar complexity order to that of the original problem.

4.5 Analysis of SDP-based Optimal Power Flow as an Alternative for MATPOWER

The OPF problem can be formulated in SDP format based on the SDP formulation of power system equations presented in [94, 33]. Employing the SDP representation of power system equations, which have been used for state estimation problem as well [95], all the system parameters can be expressed by the matrix $W = XX^T$ where X is the vector of real and imaginary values of voltage phasors with the size of $2n$ for an n-bus system.

Denoting $e_1, e_2, ..., e_n$ as the standard basis vectors in R^n, let us define a number of matrices for every node k, and any branch lm between the sending node l and receiving node m. These matrices will be denoted as SDP matrices hereafter in this dissertation.

$$y_{lm} = Y_{bus}(l, m) \tag{4.27}$$

$$Y_k = e_k e_k^T Y_{bus} \tag{4.28}$$

$$Y_{lm} = (y_{lm}^* + y_{lm})e_l e_l^T - (y_{lm}^* + y_{lm})e_l e_l^T \tag{4.29}$$

$$\mathbf{Y}_k = \frac{1}{2} \begin{bmatrix} Re\{Y_k + Y_k^T\} & Im\{Y_k^T - Y_k\} \\ Im\{Y_k - Y_k^T\} & Re\{Y_k + Y_k^T\} \end{bmatrix} \tag{4.30}$$

$$\overline{\mathbf{Y}_k} = \frac{-1}{2} \begin{bmatrix} Im\{Y_k + Y_k^T\} & Re\{Y_k - Y_k^T\} \\ Re\{Y_k^T - Y_k\} & Im\{Y_k + Y_k^T\} \end{bmatrix} \tag{4.31}$$

$$\mathbf{Y}_{lm} = \frac{1}{2} \begin{bmatrix} Re\{Y_{lm} + Y_{lm}^T\} & Im\{Y_{lm}^T - Y_{lm}\} \\ Im\{Y_{lm} - Y_{lm}^T\} & Re\{Y_{lm} + Y_{lm}^T\} \end{bmatrix} \tag{4.32}$$

$$\overline{\mathbf{Y}_{lm}} = \frac{-1}{2} \begin{bmatrix} Im\{Y_{lm} + Y_{lm}^T\} & Re\{Y_{lm} - Y_{lm}^T\} \\ Re\{Y_{lm}^T - Y_{lm}\} & Im\{Y_{lm} + Y_{lm}^T\} \end{bmatrix} \tag{4.33}$$

$$M_k = \begin{bmatrix} e_k e_k^T & 0 \\ 0 & e_k e_k^T \end{bmatrix} \tag{4.34}$$

61

$$X = [Re\{V\}^T, Im\{V\}^T]^T \tag{4.35}$$

$$W = XX^T \tag{4.36}$$

According to the matrices defined in (4.27)-4.36, the parameters of power system can be defined as below:

i Net active power injection from bus k into the grid: $P_{(inj,k)} = tr\{\mathbf{Y}_k W\}$

ii Net reactive power injection from bus k into the grid: $Q_{(inj,k)} = tr\{\overline{\mathbf{Y}_k} W\}$

iii Active power drawn by bus l from branch $l - m$ (direction is defined based on [33]): $P_{lm} = tr\{\mathbf{Y}_{lm} W\}$

iv Reactive power drawn by bus l from branch $l - m$: $Q_l m = tr\{\overline{\mathbf{Y}_{lm}} W\}$

v Voltage magnitude on bus k: $|V_k|^2 = tr M_k W$

Therefore, the OPF problem introduced in (4.5) can be presented as below:

$$\min \ \sum_{i \in N} C_i(P_{g_i})$$

$$\text{s.t} \ \ \forall i \in N, \ \forall_{(i,j) \in B}$$

$$P_{g_i} - P_{L_i} - tr\{\mathbf{Y}_i W\} = 0$$

$$Q_{g_i} - Q_{L_i} - tr\{\overline{\mathbf{Y}_i} W\} = 0$$

$$(V_i^m)^2 \leq tr\{M_i W\} \leq (V_i^M)^2$$

$$P_{g_i}^m \leq P_{g_i} \leq P_{g_i}^M$$

$$Q_{g_i}^m \leq Q_{g_i} \leq Q_{g_i}^M$$

$$(tr\{\mathbf{Y}_{ij} W\})^2 + (tr\{\overline{\mathbf{Y}_{ij}} W\})^2 - (S_{ij}^M)^2 \leq 0$$

$$W \succeq 0$$

$$\text{rank}(W) = 1 \tag{4.37}$$

where $W \succeq 0$ necessitates the matrix W to be positive semidefinite.

If the cost function of each generator i has the quadratic form of $C_i(P_{g_i}) = a_i P_{g_i}^2 + b_i P_{g_i} + c_i$, the objective function can be translated to an SDP format through the following two steps:

i The function $C_i(P_{g_i})$ is replaced by γ_i in the objective function. Instead, the constraint $\gamma_i \geq a_i P_{g_i}^2 + b_i P_{g_i} + c_i$ is added to the constraints for each $i \in N$.

ii Since the determinant of a positive semidefinite matrix is always non-zero, the newly added constraint for bus $i \in N$ can be easily explained in SDP format as follows:

$$\begin{bmatrix} \gamma_i - c_i - b_i \cdot tr\{\mathbf{Y}_{ij}W\} & \sqrt{a_i}tr\{\mathbf{Y}_{ij}W\} \\ \sqrt{a_i}tr\{\mathbf{Y}_{ij}W\} & 1 \end{bmatrix} \succeq 0 \tag{4.38}$$

The line power flow constraint, $i.e.$, $(Tr\mathbf{Y}_{lm}W)^2 + (Tr\overline{\mathbf{Y}_{lm}}W)^2 - (S_j^M)^2 \leq 0$ is always fulfilled if the following matrix is positive semidefinite, since the determinant of a positive semidefinite matrix is always non-zero:

$$\begin{bmatrix} (S_{ij}^M)^2 & tr\{\mathbf{Y}_{ij}W\} & tr\{\overline{\mathbf{Y}_{ij}}W\} \\ tr\{\mathbf{Y}_{ij}W\} & 1 & 0 \\ tr\{\overline{\mathbf{Y}_{ij}}W\} & 0 & 1 \end{bmatrix} \succeq 0 \tag{4.39}$$

The semidefinite programming problem introduced in (4.37) is non-convex due to its rank constraint. It is proposed in the literature [33] that removing the rank constraint makes the problem convex. It is also claimed that formulation certainly leads to valid optimal solutions fulfilling the rank constraint for radial networks. For the meshed networks, however, solving the problem via SDP solvers does not necessarily lead to valid results. Therefore, the results are useful if the rank of the matrix W is one, and they are not correct otherwise. The adverse point is that no modification can help SDP-OPF seek the valid solution if it converges to an invalid solution.

In our problem, the SDP-OPF is supposed to replace MATPOWER to solve the OPF problem once, at least, in each iteration. Since it is not guaranteed to solve the OPF problem for meshed networks, replacing MATPOWER with SDP-OPF causes serious problem in the multi-agent algorithms proposed in this chapter. If the SDP-OPF converges to an invalid solution at any iteration,

the multi-agent algorithm fails since there are no valid parameters for the next iteration. According to the simulation results, using SDP-OPF for radial network also leads to invalid results in some iterations, which makes the multi-agent algorithms crash. The reasons why the SDP-OPF may have some duality-gap which causes the algorithm converge to an invalid solution has been studied in [96] in detail. This transaction paper proves the inexactness of the SDP relaxation. It is shown that even for a small power network (2-bus 1-generator system), the SDP relaxation may result in all possible approximation outcomes, *i.e.* 1) It may be exact and converge to a valid solution, 2) it may be inexact and lead to an invalid solution, or 3) it may be feasible while the optimal power flow (OPF) instance may be infeasible, which offers misleading results.

Regarding the inaccuracy and uncertainty involved with SDP-OPF even for radial networks, MATPOWER has been used to solve the utility's OPF problem.

4.6 Numerical Results

To demonstrate the strength of the algorithms, three different test systems are selected. The first one is the radial test feeder introduced in IEEE standard 399 [97], which is presented in Fig 4.7. All normally-open switches are assumed to be open to have a redial system. Four community microgrids are connected to buses 9, 29, 30 and 50 of this system. The cost function parameters of all generators are presented in Table 4.1. The second test system is IEEE 30-bus test power

Table 4.1. Parameters and cost functions of generators in Fig. 4.7.

$$C(P_g) = 0.5aP_g^2 + bP_g + c$$

Bus #	Owner	P_g^m	P_g^M	Q_g^m	Q_g^M	a	b	c
100	Utility	0	2	-99	99	0.1	55	0
4	Utility	0	8	-2	8	0.3	50	0
9	$\mu G1$	0	1	-0.25	1	0.4	42	0
29	$\mu G2$	0	3	-0.75	3	0.4	35	0
30	$\mu G3$	0	2	-0.5	2	0.2	38	0
50	$\mu G4$	0	11	-2	8	0.2	49	0

system [98], shown in Fig. 4.8 to demonstrate that the algorithms work for meshed power systems. Three community microgrids embedded to the system on buses 2, 13 and 27 are responsible to operate the generators and supply the loads already connected to these buses. The third case is

Figure 4.7. IEEE standard 399 radial 42-bus test feeder with four community microgrids.

Table 4.2. Power and energy ratings of communities' battery packages in different cases.

Case Study	Network Studied	Number of Generators	Number of Microgrids	Total Capacity (MW)	Microgrid Capacity (MW)	Capacity Ratio
1	IEEE Std 399	6	4	27	17	63%
2	IEEE 30-bus	6	3	335	175	52.2%
3	IEEE 300-bus	69	3	32678	300	0.9%
4	IEEE 300-bus	69	40	32678	19203	58.8%

based on IEEE 300-bus test system with three community microgrids integrated to buses 9002, 9051, and 9053.

Table 4.2 summarizes the capacity and generation ratio of the microgrids versus the entire networks in the cases designated. Both Modified Subgradient and LUBS methods are applied on these test systems and the results are compared. Convergence criteria of Subgradient method are: $|\lambda(k) - \lambda(k-1)| < \$0.1/\text{MWh}$, $|P_{err}(k)| < 10^{-3}\text{pu}$ and $|Q_{err}(k)| < 10^{-3}\text{pu}$ for all communities. Convergence criteria of LUBS algorithm are: $gap < \$0.1$, $|\lambda(k) - \lambda(k-1)| < \$0.1/\text{MWh}$, $|P_{imp}(k) - P_{imp}(k-1)| < 10^{-3}\text{pu}$, and $|Q_{imp}(k) - Q_{imp}(k-1)| < 10^{-3}\text{pu}$ for all communities.

Figure 4.8. IEEE 30-bus test system with three community microgrids.

The final solutions of all cases exactly match the optimal power flow solutions of the test systems, which demonstrates the accuracy of the final results for both algorithms.

4.6.1 Case 1: IEEE Standard 399 Test Feeder

Case 1 is related to IEEE 399 system in Fig. 4.7. Fig. 4.9 presents the simulation results of both algorithms corresponding to the community microgrid 4 at bus 50. The plots on the left side show utility power import level versus community power export level and active power price at Bus 50 via Modified Subgradient algorithm. The algorithm converges in 38 iterations or less than 30 seconds. The plots at the right side presents reactive power import, active power import announced by the utility and the active power price of Community 4. They converge to their final values in 9 iterations using Lower-Upper-Bound Switching (LUBS) algorithm with $\sigma = 1$.

The top left plot in Fig. 4.10 shows the upper bound and lower bound in LUBS algorithms of Case 1. The optimality of solution is confirmed through the convergence of upper bound and lower bound.

Figure 4.9. Case 1 simulation results. Reactive power, active power, and active power price of Community $\mu G4$. Subgradient method (Left) and LUBS algorithm (Right).
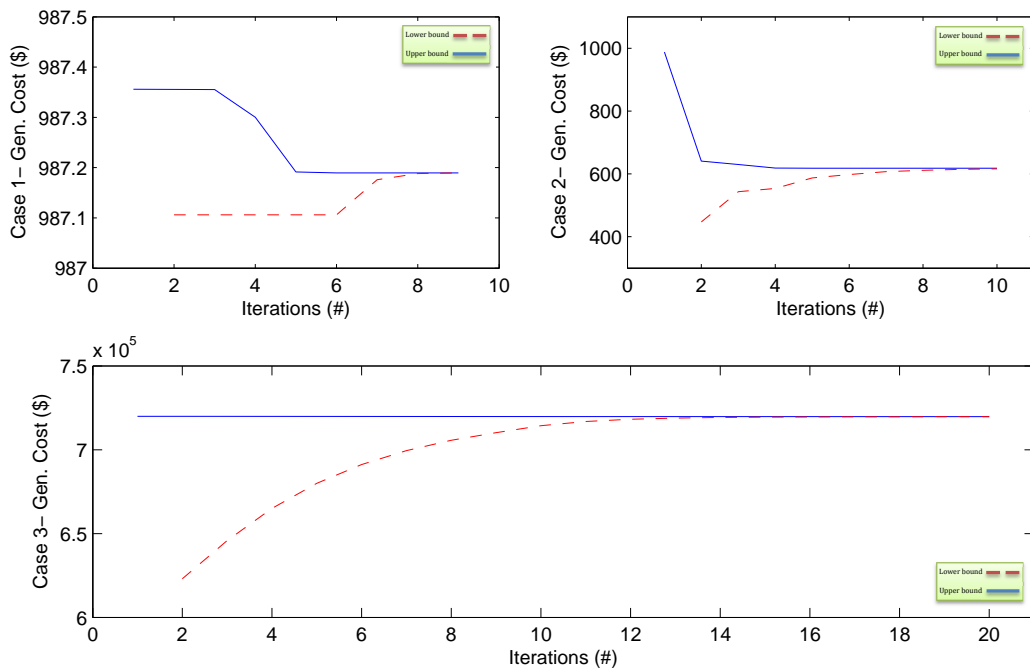
Figure 4.10. Convergence of upper bound and lower bound. Case 1 (up-left), case 2 (up-right), and case 3 (down)

4.6.2 Case 2: IEEE 30-Bus Test System

In the second case, three community microgrids are integrated to IEEE 30-bus test system as depicted in Fig. 4.8. The simulation results of both Modified Subgradient algorithm and LUBS method for community microgrid 3 connected to bus 27 are presented in Fig. 4.11.

The left side plots show community's export and utility's import levels of reactive and active power applying Modified Subgradient algorithm. These values converge in 48 iterations and less than 40 seconds. The right side plots are related to LUBS algorithm, showing the utility active and reactive power import level from community 3 as well as active power price. The numerical results demonstrate that the LUBS algorithm with $\sigma = 0.5$ converges in 10 iterations. According
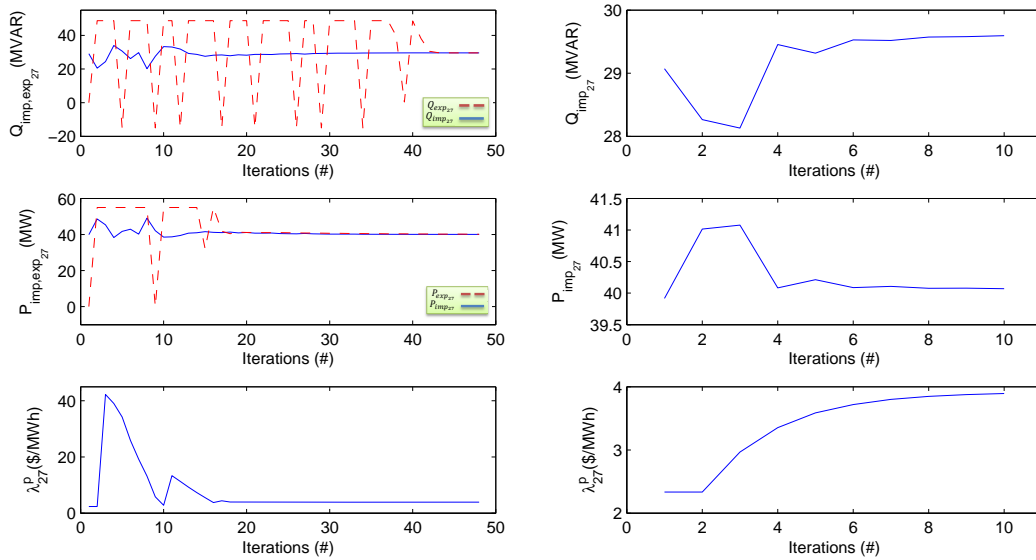
Figure 4.11. Case 2 simulation results. Reactive power, active power, and active power price of community $\mu G3$. Subgradient method (Left) and LUBS algorithm (Right).

to the top-right graph of Fig. 4.10, the upper bound and lower bound in LUBS algorithm converge as well.

4.6.3 Case 3: IEEE 300-Bus Test System with 3 Microgrids

The third case is based on IEEE 300-bus test system with three community microgrids embedded. The simulation results of Modified Subgradient and LUBS algorithms for community

microgrid 2 are shown in Fig 4.12. In the left side plots, the utility's import level and commu-
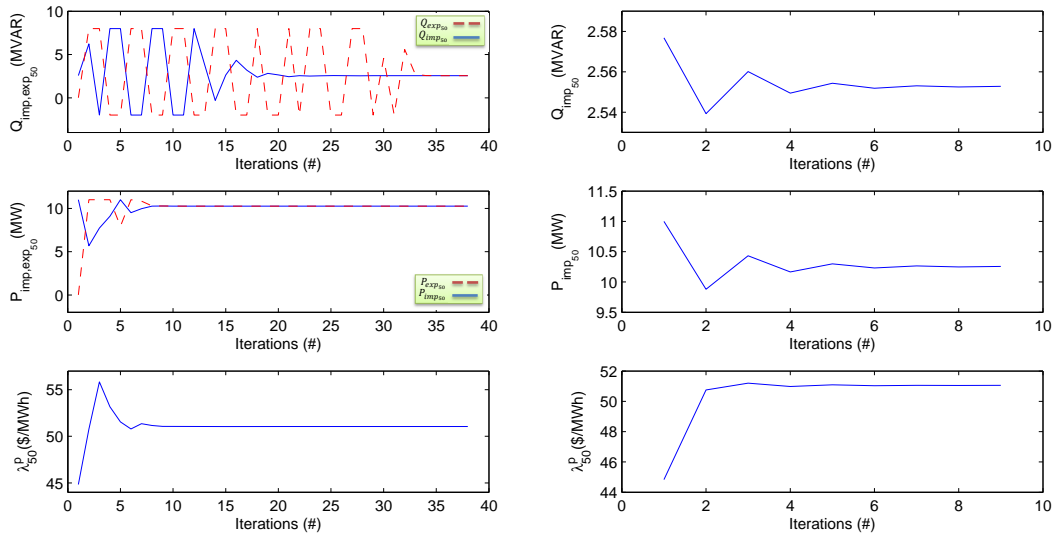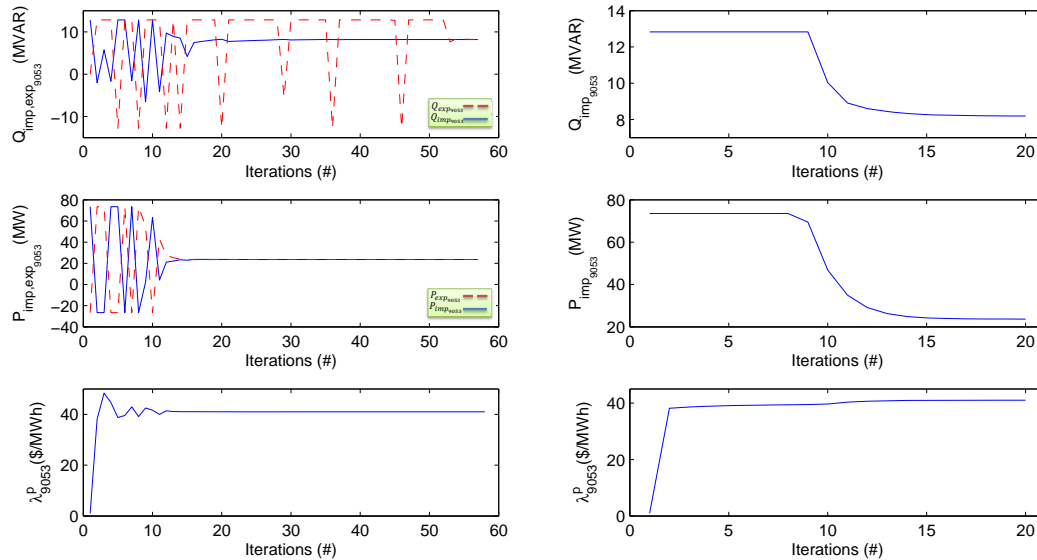

Figure 4.12. Case 3 simulation results. Reactive power, active power, and active power price of community $\mu G2$. Subgradient method (Left) and LUBS algorithm (Right).

nity's export level of active and reactive powers reach together in 57 iterations. This convergence is reached in response to the power price levels which are updated by Price Update Center using (5.15) and (4.11). The right-hand side graphs illustrated that the convergence of LUBS algorithm for case 3 with $\sigma = 0.3$ only takes 20 iterations or 15 seconds, and active and reactive power import levels and active power price are settled on their final values finally. The second-row graph of Fig. 4.10 shows upper bound and lower bound solutions and demonstrates that the optimality gap of the solution found is remarkably low.

4.6.4 Case 4: IEEE 300-Bus Test System with 40 Microgrids

In the last case, which is designated to demonstrate the scalability of the LUBS algorithm, 40 generation units of 69 units connected to IEEE 300-bus test system are considered as microgrids.

In order to guarantee the convergence of LUBS algorithm, the value of σ has to best as low as 0.01 for smooth convergence. Fig. 4.13 shows reactive power, active power and nodal price of 10 selected microgrids which are connected to buses 63, 20, 10, 8, 238, 239, 241, 242, 243, and 7001. The results demonstrate that the convergence in 221 iterations or less than 3 minutes, which is still

a reasonable time even for realtime market applications. The results exactly match the optimal results obtained from OPF benchmarked via MATPOWER.

Fig. 4.14 also illustrates how upperbound and lowerbound converge to the optimal value by the iteration, demonstrating zero duality gap of the solution.
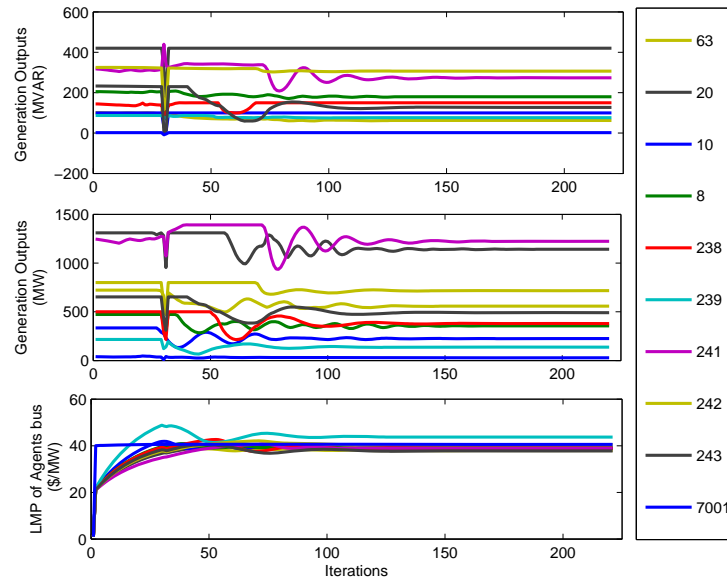

Figure 4.13. Case 4 simulation results. Reactive power, active power, and active power price of 10 selected communities through LUBS algorithm.
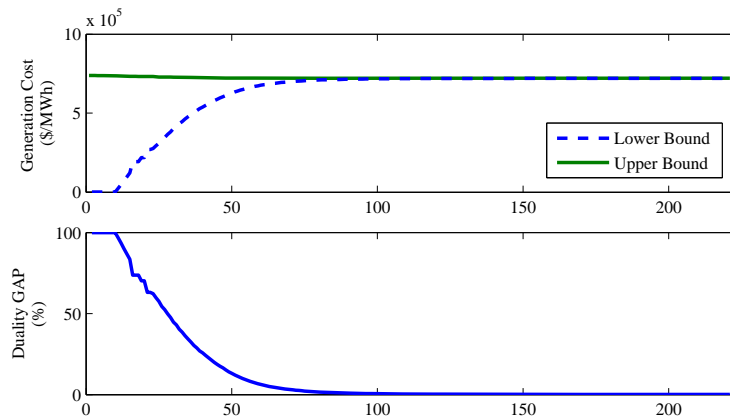

Figure 4.14. Convergence of upper bound and lower bound for Case 4.

CHAPTER 5

PRIVACY-PRESERVING DECISION MAKING PARADIGMS

5.1 Introduction

Significant increase in penetration of private agents having their own microgrid to the power network is highly expected in the future of Smart Grid, which makes control and optimization of the power network more challenging than before. In fact, any of these microgrids may have different types of Distributed Energy Resources (DER) such as Renewable Energy Systems (RES) and Energy Storage Systems (ESS), each of which introduces one type of complexity to the system. Renewable resources normally carry some level of uncertainty while storage systems are constrained by energy limitations which makes the problem be analyzed in a horizon of time instead of in one snapshot. Further, the private agents always have their own specific interests and do not like to share their private information with the system operator due to economical or privacy-related reasons. From the operator's point of view, it is desired to operate the entire power network including the microgrids in its optimal operation point which is normally defined as the least cost operation. In such optimization problem which is known as Optimal Power Flow (OPF), however, the network constraints such as network congestion and voltage limits must be considered. OPF problem sometimes is combined with a constraint on the spinning reserve availability in the system, which guarantees the system to be ready to quickly respond to the contingencies affecting the power balance in the grid.

According to inherent nonlinearity and nonconvexity of OPF problem, it has always been a complicated problem to handle in power system operation. Its complicatedness even increases when some private microgrids are connected to the grid and conduct power transaction with the main grid, where the OPF problem must be tackled in a distributed fashion. In the literature,

there are several works developing distributed algorithm for both AC-OPF [30, 31, 23, 32, 15] and DC-OPF problems [35, 36, 37, 17]. All of these algorithms decompose the problem to smaller subproblems and design an iterative process to seek the optimal solution, where one agent is responsible to each one of these subproblems. After the agents solve their own OPF problem mostly using interior point method, these algorithms performs an update process to push the solution toward the optimal solution, following an information flow scheme which needs the agents to share as minimum as possible amount of private data. Coarse-grained distributed implementation is proposed to parallelize the OPF problem in [30], followed by its extension and comparison versus some other distributed approaches in [31]. The other algorithm used to develop distributed solution for OPF problem is Alternative-Direction Method of Multipliers (ADMM) which is employed in [23]. This algorithm first modifies the updating process of Lagrange multipliers to increase the robustness of the solution with a slight change compared to subgradient method [32]. ADMM is also employed in [32] to develop a distributed solution for semi-definite program-based (SDP-based) OPF problem, which is first presented in [33]. A modified subgradient-based method is proposed in [15], where the microgrids and utility name their desired level of power transactions and a price updating trajects the solution toward the optimal solution. The other method proposed in [15] is named Lower-Upper-Bound-Switching (LUBS), where the microgrids update their desired prices based of which the main grid iteratively defines its optimal power export/import level from each microgrid. To guarantee the optimality of the final solution, the main grid checks the duality gap by comparing the upperbound and lowerbound at each iteration as the most significant signal of convergence.

Spinning reserve adequacy is a constraint which is considered not only in unit commitment problem [52] but also in OPF problem [53, 54]. A reserve-constrained OPF problem is developed in [53] to incorporate the expected security costs in the system using reserve marginal value (reserve price) which indicates how much cost is imposed to the system operation if one more unit of reserve is needed. The extension of MATPOWER 4.1 which solves OPF with co-optimization of energy and reserve is proposed in [54], and its capability is employed later in this chapter to solve reserve-constrained OPF problems.

To handle the time-correlated constraints of ESS, OPF must be considered in a horizon of time instead of just one snapshot. Several approaches has been addressed in the literature to tackle Multi-Horizon Optimal Power Flow (MHOPF) problem. A Benders decomposition method is developed in [27] to tackle energy constraints of hydroelectric plants integrated in irrigation systems. Another thread of research [49, 50] develops a KKT-based solution for MHOPF considering battery storage systems. An optimization model is also proposed in [51] for MHOPF embedded with wind generation and battery storage.

In some other research works, the capability of ESS to provide ancillary services such as reserve is taken into account to tackle reserve constraints in OPF problem without considering their time-correlated constraints [55, 56].

In this chapter, two iterative distributed algorithms are developed to solve reserve-constrained MHOPF problem, which has not been studied yet in the literature. Having identified the private agents as communities and main grid operator as utility, the entire problem is decomposed between utility and communities. Consequently, the entire multi-horizon nonconvex problem is decomposed into several single-horizon nonconvex subproblems for utility and several multi-horizon convex problems for communities along with an update process to make the algorithm iteratively converge to the global optimal solution. The proposed information flow structure completely complies with the economical and privacy-related concerns of the private agents. This chapter also represents a novel analysis on sensitivity of power generation, reserve availability, and price of energy and reserve versus size of energy storage systems [16].

5.2 Information Flow Structure Design

5.2.1 Dual Decomposition of Multi-Horizon Optimization Problems

Consider a nonconvex/nonlinear optimization problem such as AC Optimal Power Flow which can be solved through commercial software packages like MATPOWER. This problem can be easily expanded to be solved at different time steps if there is no coupling between the decision variables at different times, that is, such a multi-horizon problem can be decoupled to several subproblems across the time horizon which can be solved independently from the others. However, energy

storage systems which enable the system to transfer power from one time to another time introduces coupling constraint involving some decision variables of AC OPF problems. Further, the energy storage systems might be operated by private agents with their own objectives and privacy policies. Knowledge about how an OPF problem is mixed with the multi-horizon behavior of the storage systems, implies decomposition of the entire problem between the communities who operate their own internal grid (including generators, renewable energy resources and energy storage systems) and utility which maintain the power network security constraints considered in OPF problem.

Without loss of generality, let us consider the following optimization problem with two agents,

$$\min_{x_1, x_2} \quad \sum_{t \in \mathcal{T}} f_1(x_{1,t}) + f_2(x_{2,t})$$

$$\text{s.t.} \quad \forall t \in \mathcal{T}$$

$$x_{1,t} \in \mathcal{C}_{1,t}$$

$$x_{2,t} \in \mathcal{C}_{2,t}$$

$$x_2 \in \mathcal{C}_{2,\mathcal{T}}$$

$$g_1(x_{1,t}) - g_2(x_{2,t}) = 0$$

$$h_1(x_{1,t}) + h_2(x_{2,t}) <= 0 \tag{5.1}$$

where agent 1 and 2 resemble the utility and the single community, and $x_{i,t}$ and $\mathcal{C}_{i,t}$ denote the vector of decision variables and their feasible set of the agent i, respectively. The set $\mathcal{C}_{2,\mathcal{T}}$ is the biggest set satisfying the constraints defined across the horizon $\mathcal{T}$. The set $\mathcal{C}_{2,t}$ as well as the functions $f_2(x_{2,t})$, $g_2(x_{2,t})$, and $h_2(x_{2,t})$ are convex assumed to be convex, while the convexity of similar parameters corresponding to the first agent is not necessary. The problem includes an equality constraints which is the coupling constraint between the agents. Defining $y_{i,t} := g_i(x_{i,t})$ and $z_{i,t} := h_i(x_{i,t})$ and applying dual decomposition, the problem is decomposed to two following subproblems:

i *Master subproblem:*

$$\Phi_1(\lambda, \mu) = \min_{x_1, y_1} \sum_{t \in \mathcal{T}} f_1(x_{1,t}) + \lambda_t y_{1,t} + \mu_t z_{1,t}$$

$$\text{s.t.} \quad \forall t \in \mathcal{T}$$

$$x_{1,t} \in \mathcal{C}_{1,t}$$

$$y_{1,t} = g_1(x_{1,t})$$

$$z_{1,t} = h_1(x_{1,t}) \tag{5.2}$$

ii *Multi-horizon subproblem:*

$$\Phi_2(\lambda, \mu) = \min_{x_2, y_2} \sum_{t \in \mathcal{T}} f_2(x_{2,t}) - \lambda_t y_{2,t} + \mu_t z_{2,t}$$

$$\text{s.t.} \quad \forall t \in \mathcal{T}$$

$$x_{2,t} \in \mathcal{C}_{2,t}$$

$$x_2 \in \mathcal{C}_{2,\mathcal{T}}$$

$$y_{2,t} = g_1(x_{2,t})$$

$$z_{2,t} = h_1(x_{2,t}) \tag{5.3}$$

The parameters $\lambda = [\lambda_1, \lambda_2, \cdots, \lambda_{|\mathcal{T}|}]^T$ and $\mu = [\mu_1, \mu_2, \cdots, \mu_{|\mathcal{T}|}]^T$ denote the Lagrange multiplier vectors corresponding to the equality and nonequality constraints in (5.1), respectively.

As there is no coupling constraint or objective function in the first subproblem (5.2), it can be decoupled to $|\mathcal{T}|$ smaller problems. They are just needed to be solved for different time steps. However, the second subproblem (5.4) may not be separated across the horizon $\mathcal{T}$ since there is one coupling constraint involving decision variables from different time steps. Our convexity assumptions for corresponding set and functions makes this subproblem a convex optimization problem, which enables a convex solver to seek the optimal value directly. In case of more than one community, more subproblems similar to the subproblem (5.4) appear.

5.2.2 Multi-Horizon Iterative Solutions

Two iterative methods named SubGradient (SG) and Lower-Upper-Bound-Switching (LUBS) methods are introduced in the authors' previous work [15] to solve the OPF problem as a multiagent optimization problem. The multi-horizon iterative solutions introduced in this chapter are founded on these two algorithms and are explained as follows.

For a two-agent platform, the multi-horizon subgradient method each agent i picks its initial or updated Lagrange multiplier at iteration k and seeks its own optimal solution to defines the decision variable vectors $y_i^\dagger(k)$ and $z_i^\dagger(k)$. Then, a price updating sector updates the multiplier vectors λ and μ regarding the values announced by the agents using the following equation if $\min\{b, \max\{a, \cdot\}\}$ is denoted as $[\cdot]_a^b$:

$$\lambda(k+1) = \lambda(k) + \alpha\left(y_1^\dagger(k) - y_2^\dagger(k)\right)$$
$$\mu(k+1) = \left[\mu(k) + \alpha\left(z_1^\dagger(k) + z_2^\dagger(k)\right)\right]_0^\infty \tag{5.4}$$

The updated multipliers are sent back to the agents for next iteration. The algorithm iterates until convergence is met.

It must be noted that one Lagrange multiplier is assigned to each equality or nonequality constraint. The example of OPF would make it more clear. In AC OPF problem, one equality constraint must be determined for each bus to address the nonlinear nature of network loss, so different Lagrange multipliers are introduced on different nodes which are called Locational Marginal Prices (LMP). Therefore, price update sector must update one set of λ for the interaction between utility and each community, which has been discussed in [15]. In contrary, at each time step, the reserve constraint in OPF problem is a single nonequality constraint and only one global Lagrange multiplier must be considered.

The other iterative method which is called Lower-Upper-Bound-Switching (LUBS) method creates direct negotiation between agent 1 and 2, where the first agent names its $y_1^\dagger$ and $z_1^\dagger$ vector as a demand from the other agent. Then, the second agent responds its desired price vectors $\lambda^\dagger$ and

$\mu^\dagger$ which are derived as

$$\left(\lambda^\dagger(k), \mu^\dagger(k)\right) = \operatorname{argmax} \quad \Phi_2(\lambda, \mu) \tag{5.5}$$
$$\text{s.t.} \quad y_2 = y_1^\dagger(k)$$
$$z_2 = z_1^\dagger(k)$$

The agent 1 then performs an update process as below for smooth transition toward the global optimal solution.

$$\lambda(k+1) = \sigma_\lambda \lambda^\dagger(k) + (1 - \sigma_\lambda)\lambda(k) \tag{5.6}$$
$$\mu(k+1) = \sigma_\mu \mu^\dagger(k) + (1 - \sigma_\mu)\mu(k) \tag{5.7}$$

However, there are some drawbacks with LUBS problem in the cases where there are some joint constraints between y_2 and z_2 in multi-horizon subproblem. The most significant drawback of LUBS method is that the values of $y_1^\dagger$ and $z_1^\dagger$ should not make the multi-horizon problem infeasible. Therefore, the agent 2 needs to reveal some level of its privacy such as the limits and internal constraints to the other agent. Second, if the agent 1 considers the constraints revealed by the other agent, the inequality constraint never binds and there will be no meaningful shadow price signals for such constraints. Thus, the LUBS method is not able to address nonequality constraints. To compensate such drawback of LUBS method, the decomposition applied to the nonequality constraints is withdrawn and the first agent remains responsible to maintain these constraints. The other agents are then responsible to update the limits at each iteration.

5.3 Algorithm Design

5.3.1 Decomposition of Reserve-Constrained Multi-Horizon OPF Problem

Consider a power network consisting of a set $\mathcal{N}$ of buses and a set $\mathcal{E}$ of branches. The utility is responsible to operate the power grid, its generation units and transactions with transmission systems. As shown in Fig. 5.1, community microgrids may have energy storage systems, renewable

energy resources, and internal loads. These microgrids are connected to the network and behave as private agents who are willing to share only limited information with the utility. The set $\mathcal{A}$ includes all buses which the agents are connected to.
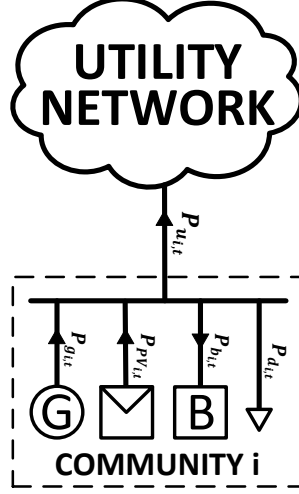
Figure 5.1. A community microgrid including generator, RES, ESS and internal load.

The reserve-constrained multi-horizon Optimal Power Flow problem considering renewable and storage systems is defined as below:

$$\min \quad \sum_{t=1}^{24} \sum_{i \in \mathcal{N}} C_i(P_{g_i}) \tag{5.8a}$$

$$\text{s.t.} \quad \forall_{i \in \mathcal{N}}, \ \forall_{j \in \mathcal{E}}, \ \forall_{t \in \mathcal{T}}$$

$$P_{g_{i,t}} - P_{L_{i,t}} + P_{PV_{i,t}} - P_{b_{i,t}} - P_{i,t}(V, \theta) = 0 \tag{5.8b}$$

$$Q_{g_{i,t}} - Q_{L_{i,t}} - Q_{i,t}(V, \theta) = 0 \tag{5.8c}$$

$$E_{b_{i,t+1}} = E_{b_{i,t}} + P_{g_{i,t}} \tag{5.8d}$$

$$V_i^m \leq V_{i,t} \leq V_i^M \tag{5.8e}$$

$$P_{g_i}^m \leq P_{g_{i,t}} \leq P_{g_i}^M \tag{5.8f}$$

$$Q_{g_i}^m \leq Q_{g_{i,t}} \leq Q_{g_i}^M \tag{5.8g}$$

$$S_{j,t}(V, \theta) - S_j^M \leq 0 \tag{5.8h}$$

$$P_{b_i}^m \leq P_{b_{i,t}} \leq P_{b_i}^M \tag{5.8i}$$

$$E_{b_i}^m \leq E_{b_{i,t+1}} \leq E_{b_i}^M \tag{5.8j}$$

$$E_{b_i,25} = E_{b_i,1} \tag{5.8k}$$

$$\sum_{i \in \mathcal{A}} R_{g_{i,t}} + R_{b_{i,t}} \geq R_{d_t} \tag{5.8l}$$

$$R_{g_{i,t}} \leq R_{g_i}^M \tag{5.8m}$$

$$R_{g_{i,t}} \leq P_{g_i}^M - P_{g_{i,t}} \tag{5.8n}$$

$$R_{b_{i,t}} \leq -P_{b_i}^m + P_{b_{i,t}} \tag{5.8o}$$

The function $C(\cdot)$ is the cost function, superscripts M and m denote upper and lower bounds. Subscripts $i \in \mathcal{N}$ and $t \in \mathcal{T}$ refer to the variables corresponding to bus i and hour t where the set $\mathcal{T} = \{t \in \mathbb{Z} | 1 \leq t \leq 24\}$ denotes the time horizon of the day ahead. P_g, Q_g, P_L and Q_L are the vectors of bus real and reactive power generations, and real and reactive loads. P_b and P_{PV} denote the battery charging power and PV output power respectively. $P(V, \theta)$ and $Q(V, \theta)$ are the active and reactive power injections in terms of bus voltage magnitude and phase angles, and $S(V, \theta)$ is the vector of line complex power flow. E_b also determines the energy stored in the storage systems. The parameters R_g and R_b also denote the reserve provided by the generators and battery systems respectively.

In the optimization problem (5.8), the objective function (5.8a) is defined so as to minimize the total generation cost in the entire system during the day ahead. Active and reactive power balance constraints are defined in (5.8b) and (5.8c) for all buses at all hours. The dependency between battery charging power and energy stored in the battery is stated in (5.8d). The constraints (5.8e)-(5.8d) describe minimum and maximum limits of the corresponding variables. The constraint (5.8k) mandates the ultimate level of energy stored in the battery to be equal to that at starting point. The minimum level of reserve is guaranteed by (5.8l) while the constraints (5.8m)-(5.8o) take care of the reserve constraints.

Similar to the definitions provided in [15], the subscript $P_{imp_{i,t}}$ denote the utility's power import from community connected to bus $i \in \mathcal{A}$ at time $t \in \mathcal{T}$ while $P_{exp_{i,t}}$ denotes the same community's power export to utility. It is noted that these parameters are determined from different points of view but in the same direction. Therefore,

$$P_{imp_{i,t}} = P_{i,t}(V, \theta)$$

$$P_{exp_{i,t}} = P_{g_{i,t}} - P_{L_{i,t}} + P_{PV_{i,t}} - P_{b_{i,t}} \quad (5.9)$$

which replace (5.8b) and (5.8c) by

$$P_{imp_{i,t}} = P_{exp_{i,t}} \quad (5.10)$$

$$(5.11)$$
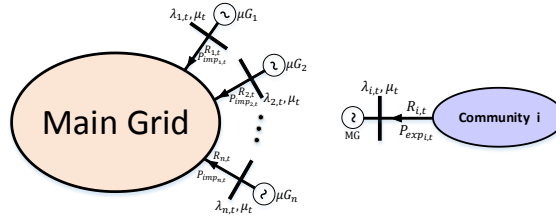
Figure 5.2. Power networks in utility and community optimization problems.

Applying the decomposition procedure proposed in [15], the main problem is divided to several subproblems each of which is solved by the utility or one of the communities. The subproblem assigned to the utility is:

$$\min_{P_{imp_t}, R_{imp_t}} \sum_{i \in \mathcal{N} - \mathcal{A}} [C_i(P_{g_{i,t}}) + \mu_t R_{i,t}] + \sum_{i \in \mathcal{A}} \lambda_{i,t} P_{\mathrm{imp}_{i,t}} \quad (5.12)$$

$$\text{s.t.} \quad \forall_{i \in \mathcal{N} - \mathcal{A}}, forall_{j \in \mathcal{A}}$$

$$P_{g_{i,t}}^m \le P_{g_{i,t}} \le P_{g_{i,t}}^M$$

$$Q_{g_{i,t}}^m \le Q_{g_{i,t}} \le Q_{g_{i,t}}^M$$

$$P_{\mathrm{imp}_{j,t}}^m \leq P_{\mathrm{imp}_{j,t}} \leq P_{\mathrm{imp}_{j,t}}^M$$

$$R_{i,t} \leq R_{g_i}^M$$

$$R_{i,t} \leq P_{g_i}^M - P_{g_{i,t}}$$

$$R_{i,t} = 0$$

while the community i solves the following problem for each hour t,

$$\min_{P_{g_i}, P_{b_i}} \sum_{t=1}^{24} [C_i(P_{g_{i,t}}) - \lambda_{i,t} P_{exp_{i,t}} - \mu_{i,t} R_{exp_{i,t}}] \tag{5.13}$$

$$\text{s.t.} \quad \forall_{t \in \mathcal{T}}$$

$$P_{g_{i,t}}^m \leq P_{g_{i,t}} \leq P_{g_{i,t}}^M$$

$$P_{b_i}^m \leq P_{b_{i,t}} \leq P_{b_i}^M$$

$$E_{b_{i,t+1}} = E_{b_{i,t}} + P_{g_{i,t}}$$

$$E_{b_i}^m \leq E_{b_{i,t+1}} \leq E_{b_i}^M$$

$$E_{b_{i,25}} = E_{b_{i,1}}$$

$$R_{i,t} = R_{g_{i,t}} + R_{b_{i,t}}$$

$$R_{g_{i,t}} \leq R_{g_i}^M$$

$$R_{g_{i,t}} \leq P_{g_i}^M - P_{g_{i,t}}$$

where $\lambda_{i,t}$ is Lagrange multipliers corresponding to power balance on bus i at time t and μ_t denotes Lagrange multiplier of global reserve adequacy constraint at time t.

5.3.2 Multi-Horizon Subgradient Method

In subgradient method, the energy price and reserve price signals are first specified by the Price Update Center (PUC) as illustrated in Fig. 5.3. The price signals are used by the utility and communities to define their power import and export levels as well as reserve for all $t \in \mathcal{T}$. For the next iteration, the energy price values $\lambda_{i,t}$ for the next iteration are then updated using the

mismatch between corresponding power import and export levels. The reserve price value μ_t is also updated to reflect the adequacy or lack of reserve in the network. Fig. 5.3 also depicts the information flow between these three blocks through the algorithm. The utility is assumed to know the maximum and minimum power export level of each community and the communities update these values at each iteration if required.
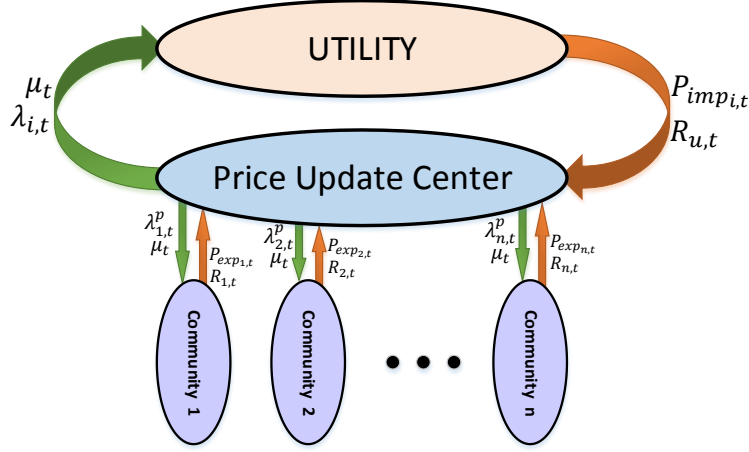

Figure 5.3. Information flow of multi-horizon subgradient algorithm.

5.3.2.1   Price Updating

Updating the energy price at each bus and the global reserve price are the functions assigned to Price Update Center, utilizing the following equations:

$$\lambda_{i,t}(k+1) = \lambda_{i,t}(k) + \alpha_{i,t}(k) \cdot (P_{imp_{i,t}} - P_{exp_{i,t}}) \tag{5.14}$$

$$\mu_t(k+1) = \mu_t(k) + \beta_t(k) \cdot (R_{d_t} - \sum_{i \in \mathcal{N}} R_{i,t}) \tag{5.15}$$

where k is the index of step, $\lambda_{i,t}(k)$ and $\beta_t(k)$ denote the step sizes to update Lagrange multipliers at k-th iteration, the values of which get updated based on the procedure proposed in [15].

5.3.2.2 Community Optimization

In order to define its power export level at different hours, each community must perform its optimization based on the given price from the PUC. In this chapter, it is assumed that each community has a generator and a defined power load as well as a PV-battery package. The optimization problem corresponding to the community connected to bus $i \in A$ is presented in (5.13).

Each community receives the updated price for energy and reserve, solves its own subproblem (5.13) and determines the amount of power to sell or to export to the main grid ($P_{exp_{i,t}}$ for all $t \in \mathcal{T}$) as well as the level of reserve it may provide.The community also updates its maximum and minimum power output to reflect the effects of their battery dispatch, which appear as below in the next utility's OPF problems:

$$P^m_{\text{imp}_{i,t}}(k+1) = P^m_{g_i} - P_{L_{i,t}} + P_{PV_{i,t}} - P_{b_{i,t}}(k)$$
$$P^M_{\text{imp}_{i,t}}(k+1) = P^M_{g_i} - P_{L_{i,t}} + P_{PV_{i,t}} - P_{b_{i,t}}(k)$$

These values are then announced to PUC for price updating process as shown in Fig. 5.3.

5.3.2.3 Utility Optimization

For each hour t, the utility updates the import level limits and employs MATPOWER 4.1 [99] to solve the reserve-constrained OPF problem where the the communities are assumed as traders selling their power by the price announced by PUC. These values create the power import matrix P_{imp} from different communities at different hours as well as the reserve matrix R, which are sent to the PUC for price updating process for the next iteration.

5.3.3 Multi-Horizon LUBS Method

In this structure, communities are responsible to determine the optimal price vectors at different hours to be fed into the utility's OPF problems. At each iteration, communities update utility about maximum and minimum power and reserve they can provide. The values of lower and upper bounds of the total system cost for the entire horizon are defined based on the method proposed in [15].

The information flow platform for utility and communities in multi-horizon LUBS algorithm is illustrated in Fig. 5.4.
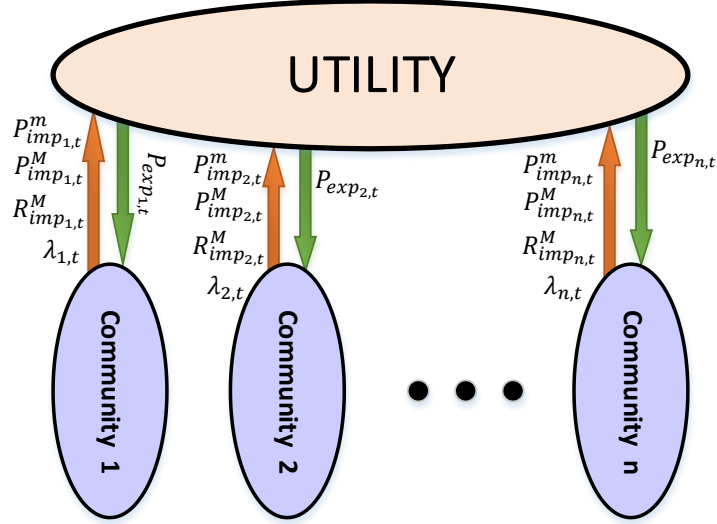

Figure 5.4. Information flow of multi-horizon LUBS algorithm.

5.3.3.1 Community Optimization and Price Updating

Once the communities receive the utility's power import vector which can initially start from zero vector, they must determine their local generator and battery dispatch at different hours and announce the corresponding price signals back to the utility.

Generally, the community connected to the bus $i \in A$ determines its Lagrange multipliers corresponding to the power balance constraints $(\lambda_{i,t}^{p*}, \lambda_{i,t}^{q*})$ for any $t \in \mathbb{Z}_1^{24}$. When the limits are not binding, the prices are same as the marginal prices of the generators.

$$
\begin{aligned}
\min \quad & C_i(P_{g_i}) \\
\text{s.t.} \quad & P_{g_i} - P_{L_i} = P_{imp_i} \\
& P_{g_i}^m \leq P_{g_i} \leq P_{g_i}^M
\end{aligned} \tag{5.16}
$$

One of the requirements in LUBS method is that the solution sought by utility for power and reserve must be feasible in communities subproblems. Since the multi-horizon energy constraints of communities may not be considered in utility subproblems which are solved separately for different hours, utility solution may be infeasible in some cases. For example, if community i's marginal cost function is cheaper than minimum marginal cost of the other generators, utility wills to demand its maximum generator and battery powers at all hours, which may be infeasible due to the energy constraints of the battery. Same scenario may happen for the communities with very expensive generators. Communities are then required to update the maximum and minimum power at each iteration in order to prevent such issues.

According to the constraint (5.8k) which mandate the final and initial SOC of the batteries to be equal, total power output of each battery is zero during the horizon T, i.e., $\sum_{t \in \mathcal{T}} P_{b_{i,t}} = 0$. Thus, the community i's subproblem will be infeasible if

$$24 * P_{g_i}^m \leq \sum_{t=1}^{24} [P_{\text{imp}_{i,t}} + P_{d_{i,t}} - P_{PV_{i,t}}] \leq 24 * P_{g_i}^M \tag{5.17}$$

which may be resolved by updating maximum and minimum limits of community power output as below,

$$P_{\text{imp}_{i,t}}^m(k+1) = P_{g_i}^m - P_{L_{i,t}} + P_{PV_{i,t}} - P_{b_i}^M + P_{b_{\text{adj}_i}}^m(k) \tag{5.18}$$

$$P_{\text{imp}_{i,t}}^M(k+1) = P_{g_i}^M - P_{L_{i,t}} + P_{PV_{i,t}} - P_{b_i}^m - P_{b_{\text{adj}_i}}^M(k) \tag{5.19}$$

where

$$P_{b_{\text{adj}_i}}^m(k) = \left[P_{b_{\text{adj}_i}}^m(k-1) + \pi \left(24 * P_{g_i}^m - \sum_{t=1}^{24} [P_{\text{imp}_{i,t}} + P_{d_{i,t}} - P_{PV_{i,t}}] \right) \right]_0^\infty \tag{5.20}$$

$$P_{b_{\text{adj}_i}}^M(k) = \left[P_{b_{\text{adj}_i}}^M(k-1) + \pi \left(\sum_{t=1}^{24} [P_{\text{imp}_{i,t}} + P_{d_{i,t}} - P_{PV_{i,t}}] - 24 * P_{g_i}^M \right) \right]_0^\infty \tag{5.21}$$

If the community's subproblem is not feasible due to the energy limitations of the battery, the previous price matrix will be sent to the utility; otherwise, the updated vector will be announced.

According to the adjustment process introduced for $P^m_{b_{\mathrm{adj}_i}}$ and $P^M_{b_{\mathrm{adj}_i}}$, it is expected that the battery charging power of the utility i converge to zero for the entire horizon if its generator is fully dispatch or not dispatched at all for the entire horizon.

Community i also updates the maximum reserve it can provide at each iteration according to its dispatched battery power as below and sends it to utility,

$$R^M_{\mathrm{imp}_{i,t}}(k+1) = R^M_{g_i} - P^m_{b_i} + P_{b_{i,t}}(k)$$

5.3.3.2 Utility Optimization

At iteration k, the utility solves its own subproblem given price values $\lambda_{i,t}(k)$ as well as power limits to determine the power import matrices P_{imp} at each hour considering maximum and minimum limits of power and reserve which are announced by communities. The OPF results are then announced to the communities. The procedure to solve utility OPF problem is the same as that in the subgradient method. The utility also computes the utility cost $C_u(k)$ at k-th iteration.

5.3.4 Benefits of Moving-Horizon Method

Two of the parameters being considered in the optimization problem are the power output of photovoltaic panels and the power demand, both of which are mixed with some level of uncertainty. It is obvious that prediction of a stochastic process gets more accurate as time goes on. That is, our prediction about, for example, PV power output one hour hour before it actually happens is much more accurate than what we have predicted on the day before. Thus, running the multi-horizon algorithms in a moving fashion is highly desired in such cases integrated with uncertainty.

Performing moving-horizon method for several times, as shown in Fig. 1.6, instead of running multi-horizon algorithm once, is expected to introduce two major advantages. First, as explained above, it reduces the effect of prediction error by giving more chance to the operator to correct his/her estimation of the uncertain parameters more frequently for more accurate results. Second, running the solution in moving-horizon algorithm provides the opportunity to initialize the algorithm parameters (price values) for the next run using the ultimate simulation results from the

previous run, which are very close to the expected final results in the next run. This technique significantly reduces the number of iterations and helps the algorithm to converge faster. The simulation results demonstrates the effect of this technique on the convergence speed of both algorithms. As an example, applying such initialization technique in the case studies simulated in this dissertation has reduced the number of iterations from 30 in LUBS method and 70 in subgradient method to only 10 iterations, which is a huge improvement in this scale. This technique enables the convergence to be reached in about 100 seconds while the simulation time is 5 minutes for LUBS and 11 minutes for subgradient when no initialization is performed. As stated about the timing of realtime market, algorithms are expected to solve the problems in less than 5 minutes.

5.4   Sensitivity Analysis

5.4.1   Sensitivity of Energy Market to Battery Size

To understand the effect of communities' battery size on their generation and nodal price profiles, the optimal solution of community i in two extreme cases is considered, when no reserve is required. Analyzing the extreme cases of zero- and infinite-capacity for battery system illustrates how multi-horizon optimization of storage systems are expected to behave to minimize the operation cost.

The community i, shown in Fig. 5.1, solves the following problem if it is asked by utility to provide the feasible power profile of $P_{u_{i,t}}$ $\forall_t$,

$$\min_{P_{g_i}, P_{b_i}} \sum_{t=1}^{24} C_i(P_{g_{i,t}}) \tag{5.22a}$$

$$\text{s.t.} \quad \forall_{t \in \mathbb{Z}_1^{24}}$$

$$P_{g_{i,t}} + P_{PV_{i,t}} = P_{d_{i,t}} + P_{b_{i,t}} + P_{u_{i,t}} \tag{5.22b}$$

$$P_{g_{i,t}}^m \leq P_{g_{i,t}} \leq P_{g_{i,t}}^M \tag{5.22c}$$

$$P_{b_i}^m \leq P_{b_{i,t}} \leq P_{b_i}^M \tag{5.22d}$$

$$E_{b_{i,t+1}} = E_{b_{i,t}} + P_{b_{i,t}} \tag{5.22e}$$

87

$$E_{b_i}^m \leq E_{b_{i,t+1}} \leq E_{b_i}^M \tag{5.22f}$$

$$E_{b_{i,25}} = E_{b_{i,1}} \tag{5.22g}$$

For a zero-capacity battery system, $P_{g_{i,t}} = P_{d_{i,t}} + P_{u_{i,t}} - P_{PV_{i,t}}$ is the unique solution and the optimal one. For the other case, the constraints (5.22d) and (5.22f) are ignored to imply an infinite energy storage resource. Therefore, (5.22) can be replaced by the following optimization problem,

$$\min_{P_{g_i}} \sum_{t=1}^{24} C_i(P_{g_{i,t}}) \tag{5.23a}$$

$$\text{s. t.} \quad \sum_{t=1}^{24} [P_{g_{i,t}} + P_{PV_{i,t}} - P_{d_{i,t}} - P_{u_{i,t}}] = 0 \tag{5.23b}$$

$$P_{g_{i,t}}^m \leq P_{g_{i,t}} \leq P_{g_{i,t}}^M \quad \forall_{t \in \mathbb{Z}_1^{24}} \tag{5.23c}$$

It will be shown later that the constraint (5.23c) does not affect the optimal solution, so it is neglected here. The Lagrange function of the problem (5.23) is derived as,

$$\mathcal{L}(P_{g_{i,t}}) = \sum_{t=1}^{24} \left[C_i(P_{g_{i,t}}) - \lambda(P_{g_{i,t}} + P_{PV_{i,t}} - P_{d_{i,t}} - P_{u_{i,t}}) \right] \tag{5.24}$$

the derivation of which over $P_{g_{i,t}}$ leads to

$$MC_i(P_{g_{i,t}}) = \lambda \quad \forall_{t \in \mathbb{Z}_1^{24}}$$

$$P_{g_{i,t}} = P_{g_{i,t'}} \quad \forall_{t,t' \in \mathbb{Z}_1^{24}}$$

Therefore, the optimal solution with an infinite ESS is explicitly derived as

$$P_{g_{i,t}} = \frac{1}{24} \sum_{t=1}^{24} \left[P_{d_{i,t}} + P_{u_{i,t}} - P_{PV_{i,t}} \right] \forall_{t \in \mathbb{Z}_1^{24}}$$

According to the results of both extreme cases, ESS swaps energy from peak hours to off-peak which enables the community to minimize its cost by operating the generators on a unique level which is the average power output of generator in the first case. It is obvious that the optimal solution leads to a flat profile for locational marginal price of the community. Since the optimal solution satisfies the constraint (5.23c), neglecting this constraint is proved to be valid.

Since the optimization problem (5.22) is convex, its optimal solution lies at a point between two extreme cases. That is, the optimal operation of a constrained battery system pushes the generator output toward $\frac{1}{24} \sum_{t=1}^{24} \left[P_{d_{i,t}} + P_{u_{i,t}} - P_{PV_{i,t}} \right]$ as much as the constraints allow. Fig. 5.5 provides a visual explanation of how a constrained ESS reduces total generation cost, where the horizon of the problem is reduced to two hours for better explanation. In this figure, $P_{g_t}^0$ denotes the optimal generator output at hour t in the first extreme case, and $\bar{P}_g^0 = (P_{g_1}^0 + P_{g_2}^0)/2$. The parameters $P_{g_t}^1$ are also the optimal solution at time t when the battery power is constrained by P_b^M and $-P_b^M$ as maximum and minimum limits. The surface of different partitions divided by the vertical lines are expressed by the parameters $A - E$.
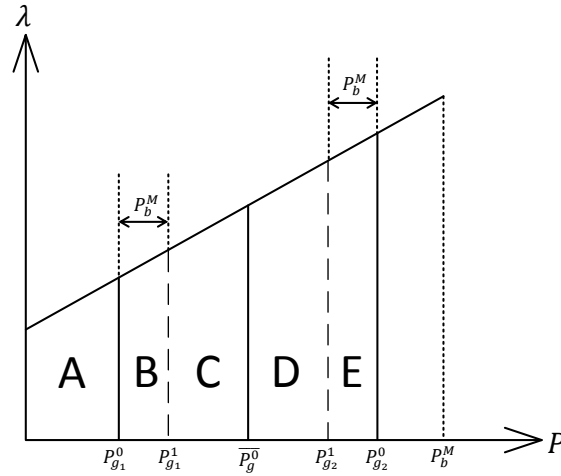

Figure 5.5. Effect of battery management on generation schedule.

It is clear in Fig. 5.5 that the cost associated with the first extreme case is equal to $2A + B + C + D + E$. The optimal solution of the second extreme case is setting the generator outputs on $\bar{P}_g^0$ at each hour and the cost drops on $2(A + B + C)$ which is the minimum generation cost the system can reach. If the battery system is constrained by maximum and minimum power limits, the battery

system pushes the operation point to the average point as much as the battery constraints tolerate. As shown, the optimal operation of the generation in the constrained case is $P_{g_1}^1 = P_{g_1}^0 + P_b^M$ and $P_{g_2}^1 = P_{g_2}^0 - P_b^M$ for the first and second hours respectively. Likewise, any constraint on energy stored in the battery limits the system to reach the solution of the second extreme case, but the trajectory is still making the generation output equal at different hours. Therefore, any release of the battery constraints is expected to result in flatter generation output and nodal price profile.

5.4.2 Sensitivity of Reserve Market to Battery Size

The battery system of community i provides the grid with a reserve capacity equal to $-P_{b_i}^m + P_{b_{i,t}}$ at any time t. As the parameter P_{b_i} has a negative value, increasing the power rating of the battery boosts the reserve available and reduces the reserve price.

The energy rating of the battery also has some impacts on the level of available reserve and its price profile. Charging and discharging the battery changes the operation point of the generator, which changes both generator reserve and battery reserve. If maximum level of the reserve provided by generator is equal to its maximum power, battery operation does not change the total reserve available by both generator and battery. However, if the generator maximum reserve is limited, the corresponding constraint most likely bind at off-peak hours. In this situation, charging the battery as the optimal operation at such hours increases the power output of the generator by ΔP_g and reduces the reserve by $0 \leq \Delta R_g \leq \Delta P_g$ where the reserve offered by the battery boosts exactly by ΔP_g. Thus, at off-peak hours, the operation of the battery is expected to lead to higher reserve in a case with higher energy rating of the battery. At peak hours when the constraint of the maximum reserve binds, increasing the energy rating of battery leads does not change the reserve availability but changes the reserve price. At other hours, the reserve available highly depends on whether the optimal operation of the battery is to be charged or discharged at such hours which may increase or decrease total reserve available.

In an optimization problem, relaxing an inequality constraint helps the solver to seek more optimal solutions, but it makes other inequality constraint more likely to bind. Similarly, increasing the battery energy rating helps the community to seek more profitable battery schedule, and it

increases the probability that the other inequality constraints such as reserve constraint bind. In this case, relaxing battery size lets the system seek better options and increases the cost incurred by other constraints if they bind.

In other words, increasing battery energy rating makes battery to discharge with higher rate at peak hours which means less reserve offered by battery to the grid, which requires the generators to provide higher reserve to the grid and higher reserve price is expected.

5.5 Numerical Results

5.5.1 Algorithms Through Iterations

Both algorithms are applied to the radial 42-bus test feeder introduced in IEEE Standard 399 [97] with the generators determined in Table 5.1. As illustrated in Fig. 5.6, one community equipped with a 200-kW PV and a battery system is assumed to be connected on bus 50. Several cases are studied for different power/energy ratings of the battery presented in Table 6.1. The demand profile of the entire test feeder is multiplied by a time-variant scaling factor $\rho(t)$ as shown in Fig. 5.7 which is corrupted by a white noise $w(t)$ to address the uncertainty of load and PV generation forecast. Therefore, assuming that the optimization horizon starts from t_0 and $P_{d_i}^0$ is the original demand level on bus i in IEEE Standard test feeder, the power demand on each bus i at each time t is updated to $P_{d_i,t} = P_{d_i}^0 * (\rho(t) + w(t - t_0))$, where $w(t - t_0) \sim \mathcal{N}(0, \sigma(t - t_0))$ with a time-variant standard deviation $\sigma(t - t_0) = 0.1\rho(t) \times (1 - e^{\frac{-(t-t_0)}{12}})$.

After the operation schedules of energy storage systems is finalized, they must be followed as reference set points by a battery management system [100].

5.5.1.1 Without Reserve Requirement

First, the system is studied through both algorithms when no reserve is required. Fig. 5.8 illustrates the parameters P_{imp}, P_{exp}, community's nodal price, and battery charging power at different hours $t \in \{1, 7, 13, 19\}$ for case 1. The algorithm results converge to the optimal values in 70 iterations.
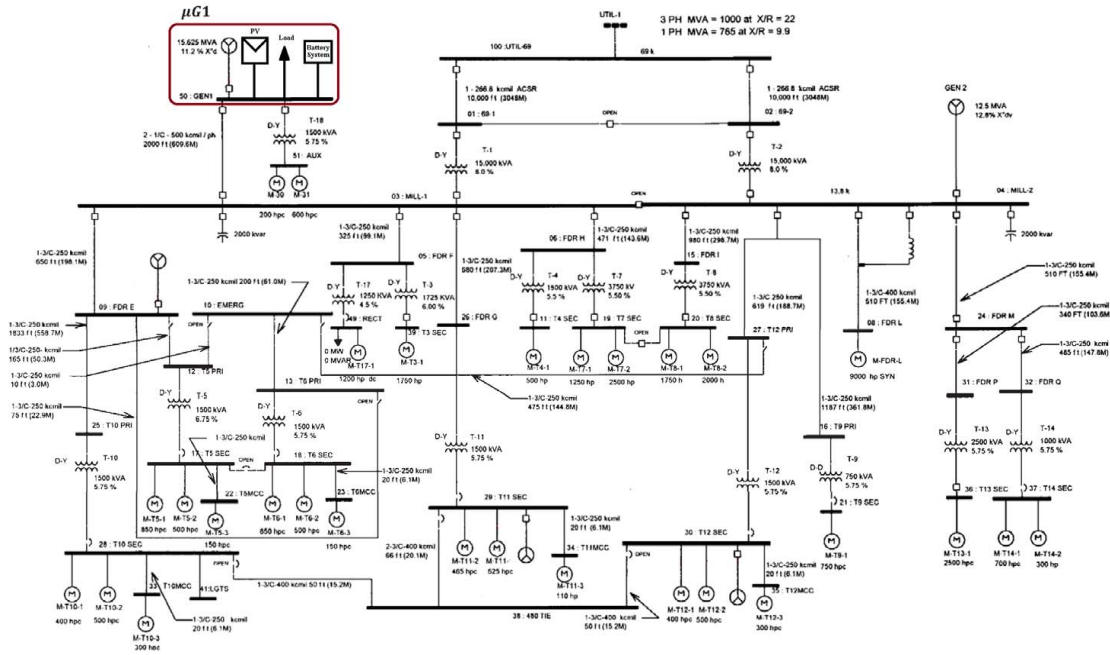
Figure 5.6. IEEE standard 399 test feeder with one interconnected microgrid.

Table 5.1. Parameters and cost functions of generators in IEEE standard 399 test feeder. $C(P_g) = 0.5\alpha P_g^2 + \beta P_g + \gamma$

Bus #	Owner	P_g^m	P_g^M	R_g^m	α	β	γ
100	Utility	0	2	0	0.1	55	0
4	Utility	0	12	2	0.3	50	0
9	$\mu G2$	0	5	0	0.4	42	0
29	$\mu G3$	0	3	0	0.4	35	0
30	Utility	0	4	0	0.2	38	0
50	$\mu G1$	0	11	8.8	0.2	49	0

Table 5.2. Power and energy ratings of communities' battery packages in different cases.

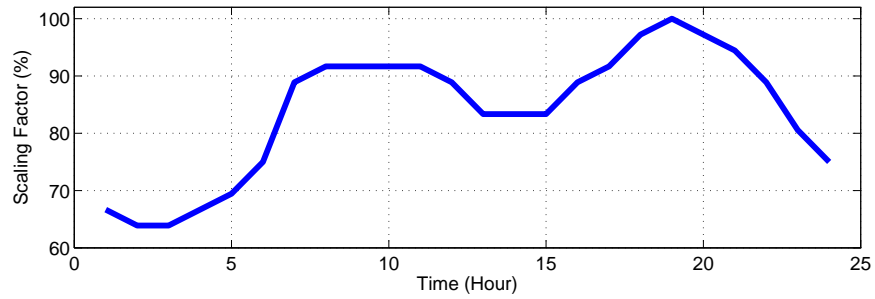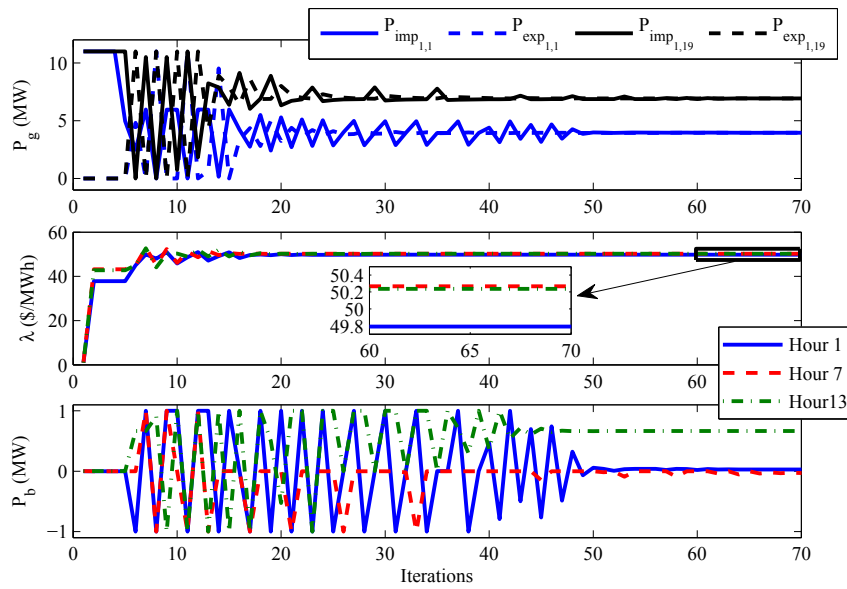| Case	$P_b^m(MW)$	$P_b^M(MW)$	$E_b^M(MWh)$	$SOC_1(\%)$
Base Case	0	0	0	0
Case 1	-1	1	2	50
Case 2	-1	1	10	50
Case 3	-10	10	20	50
Case 4	-4	4	40	50
Case 5	-4	4	20	50
Case 6	-4	4	10	50
Case 7	-4	4	4	50

Figure 5.7. 24-hour demand scaling factor.

Figure 5.8. Results of multi-horizon subgradient method with no reserve. a) power import by utility and power export by community, b) community nodal price, c) community battery charging power.

Fig. 5.9 illustrates the results of multi-horizon LUBS method at different hours $t \in \{1, 7, 13, 19\}$ through iterations for case 1. The algorithm converges to the optimal solution in just 27 iterations, less than subgradient method. The battery charging power as well as the nodal prices are exactly same as the results of the previous method. The advantage of multi-horizon LUBS method against subgradient method is the fact that the optimality of the results can be tested through duality gap in LUBS method. Fig. 5.15 depicts the lowerbound and upperbound computed in LUBS method through iterations for the first case. The convergence of these two parameters which leads to zero duality gap guarantees the optimality of the solution sought.
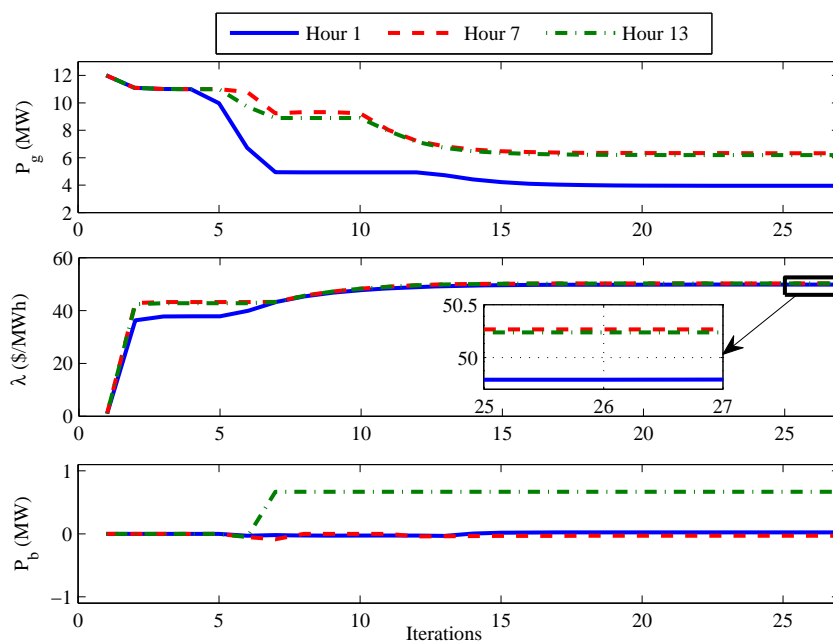

Figure 5.9. Results of multi-horizon LUBS method with no reserve. a) power import by utility and power export by community, b) community nodal price, c) community battery charging power.

5.5.1.2 With Reserve Requirement

To test the efficiency of both algorithm in the cases with reserve requirements, the system is assumed to guarantee a reserve level equal to 7 MW at each hour. The maximum limit of reserve for all generations can be found in Table 5.1. The battery system is also able to offer its free power capacity as reserve. Fig. 5.12 depicts power import and export values for $t \in \{1, 19\}$ as
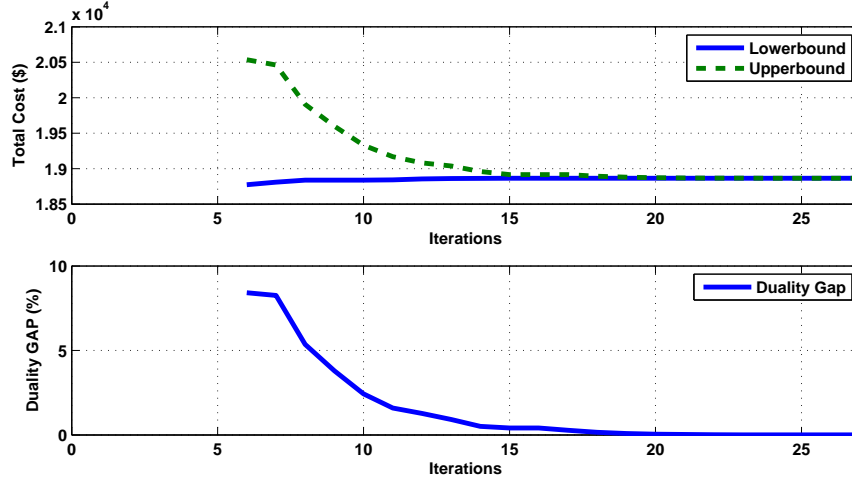
Figure 5.10. Convergence indices of multi-horizon LUBS without reserve.

well as community nodal price and battery charging power at $t \in \{1, 7, 13, 19\}$ obtained through multi-horizon subgradient method. The results illustrates the algorithm converges to the optimal solution in 90 iterations. As expected, the power import and export levels are finally equal at each hour. As shown in Fig. 5.12, the algorithm guarantees the reserve required at different hours.

According to the reserve signals and its price values, the reserve constraints binds only at $t = 19$ with a price equal to $\mu_r = \$0.53/MW$.

The results of power output of the community, energy price and battery charging power corresponding to multi-horizon LUBS method are proposed in Fig. 5.13 which shows the convergence of the algorithm in 28 iteration. As illustrated in Fig. 5.14, the reserve constraint only binds at $t = 19$ with a reserve price equal to $\$0.55/MW$.

5.5.2 Moving Horizon Simulation

Since the uncertainty of the renewable systems and demand profile is a function of time, instead of running the algorithms once for the day ahead, it is more accurate to run them in a moving-horizon fashion. Therefore, the multi-horizon problem is solved for the entire horizon at each hour. After the problem is solved, the solutions for the most immediate horizon (first hour) are used to set the generation and battery charging power levels. These values are valid until the next hour when the next multi-horizon problem is solved.
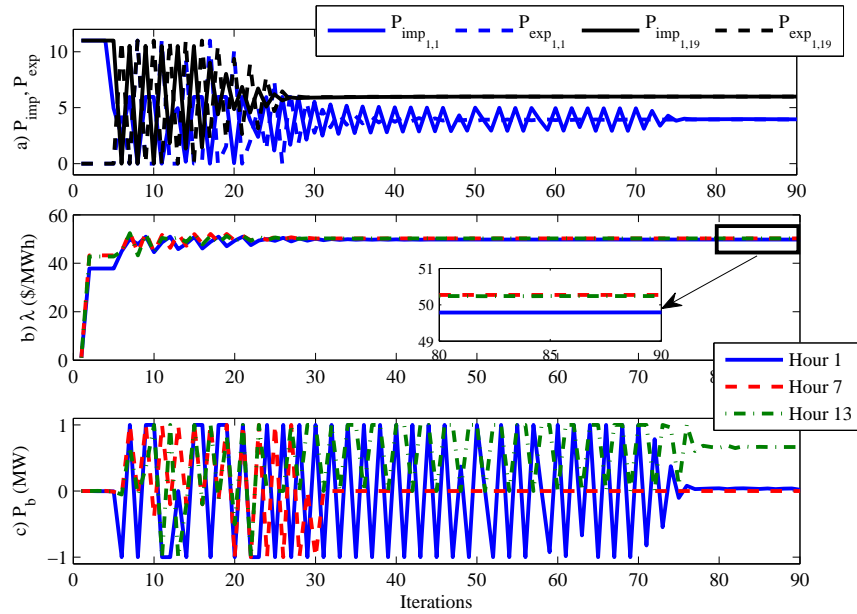
Figure 5.11. Results of multi-horizon subgradient method with reserve. a) power import by utility and power export by community, b) community nodal price, c) community battery charging power.
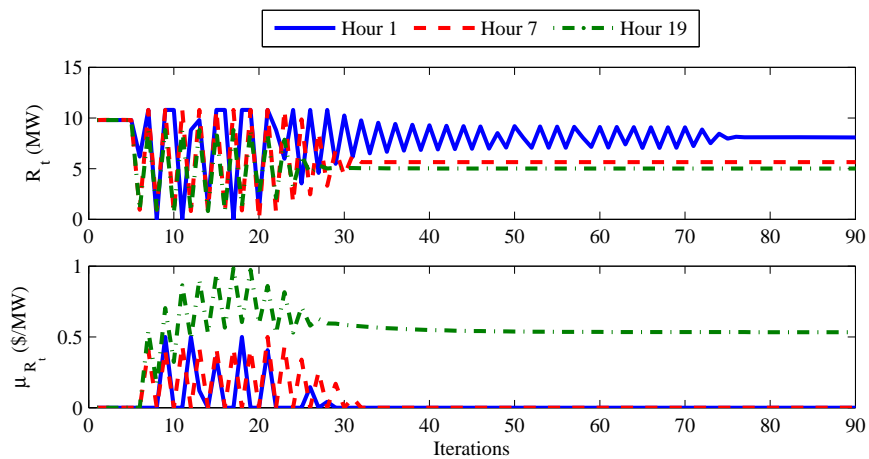

Figure 5.12. Reserve market results of multi-horizon subgradient method with reserve. a) total reserve available, b) reserve price.
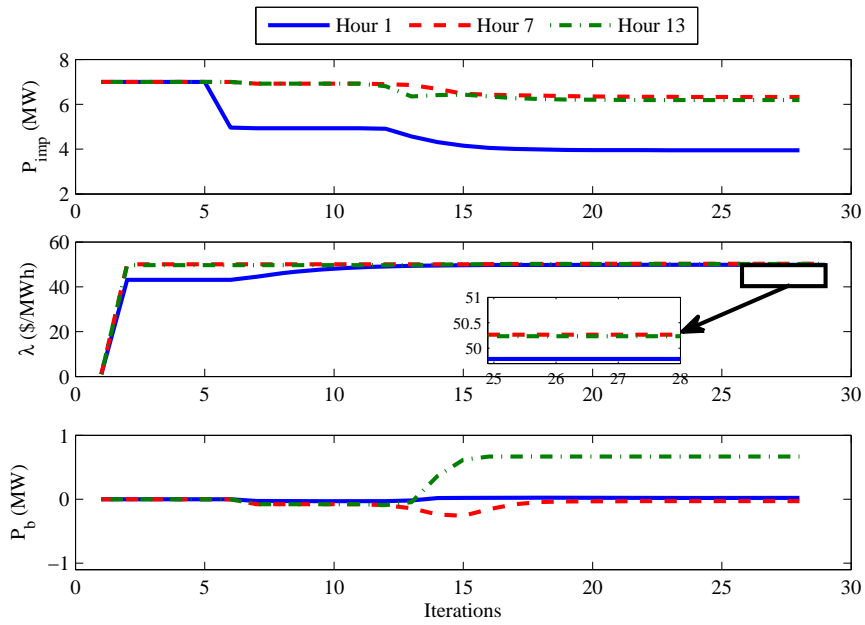
Figure 5.13. Results of multi-horizon LUBS method with reserve. a) power import by utility and power export by community, b) community nodal price, c) community battery charging power.
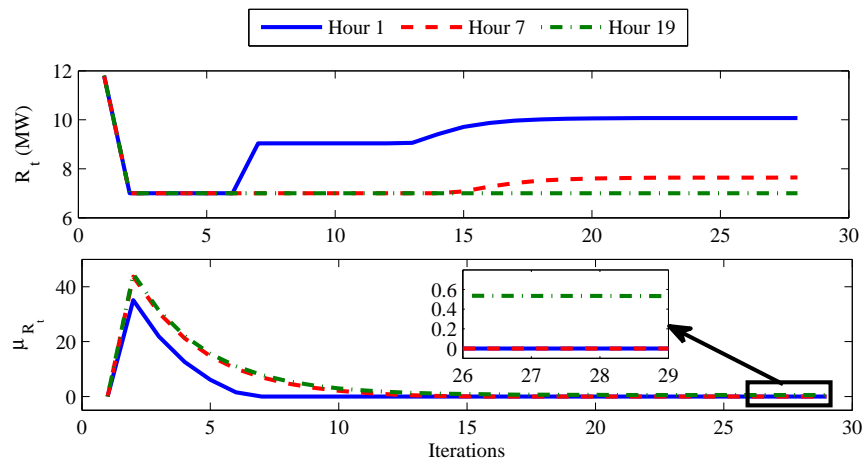

Figure 5.14. Reserve market results of multi-horizon LUBS method with reserve. a) total reserve available, b) reserve price.
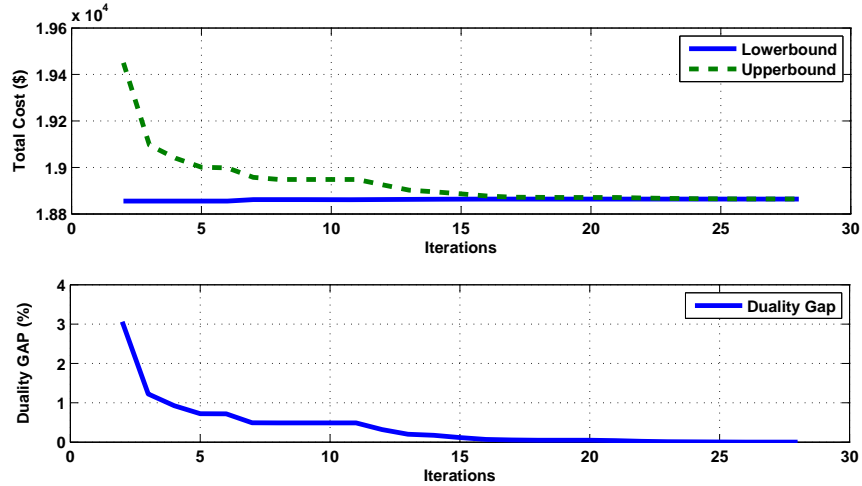
Figure 5.15. Convergence indices of multi-horizon LUBS with reserve.

Employing moving-horizon technique mitigates the prediction error of demand profile and renewable generation by updating the predictions every hour, which finally leads to less total cost of the system. The only concern about this method is the convergence speed of the algorithms as the problem must be solved within one hour instead of 24 hours. To improve the converge speed, the initial condition of each simulation are set on the final results of the previous simulation, as explained above.

For this case study, 24 consecutive moving-horizon simulations have been performed using both algorithms. Simulation of both algorithms using moving-horizon technique demonstrates that every run of LUBS method converges in 10 iterations (100 seconds) and every run of subgradient method is final in 30 iteration (3 minutes) to satisfy all convergence criteria. Both methods are proved to be fast enough to be practiced in hour-by-hour moving-horizon simulation.

5.5.2.1   Configuration 1: Single Microgrid

This study has been performed on the network shown in Fig. 5.6, which includes only one microgrid on the bus 50. The characteristics of the microgrid's energy storage system is based on the case 1 as provided in Table 6.1. A comparison of iteration behavior of community power export (P_{exp}) and utility import power (P_{imp}) is depicted in Fig. 5.16 where each iteration is assumed to

take 2 minutes for more clear presentation. For a closer look on the behavior of the power level signal through iterations, a 2-hour period is highlighted in Fig. 5.16-c. The community nodal price signals for both algorithms are shown in Fig. 5.17. To demonstrate that the results of both algorithms match each other and to compare the dynamic behavior of the price signals, a 2-hour frame of both results are shown in Fig. 5.17-c. As expected, the energy price profile follows the trend of the daily demand profile which demonstrates the accuracy of the simulation results. Also, according to the results depicted in Figs. 5.16-5.17, the results corresponding to LUBS method shows smoother and faster convergence to the optimal solution than those of subgradient method.
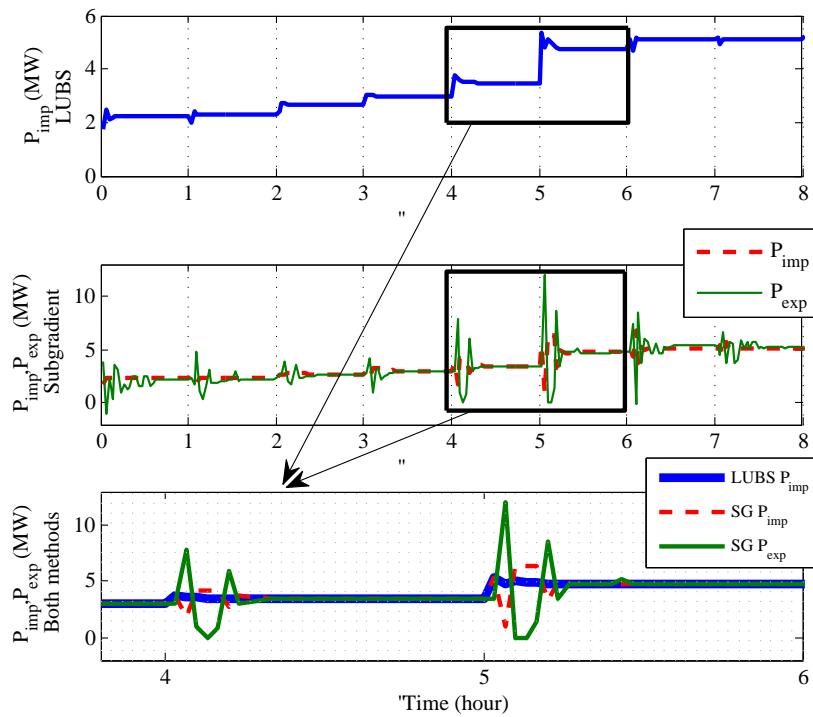

Figure 5.16. Comparison of dynamic behavior of community power export and utility import levels in LUBS and subgradient for 8 consecutive moving-horizon simulations for configuration 1. a) P_{imp} of utility in LUBS method for the first 8 hours, b) P_{imp} and P_{exp} in subgradient method for the first 8 hours, c) a closer look on P_{imp} and P_{exp} in both methods during a two-hour horizon.

Fig. 5.18 also shows the iteration of generator active and reactive power outputs as well as battery charging power and stored energy for the community during the 24-hour period. The active
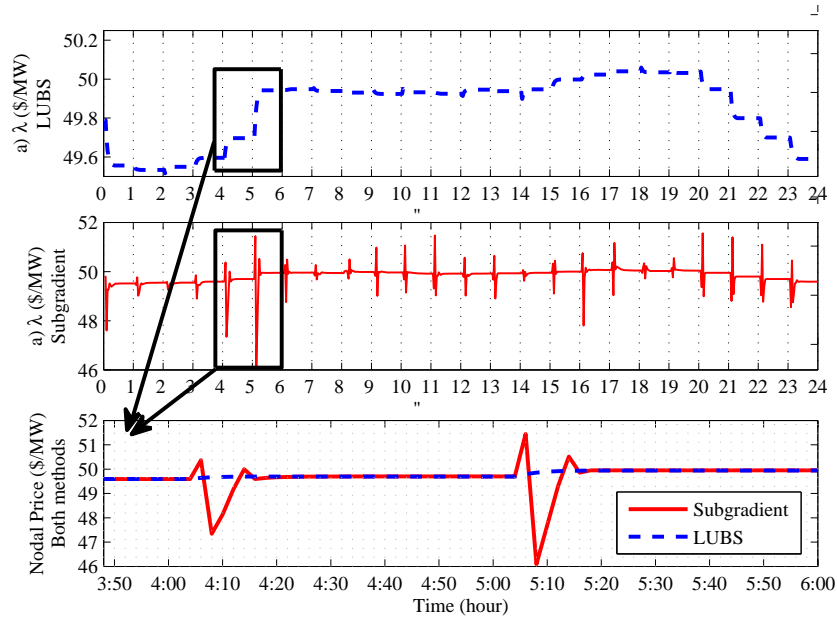
Figure 5.17. Comparison of community nodal price behavior through iterations in LUBS and sub-gradient for 24 consecutive moving-horizon simulations for configuration 1. a) λ in LUBS method throughout an entire day, b) λ in subgradient method throughout an entire day, c) a closer look on λ in both methods during a two-hour horizon.

and reactive power profiles associated with the utility's generation unit on bus 4 are depicted in Fig. 5.19.

Similar to the nodal price profile, the daily profile of all these signals follows the demand profile, too. Higher demand is expected to result in higher nodal price, higher energy generation by either utility's or community's generation units and less battery charging power.

Fig. 5.20-5.21 also show the iteration behavior of total reserve available in entire network and reserve price through both methods for 8 consecutive moving-horizon simulations, including a 2-hour frame of such signals to demonstrate the accuracy of the results and dynamic behavior comparison.

As shown in these figures, both algorithms show faster convergence to the ultimate solutions in less iterations than in multi-horizon algorithm with random initial values. That is, the initialization technique has reduced the number of iterations in both algorithms to 10 iterations which is a good achievement for suitability of such algorithms to be practiced for real world scenarios. Moreover,
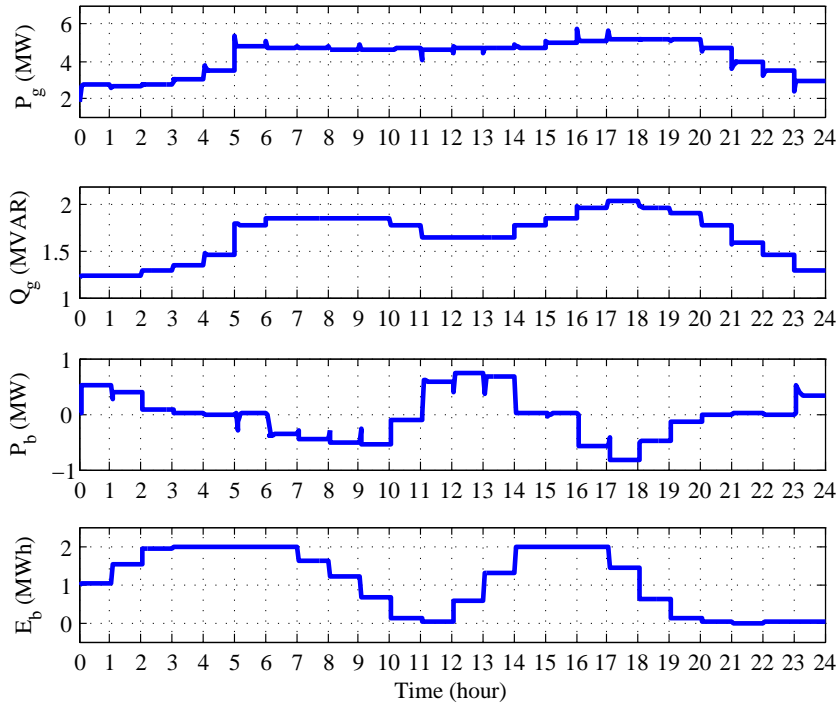
100

Figure 5.18. Community's operation parameters during 24 consecutive moving-horizon simulation for configuration 1. a) active power output of generator, b) reactive power output of generator, c) charging power of battery, d) energy stored in battery.
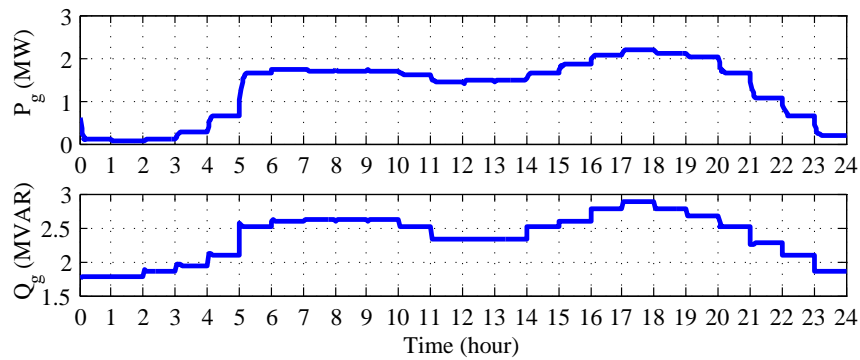

Figure 5.19. Utility's operation parameters during 24 consecutive moving-horizon simulation for configuration 1. a) active power output of generator, b) reactive power output of generator.
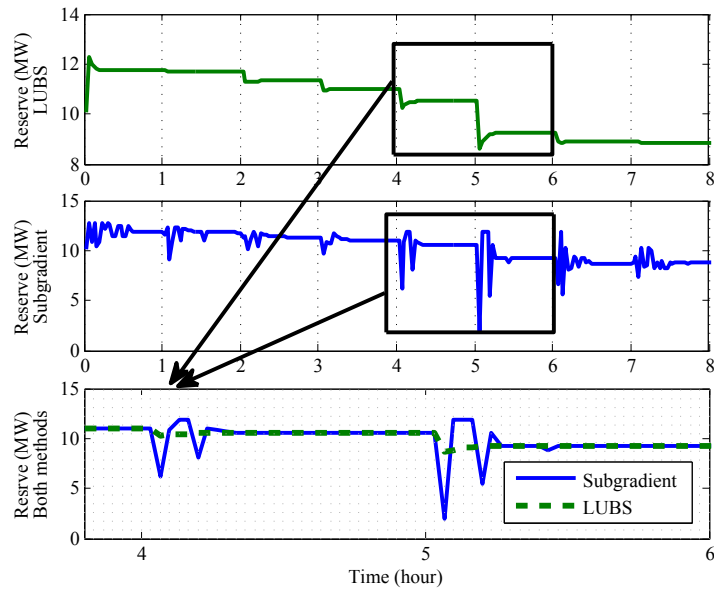
Figure 5.20. Comparison of dynamic behavior of total network reserve in LUBS and subgradient for 8 consecutive moving-horizon simulations for configuration 1. a) total reserve in LUBS method, b) total reserve in subgradient method, c) a closer look on total reserve in both methods during a two-hour horizon.
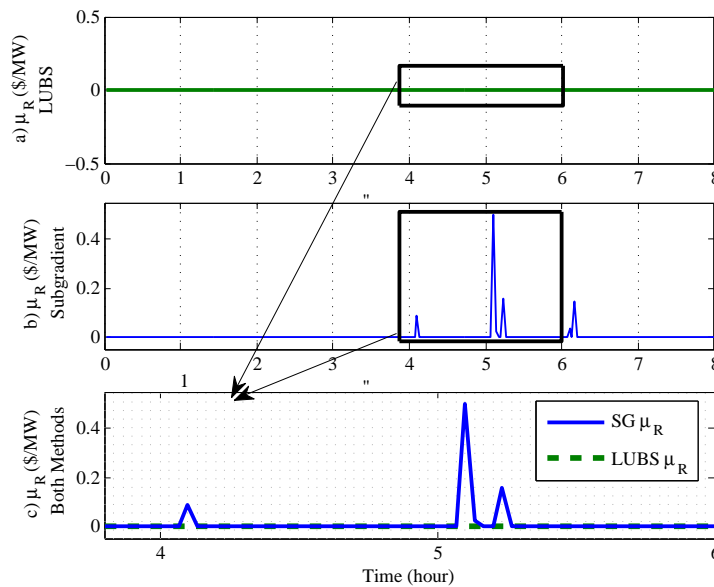

Figure 5.21. Comparison of reserve price behavior through iterations in LUBS and subgradient for 8 consecutive moving-horizon simulations for configuration 1. a) μ_R in LUBS method throughout an entire day, b) μ_R in subgradient method throughout an entire day, c) a closer look on μ_R in both methods during a two-hour horizon.

the LUBS method results in smoother and faster transition from initial values to the final value compared to the subgradient method.

5.5.2.2 Configuration 2: Three Microgrids

To demonstrate the scalability of the algorithm, another case study with three microgrids, as shown in Fig. 5.22, is performed using both algorithms. The parameters associated with the case 1 in Table 6.1 is considered for the sizing of the energy storage systems of the microgrids.
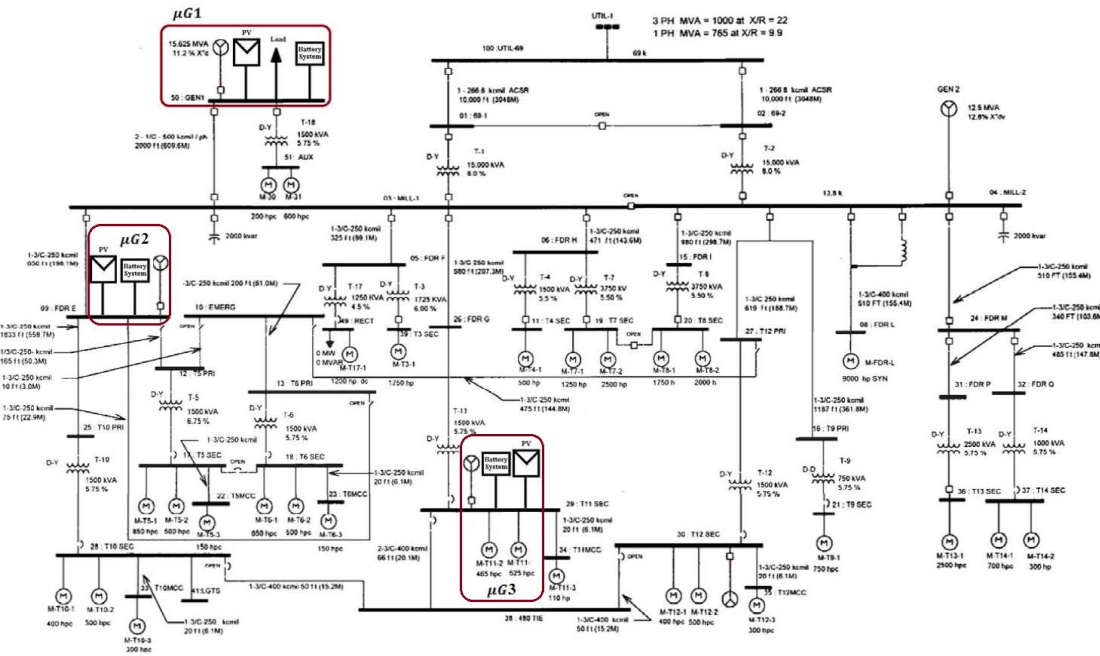

Figure 5.22. IEEE standard test feeder with three interconnected microgrids.

As expected , the results of both algorithms comply with each other and converge to the optimal solution. Fig. 5.23 illustrates the community 2's power export and utility's power import from this community through both methods. Similar to the single agent case study, a closer look over the results is provided in Fig. 5.23-c. The community nodal price signals of community 2 for both algorithms are shown in Fig. 5.24.

Fig. 5.25 also shows the iteration of generator active and reactive power outputs as well as battery charging power of the community 2 during the 8-hour period.
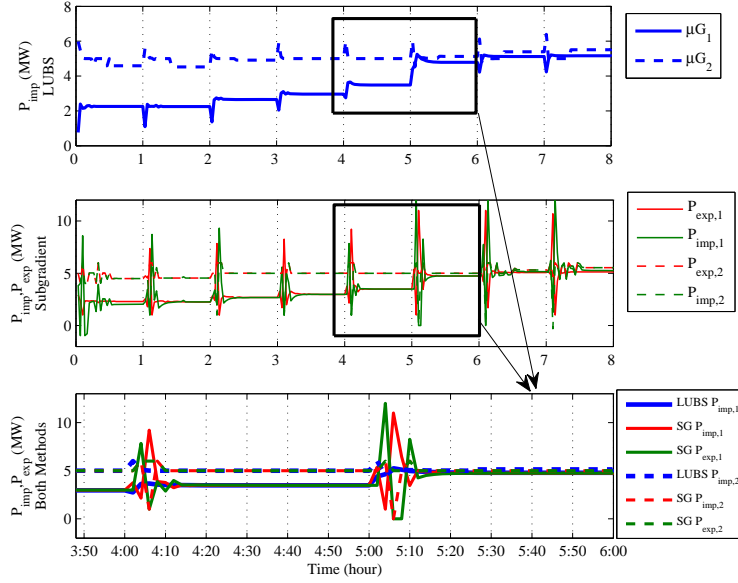
Figure 5.23. Comparison of dynamic behavior of community power export and utility import levels in LUBS and subgradient for 8 consecutive moving-horizon simulations for configuration 2. a) P_{imp} of utility in LUBS method for the first 8 hours, b) P_{imp} and P_{exp} in subgradient method for the first 8 hours, c) a closer look on P_{imp} and P_{exp} in both methods during a two-hour horizon.
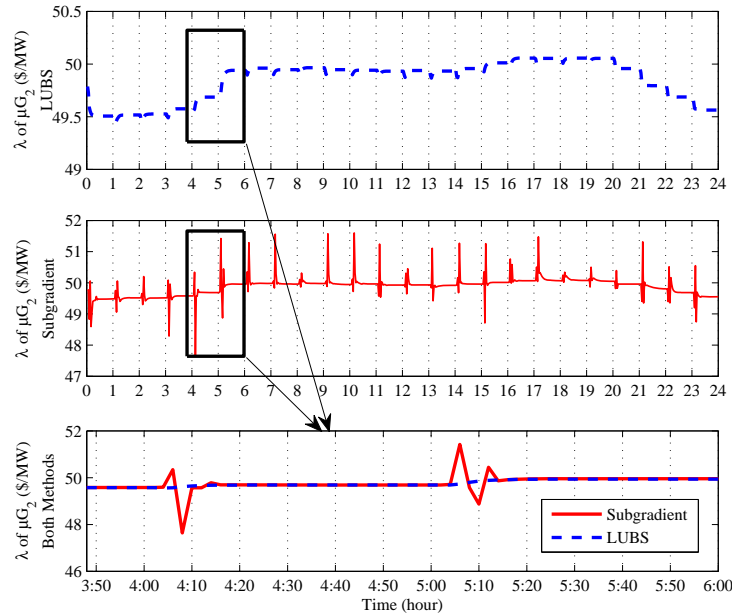

Figure 5.24. Comparison of community nodal price behavior through iterations in LUBS and subgradient for 24 consecutive moving-horizon simulations for configuration 2. a) λ in LUBS method throughout an entire day, b) λ in subgradient method throughout an entire day, c) a closer look on λ in both methods during a two-hour horizon.
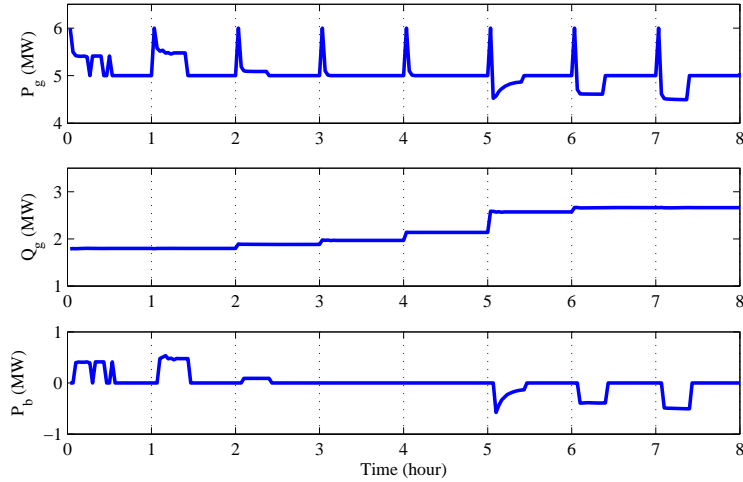
Figure 5.25. Community's operation parameters during 24 consecutive moving-horizon simulation for configuration 2. a) active power output of generator, b) reactive power output of generator, c) charging power of battery.

Due to low marginal price of community 2's generation unit, it is always dispatched for the entire horizon. Therefore, the charging power of the battery converges to zero for the entire horizon regarding the update process defined in (5.19)-(5.18).

The iteration behavior of total reserve available in the network for 8 consecutive hours is also shown in Fig. 5.26. Compared to the results illustrated in Fig. 5.20, it is obvious that more reserve is expected to be provided in the case 2 due to more energy storage systems in the entire grid.

5.5.3 Sensitivity Analysis Results

5.5.3.1 Results of Energy Market Sensitivity to Battery Size

Fig. 5.27 depicts the final results of multi-horizon subgradient method for different cases with distinct power/energy ratings of the battery. In the base case where there is no battery involved in the optimization problem, the results converge to the MATPOWER OPF results and the profile of community nodal price follows the system demand profile at different hours. As expected, the profile of battery charging power has a reverse dependency to the nodal price, which results in taking advantage of energy storage system in the network. One of the main outcomes of applying energy storage systems in a power network is to distribute the power demand evenly between
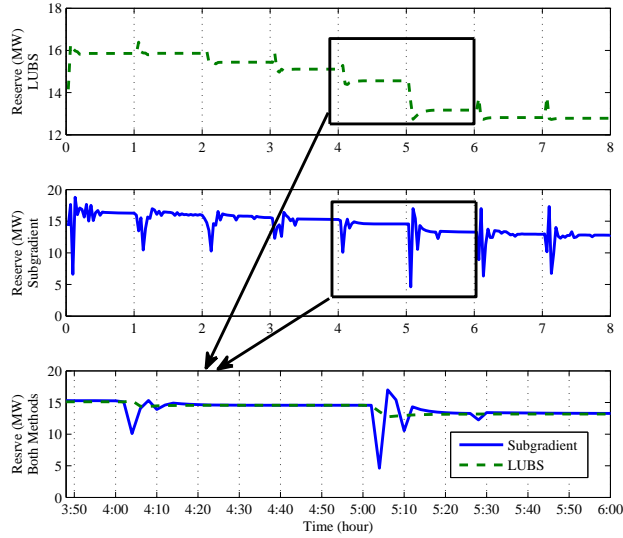
105

Figure 5.26. Comparison of dynamic behavior of total network reserve in LUBS and subgradient for 8 consecutive moving-horizon simulations for configuration 2. a) total reserve in LUBS method, b) total reserve in subgradient method, c) a closer look on total reserve in both methods during a two-hour horizon.

different hours, which can be identified by unified nodal prices. As seen in Fig. 5.27, increasing the battery ratings leads to flatter profile for community nodal price. The fourth case is designated to show an extreme case of battery rating leading to a completely flat price profile.

The effects of battery power/energy ratings on nodal prices and battery charging power profile are also tested through multi-horizon LUBS algorithm, the results of which are shown in 5.28. These results confirm the results obtained from multi-horizon subgradient method.

According to the results, battery size has significant effects on power profiles and nodal prices such that increasing the battery size results in flatter generation power and nodal price profiles.

5.5.3.2   Results of Reserve Market Sensitivity to Battery Size

Fig. 5.29 illustrates battery charging power, nodal price, reserve provided and reserve price for cases 1-4 when a 7-MW reserve required. As expected, higher battery size in case 4 results in more flexible operation of the system and a completely flat nodal price compared to the other cases where size of battery is more constrained. According to the results, nodal price is also very sensitive to battery energy rating where the nodal price in case 4 is flatter than that in case 3
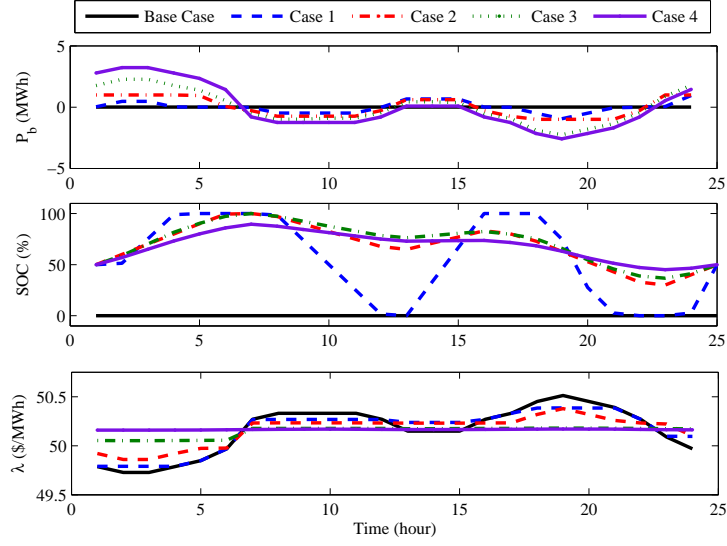
106

Figure 5.27. Final results of multi-horizon subgradient method for different ratings of battery. a) battery power output, b) battery SOC, c) community nodal price.
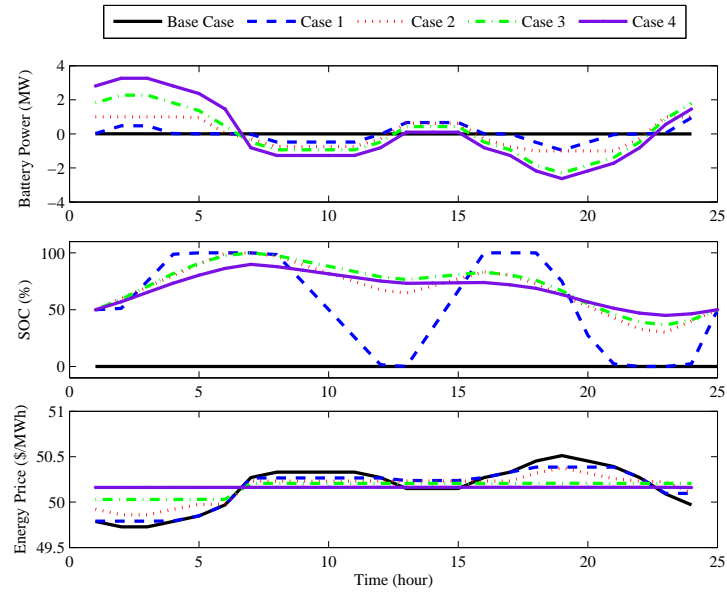

Figure 5.28. Final results of multi-horizon LUBS method for different ratings of battery. a) battery power output, b) battery SOC, c) community nodal price.

because of higher energy rating in spite of lower power limit in this case. It is also seen from Fig. 5.29 that increasing battery size allows the battery to offer higher level of reserve to the system and therefore less reserve price if its constraint binds. Reserve availability is shown to be more sensitive to battery power rating than to its energy limit.
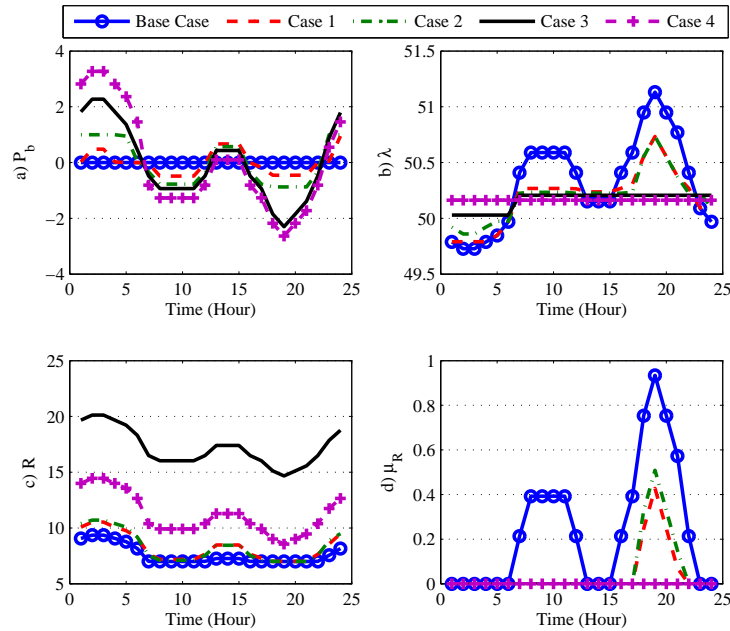
Figure 5.29. Sensitivity versus battery size. a) battery charging power, b) nodal price, c) reserve availability, d) reserve price.

Regarding the interesting impacts of energy rating of the battery on available reserve and reserve price, the sensitivity of these parameters versus battery energy level is also studied. Fig. 5.30 illustrates the sensitivity of reserve level and its price versus energy rating of battery. As depicted in Fig. 5.30-a, reserve availability at off-peak hours is higher in the cases where the energy limit of battery is higher. At peak hours, the reserve level does not change because the system is forced to maintain a specific level of reserve (10.5 MW) at any time, but it has an effect on reserve price which is shown in Fig. 5.30-b. The reserve price is non-zero only at hours when the reserve is set on the required value. As stated in the previous section, when battery has higher energy rating, discharging the battery with higher power level reduces the reserve provided by the battery more and causes the system to force the other generators to provide more reserve, which leads to

higher reserve price. The effect of reserve price on nodal prices is shown in Fig. 5.30-c, where the nodal price with and without reserve requirements are shown. For all cases, the difference between the nodal price with and without reserve is exactly equal to corresponding reserve price. It is also possible to extract the effect of battery energy constraints on nodal price by subtracting nodal price in case 4 (which is a flat line) from that in the other cases, as shown in Fig. 5.30-d. The value of μ_B^+ is summation of the Lagrange multipliers of battery power and energy limits, where μ_B^- is related to the lower limit constraints. In the cases 4-7 none of the power rating constraint binds, so the values of μ_B^+ and μ_B^- just include the multiplier of energy constraints. Since these two variables cannot take a nonzero value at the same time and none of them can be negative, any positive value of $\mu_B^+ - \mu_B^-$ is equal to μ_B^+ and any negative value defines $-\mu_B^-$. These values as well as reserve price are illustrated in Fig. 5.31 for all four cases. It is obvious in these figures that increasing energy rating of battery reduces the effects its size limits on nodal price but increases the reserve price in the system.
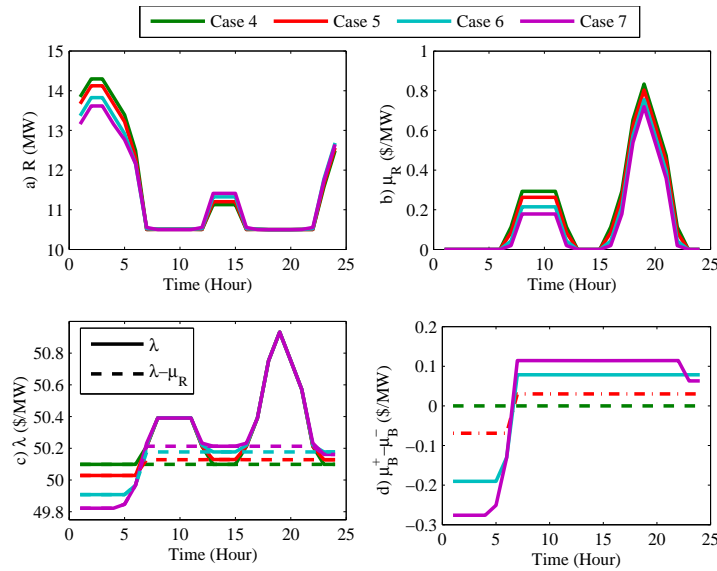

Figure 5.30. Sensitivity versus battery energy rating. a) available reserve, b) reserve price, c) nodal energy price with (solid) and without (dashed) reserve requirement, d) shadow prices of battery constraints on nodal energy price.
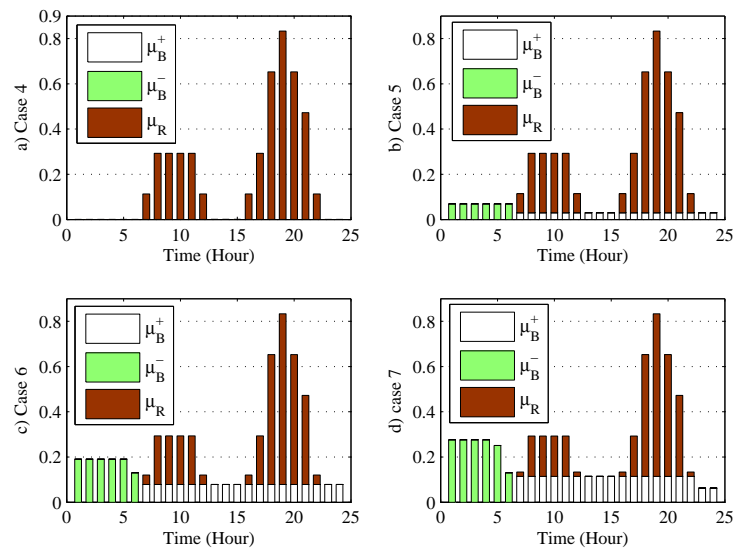
Figure 5.31. Comparison of shadow prices of battery constraints and reserve constraints for different energy ratings of battery.

CHAPTER 6

MODEL PREDICTIVE CONTROL OF MODULAR MULTILEVEL CONVERTER

6.1 Introduction

Modular Multilevel Converter (MMC) is reported in the literature as the most promising topology proposed for Voltage Source Converters (VSC) due to its salient characteristics such as scalability and modularity [57, 58, 59, 60, 61, 62, 63].

Several switching methods have been proposed for MMC. The popularly used schemes are based on Sinusoidal Pulse Width Modulation (SPWM) which defines the number of switches that must be trigged in the lower arm and the upper arm of all phases by comparing the sinusoidal reference waveforms with a set of high-frequency carrier waveforms with different dc off shifts [64, 65, 66, 67]. SPWM is popular for its simplicity of implementation. However it cannot handle the circulating currents in the converter bridges.

In a two-level VSC, the switching scheme is the output of PWM which is directly applied to the gates of IGBTs. However, in MMC, higher number of submodules on each arm makes the switching algorithm more complicated. PWM is the most widely used method for MMC as well. The main objective in MMC's PWM switching is to define the number of submodules to be turned-on on each arm at switching time using higher number of carriers instead of just one. Having the number of submodules known, the capacitor voltages and the direction of current on each arm define the arrangement of the submodules to be on or off.

In SPWM switching method, the comparison of the sinusoidal reference waveforms with the multi-carrier triangular waveforms defines how many submodules are required to be switched on on each arm. Then, the switching algorithm sorts the submodules based on their capacitor voltages, either in ascending or descending order according to the direction of the corresponding arm. Since,

the total voltage of submodules selected are not necessarily equal for all bridges, the currents flowing through the bridges is prone to have some unbalanced components. This unbalanced component, which is address as circulating current, increases the converter loss and mandates higher ratings for power electronic switches [68, 69, 57, 70]. Therefore, mitigation of circulating current is highly desired in MMC switching and control design.

Although SPWM switching method can be simply implemented for MMC applications, it cannot address the issue of circulating current. Therefore, several PWM-based algorithms are introduced in the literature. The main idea of all these algorithms is to appropriately change either the sinusoidal reference waveforms or multi-carrier triangular waveforms. Phase-shifted Carrier PWM (PSPWM) is the method widely used for circulating current mitigation, which shifts the phase of the sinusoidal reference waveforms to regulate the capacitor voltages and to mitigate the circulating current simultaneously [71, 72, 73]. This switching scheme changes the the upper and lower arms' modulation signals to obtain the capability of dynamically adjusting the capacitor voltages. However, the method causes more harmonics in the arm current, changes the characteristics of circulating current, and may get unstable. Therefore, it is valid only to a limited extent [74]. The other method which is proposed for circulating current mitigation is Phase-disposition PWM (PDPWM) [74]. This method, instead of changing the reference waveform, makes changes to the carrier waveforms to increase the stability of the control method while mitigating the circulating current and capacitor voltage deviation [74]. Several other works have been also proposed in the literature to address the circulating current issue by adding additional components to the current reference waveforms. It has been shown in the literature that circulating current has has a dc component and a second-order frequency component at steady state [75, 76]. Eliminating the second-order component needs a proportional-resonance (PR) controller. A strategy for MMC circulating current suppression using PR controller has been presented in [69]. In [68], a control strategy has been developed to convert the ac component of circulating current into dc signal through acb/dq transform to mitigate the circulating current. Recently, an integrated MMC control is proposed in [70], which includes the conventional vector control (outer PQ control, inner line current control), circulating current mitigation control, phase-shifted PWM scheme, and submodule voltage balancing block.

Along with the research works on improving MMC switching control using PWM technique, there is another thread of research focusing on model predictive control as a solution to this problem [57, 77]. In these research works, the MMC switching problem is modeled as an optimization problem with specific objective functions such as following the reference ac current, circulating current suppression, and capacitor voltage regulation. The decision variables in MPC control method are the binary variables indicating the status of each submodules at each switching time step. Simultaneous regulation of submodule capacitor voltages and elemination/minimization of the circulating current flowing through three phases of the converter is still one of the technical challenges associated with MMC application due to their mutual effects. Circulating current, in fact, not only is a function of the capacitor voltages of the submodules turned on at each time step, but also determines how the capacitor voltages of the same submodules change until the next switching time step arrives, which may lower the efficiency of the converter and cause more ripples in the capacitor voltages if it is not well suppressed. However, it should be noted that the circulating current is a useful mean to balance the energies between all six arms in situations where some energy unbalance are caused by asymmetric operations and fault situations and tolerances of the components [78].

The method proposed in [57] compares all possible switching combinations for the MMC switches in one bridge for their predicted performance one step ahead. This method requires significant computing effort. At each time step with the step size defined by the switching frequency, e.g. 100 μs for 10 kHz, the solution must be sought. For a 5-level MMC, there are 8 submodules in each bridge. Among the eight submodules, four submodules should be turned on to keep the dc-link voltage constant. Therefore, the number of the combination is $C_8^4 = 70$. The algorithm needs to check 70 possible on/off sequences and find the best one. For a 13-level MMC, C_{24}^{12}, or 2.7 million combinations should be checked. For a 16-level MMC, 155 million combinations should be checked.

In [77], a one-step model predictive control has been proposed. The proposed method aims to track the ac reference currents and eliminate the circulating currents. Based on the two objectives, the optimal upper-arm voltage and lower-arm voltage for a MMC bridge can be found. Based on

the desired voltage level, capacitor voltages are sorted in order. When the arm current is positive, the capacitors with lowest voltages will be switched on to get charged. When the arm current is negative, the capacitors with the highest voltages will be switched off to get discharged. This method requires only sorting algorithms, which makes it efficient for MMCs with a large number of submodules.

The disadvantage of the above algorithm is its omission of the dc-voltage constraint. The number of submodules to be switched on is required to be fixed in PWM scheme and the MPC scheme proposed in [57]. In order to take this constraint into account, a mathematical programming problem is formulated and solved using heuristic way. In many papers, commercial solvers such as CPLEX are employed to solve MIP problems [79, 80]. However, for this power electronics application, it is not feasible to employ a commercial solver. Firstly, the switching scheme will be programmed in a chip. It is not possible to have a commercial solver on a chip. Secondly, commercial solvers use general methods to solve optimization problems. In many cases, CPLEX has convergence issues due to its adoption of enumeration. For special optimization problems, a specific solving method will achieve much faster solving speed than a commercial solver.

In this chapter, the mathematical model of MPC-based (n+1)-level MMC, which has n submodules at each arm, is proposed in order to track ac reference current, mitigate circulating current and to keep capacitor voltage nominal subject to selection of exactly n submodules to be trigged at each arm. The multi-objective optimization problem is then reformulated to a new model and the weighting sum method is employed to merge the objectives. To solve such problem, two algorithms are represented to seek the optimal solution for switching pattern. The first search algorithm design remarkably reduces the size of feasible solution to n instead of C_{2n}^n, but the simulation results shows that it has serious drawbacks in satisfying the objectives of MPC, which has led the authors to an alternative algorithm for better performance while maintaining the computation advantages. The second algorithm is developed by applying a relaxation on the constraint of number of switched-on submodules and increases the size of the feasible set to n^2, which introduces additional computation burden compared the first algorithm especially for high values of n. However, it is proved in this chapter that this size can be cut down to 4 if appropriate weighting factors are selected

and checking just 4 of the solutions is enough to find the optimal solution. The efficiency of the algorithms are finally tested via simulations in MATLAB SimPowerSystems.

6.2 MMC Background

6.2.1 System Topology

Fig. 6.1 shows a simplified scheme for a three-phase MMC. At each phase of A, B, or C, there are two groups of switches on upper and lower arms. Fig. 6.2 shows the structure of each arm of a 7-level MMC. Each arm consists of 6 submodules (SM) each of which has two IGBT switches and a capacitor. There are two inductors in each phase in order to provide current control and limit the fault currents. The voltage of each submodule is either equal to its capacitor voltage $V_{C,i}$ or zero depending on the states of the two switches. Table 6.1 lists the submodule output voltage. The on/off states of the two switches of a submodule are always opposite to each other. The total voltage of one arm will be the sum of its submodules' voltages and the voltage across the inductor.
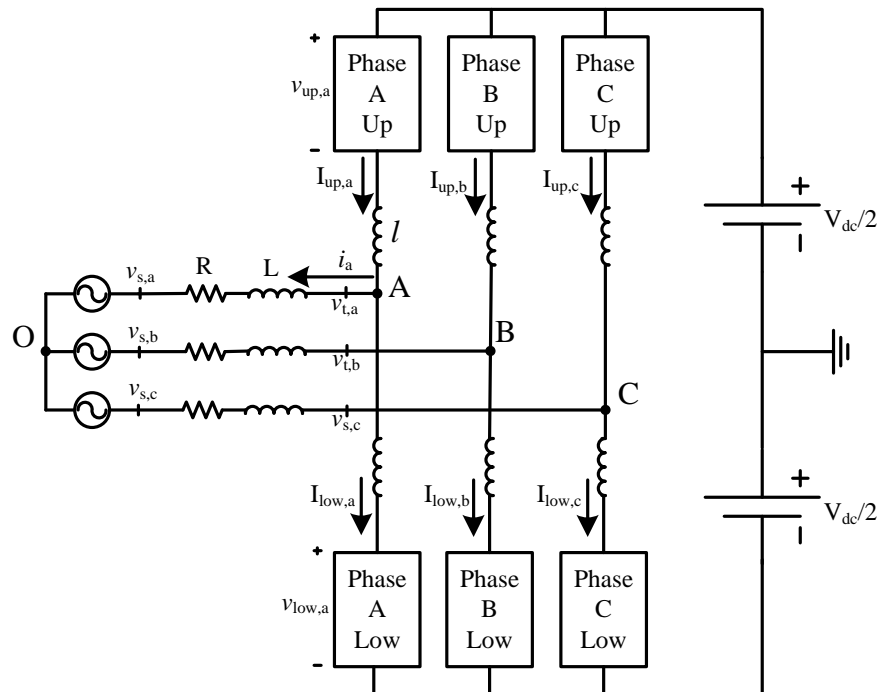

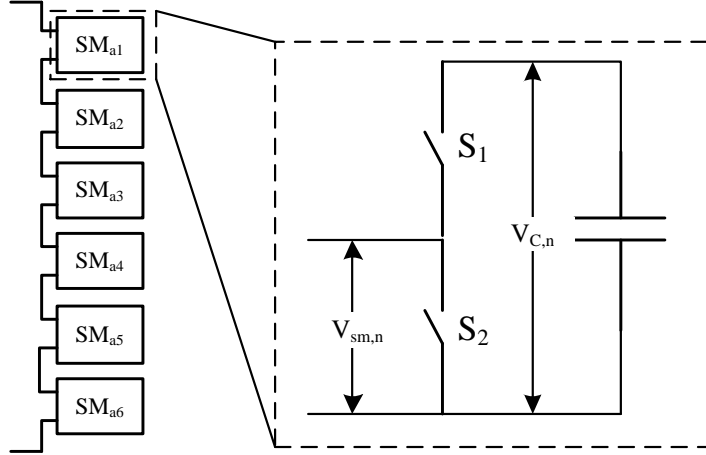Figure 6.1. Simplified scheme of a multilevel modular converter.

Figure 6.2. The structure of MMC submodules.

Table 6.1. Submodule parameters for different states.

State	$S1$	$S2$	V_{SM}
$0(inactive)$	OFF	ON	0
$1(active)$	ON	OFF	V_C

6.2.2 PWM Control Strategy

6.2.2.1 AC Side Voltage Control & Command Signal Generation

SPWM is the conventional switching method to synthesize a multilevel waveform at the ac-side of the converter[101]. To operate an n-level MMC, this method, each phase requires $n + 1$ carrier waveforms which are displaced symmetrically with respect to the zero-axis [102], as shown waveforms in Fig. 6.3 as the sawtooth. Fig. 6.3 illustrates the comparison of the reference waveform and the carrier waveforms for phase a. Note that a *third order* harmonic is injected to the reference waveform to enhance the linear operating rang of PWM. The magnitude of the third harmonic is as much as $\frac{1}{6}$ of the fundamental frequency magnitude to get the maximal ac-side voltage [77].

The ac voltage v_{ta} is defined by the voltage on the lower arm $v_{low,a}$. This voltage is derived by the number of submodules in the lower arm which are switched on. Fig. 6.4 is the comparison results of two signals depicted in Fig. 6.3. The output of the comparison (N_{low}) defines the number of the submodules to be switched on. In any PWM switching method, the value of N_{low} defines
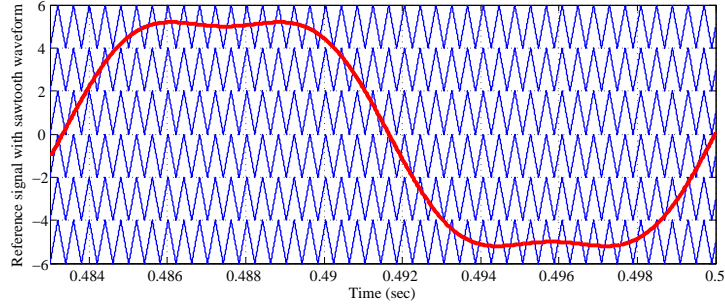
116

Figure 6.3. Reference and carrier waveforms of a 7-level MMC.

how many submodules must be switched on on the lower arm and $n - N_{low}$ determines the number
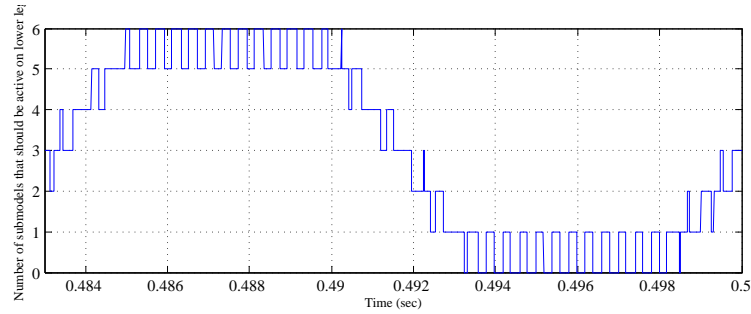of active submodules on the upper arm.

Figure 6.4. The number of active submodules in the lower arm.

6.2.2.2 Capacitor Voltage Regulation in PWM

To regulate the capacity voltage over the switching of MMC, the sequence of active submodules
must be selected wisely. For this purpose, reducing higher capacitor voltages and increasing lower
ones are desired. If the arm current is positive, the capacitors of the active submodules are expected
to be charged; when the arm current is negative, they are expected to be discharged. Therefore, it
is better to switch on the submodules with lowest capacitor voltages if the arm current is positive,
and to activate the submodules with highest capacitor voltages when the arm current is negative.
Fig. 6.5 is a block diagram showing the algorithm of selecting submodules and generating gate
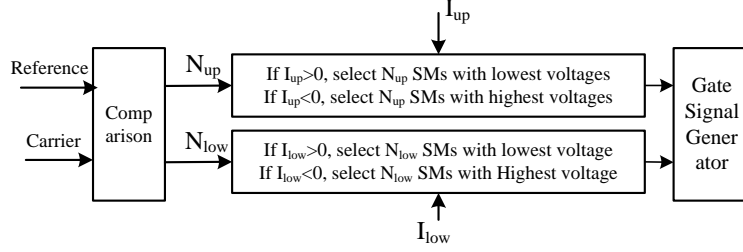driving signal generation.

117

Figure 6.5. Block diagram of the per-phase gate signal generation.

6.2.3 Definition of Circulating Current for MMC

The concept of circulating current is always one of the concerns is circuit analysis when two or more branches with different voltage levels are connected in a parallel way. This parameter does not show up while dealing with a two-level VSC with a single capacitor since the voltage over all the branches are equal at any time. In contrary, since the DC link is distributed between the submodules in terms of small capacitors, difference between the voltages over the parallel branches (phases) may cause unbalanced currents through the branches which is the source of circulating current.

Circulating currents hold such a name because they circulate within the converter circuit and have no effect on the currents on DC or AC side. High values of the circulating current has been claimed in the literature [57] to have two major effects on the converter: 1) it increase the loss of the system; 2) it makes the converter consist of higher-rate IGBTs, capacitors, and inductances.

Although Circulating current is defined in the literature as,

$$i_z = \frac{i_{up} + i_{low}}{2} - \frac{i_{dc}}{3} \tag{6.1}$$

it is worth here to elaborate why such definition has been introduced for circulating current and why it is preferred to be mitigated in MMC control. It is shown in this section that circulating current is defined as (6.1) to reflect the portion of phase currents which unnecessarily increases the converter loss.

Let us start with the internal circuit loss of a modular multilevel converter. An inductor is always combined with a resistance which is normally neglected in circuit analysis because of its small value,

118

but it must be considered while analyzing the MMC internal loss. Also, each IGBT has a resistance which cause additional power loss in the converter. Therefore, total resistance corresponding to each inductor l and IGBT's of the switched-on submodules on each arm is denoted by r. It is obvious that the internal power loss of the MMC is equal to,

$$P_{loss} = ri_{up,a}^2 + ri_{up,b}^2 + ri_{up,c}^2 + ri_{low,a}^2 + ri_{low,b}^2 + ri_{low,c}^2 \tag{6.2}$$

Let us determine what values of $i_{up,a}$, $i_{up,b}$, $i_{up,c}$, $i_{low,a}$, $i_{low,b}$, and $i_{low,c}$ minimize the internal loss of MMC, given the values of ac and dc currents. The associated optimization problem is, therefore, defined as below:

$$\min \quad L = ri_{up,a}^2 + ri_{up,b}^2 + ri_{up,c}^2 + ri_{low,a}^2 + ri_{low,b}^2 + ri_{low,c}^2 \tag{6.3}$$

$$\text{over: } \{i_{up,a}, i_{up,b}, i_{up,c}, i_{low,a}, i_{low,b}, i_{low,c}\}$$

$$\text{s.t. } i_{up,a} - i_{low,a} = i_a \tag{6.4}$$

$$i_{up,b} - i_{low,b} = i_b \tag{6.5}$$

$$i_{up,c} - i_{low,c} = i_c \tag{6.6}$$

$$i_{up,a} + i_{up,b} + i_{up,c} = i_{dc} \tag{6.7}$$

$$i_{low,a} + i_{low,b} + i_{low,c} = i_{dc} \tag{6.8}$$

$$i_a + i_b + i_c = 0 \tag{6.9}$$

where the objective function (6.3) is to minimize the power loss inside MMC, the constraints (6.4)-(6.6) are simple KCL equations on ac side, the constraints (6.7)-(6.8) are KCL equations on dc side, and (6.9) holds as the ac grid is assumed balanced.

Applying the equality constraints (6.4)-(6.9) to the objective function (6.3), simplifies the optimization problem as below,

$$\min \quad f(i_{up,a}, i_{up,b}) = i_{up,a}^2 + i_{up,b}^2 + (i_{dc} - i_{up,a} - i_{up,b})^2 +$$

$$(i_{up,a} - i_a)^2 + (i_{up,b} - i_b)^2 + [i_{dc} - (i_{up,a} - i_a) - (i_{up,b} - i_b)]^2 \tag{6.10}$$

over: $\{i_{up,a}, i_{up,b}, i_{up,c}, i_{low,a}, i_{low,b}, i_{low,c}\}$

To calculate the optimal values of $i^*_{up,a}$ and $i^*_{up,a}$, it is enough to solve the following two equations:

$$\frac{\partial P_{loss}}{\partial i_{up,a}}(i^*_{up,a}, i^*_{up,b}) = 0 \quad \Rightarrow \quad 8i^*_{up,a} + 4i^*_{up,b} - 4i_{dc} - 4i_a - 2i_b = 0$$

$$\frac{\partial P_{loss}}{\partial i_{up,b}}(i^*_{up,a}, i^*_{up,b}) = 0 \quad \Rightarrow \quad 8i^*_{up,b} + 4i^*_{up,a} - 4i_{dc} - 4i_b - 2i_a = 0$$

Solving the these two equations together defines $i^*_{up,a}$ and $i^*_{up,a}$ as following:

$$i^*_{up,a} = \frac{i_a}{2} + \frac{i_{dc}}{3} \tag{6.11}$$

$$i^*_{up,b} = \frac{i_b}{2} + \frac{i_{dc}}{3} \tag{6.12}$$

According to (6.4)-(6.9), the ideal values for other upper/lower arm currents can be derived as below,

$$i^*_{up,c} = \frac{i_c}{2} + \frac{i_{dc}}{3} \tag{6.13}$$

$$i^*_{low,a} = -\frac{i_a}{2} + \frac{i_{dc}}{3} \tag{6.14}$$

$$i^*_{low,b} = -\frac{i_b}{2} + \frac{i_{dc}}{3} \tag{6.15}$$

$$i^*_{low,c} = -\frac{i_c}{2} + \frac{i_{dc}}{3} \tag{6.16}$$

Regarding (6.11), any current deviation between the upper arm current of phase a can be expressed as

$$\Delta i_{up,a} = i_{up,a} - i^*_{up,a} = i_{up,a} - \frac{i_a}{2} - \frac{i_{dc}}{3} \tag{6.17}$$

which leads to the following equation if (6.4) is applied:

$$\Delta i_{up,a} = \frac{i_{up,a} + i_{low,a}}{2} - \frac{i_{dc}}{3} \tag{6.18}$$

Similarly, we have

$$\Delta i_{low,a} = \frac{i_{up,a} + i_{low,a}}{2} - \frac{i_{dc}}{3} \tag{6.19}$$

$$\Delta i_{up,b} = \frac{i_{up,b} + i_{low,b}}{2} - \frac{i_{dc}}{3} \tag{6.20}$$

$$\Delta i_{low,b} = \frac{i_{up,b} + i_{low,b}}{2} - \frac{i_{dc}}{3} \tag{6.21}$$

$$\Delta i_{up,c} = \frac{i_{up,c} + i_{low,c}}{2} - \frac{i_{dc}}{3} \tag{6.22}$$

$$\Delta i_{low,c} = \frac{i_{up,c} + i_{low,c}}{2} - \frac{i_{dc}}{3} \tag{6.23}$$

Comparing the equations just obtained and the definition of the circulating current mentioned in (6.1) demonstrates the fact that circulating current on each phase is exactly equal to the deviation of the arm currents of that phase from their optimal value. With such findings, it is not difficult to describe why it is desired to mitigate the circulating current in MMC switching scheme. That is, the MMC internal loss is minimum whenever the circulating current is eliminated.

6.3 MMC Circuit Analysis

The ac current of each phase (e.g., phase a) can be represented by the corresponding upper-arm (i_{up}) and lower-arm (i_{low}) currents, as below:

$$i_a = i_{up,a} - i_{low,a} \tag{6.24}$$

Hereafter, the subscripts "a", "b", and "c" standing for three phases will be ignored for simplicity of the equations. One of the objectives of the MPC control to mitigating the circulating currents in the arms. The total current in an upper-arm or lower-arm has three components: $\frac{1}{3}$ of the dc current i_{dc}, a component related to the ac current, and the circulating current i_z. The following equations represent the relationship of the currents:

$$i_{up} = \frac{i}{2} + \frac{i_{dc}}{3} + i_z \tag{6.25}$$

$$i_{low} = -\frac{i}{2} + \frac{i_{dc}}{3} + i_z \tag{6.26}$$

Although i_z only circulates through the converter legs and does not affect the AC side current, the circulating current has adverse impact on the voltage ripples of the capacitors, converter loss, and rating of power electronic components of MMC. Hence, the circulating current must be mitigated.

Based on the above mentioned equations (6.25) and (6.26), the circulating current flowing through each phase can be expressed in terms of its upper-arm and lower-arm currents as well as converter dc-side current as follows:

$$i_z = \frac{i_{up} + i_{low}}{2} - \frac{i_{dc}}{3} \tag{6.27}$$

According to Fig. 6.1, the dynamic behavior of the each phase of MMC is determined by the following equations:

$$v_{up} = \frac{V_{dc}}{2} - l\frac{di_{up}}{dt} - Ri - L\frac{di}{dt} - v_s \tag{6.28}$$

$$v_{low} = \frac{V_{dc}}{2} - l\frac{di_{low}}{dt} + Ri + L\frac{di}{dt} + v_s \tag{6.29}$$

where v_s denotes the grid voltage.

Subtracting (6.29) from (6.28) leads to

$$v_{low} - v_{up} = l\frac{di}{dt} + 2Ri + 2L\frac{di}{dt} + 2v_s \tag{6.30}$$

$$\tag{6.31}$$

while adding the two equations results in

$$v_{low} + v_{up} = V_{dc} - 2l\frac{di_z}{dt} \tag{6.32}$$

The dynamic of capacitor voltage of the submodule i is also described by

$$C\frac{dv_{Cj}}{dt} = i_{up}u_j \quad \forall j \in [1, n] \tag{6.33}$$

$$C\frac{dv_{Cj}}{dt} = i_{low}u_j \quad \forall j \in [n+1, 2n] \tag{6.34}$$

where $u_j = 1$ if submodule j is active, and $u_j = 0$ otherwise.

6.3.1 Discrete Model of MMC

According to (6.30) and its Euler's approximation of the current derivative, the next step value for ac-side current can be written as

$$i(t + T_s) = \frac{1}{K'} \left(\frac{v_{low}(t + T_s) - v_{up}(t + T_s)}{2} - v_s(t + T_s) + \frac{L'}{T_s}i(t) \right) \tag{6.35}$$

where T_s is an adequately small sampling time step, $L' = L + l/2$, and $K' = R + L'/T_s$. The time indices (t) and $(t+T_s)$ denotes the measured values at current time and the predicted values for the next time step, respectively. As the sampling frequency is assumed to be large enough compared to grid frequency, the predicted value of grid voltage $v_s(t + T_s)$ can be replaced by its measured value $v_s(t)$. $v_{up}(t+T_s)$ and $v_{low}(t+T_s)$ are the predicted upper-arm and lower-arm voltages which are defined as

$$v_{up}(t + Ts) = \sum_{j=1}^{n} v_{Cj}(t + Ts)u_j \tag{6.36}$$

$$v_{low}(t + Ts) = \sum_{j=n+1}^{2n} v_{Cj}(t + Ts)u_j \tag{6.37}$$

where, according to (6.33)-(6.34),

$$v_{Cj}(t + Ts) = v_{Cj}(t) + \left(\frac{T_s i_{up}(t)}{C} \right) u_j \quad \forall j \in [1, n] \tag{6.38}$$

$$v_{Cj}(t + Ts) = v_{Cj}(t) + \left(\frac{T_s i_{low}(t)}{C} \right) u_j \quad \forall j \in [n+1, 2n] \tag{6.39}$$

The discrete description of (6.32) leads to the following equation to represent the next-step circulating current:

$$i_z(t + T_s) = \frac{T_s}{2l} \left(V_{dc} - v_{low}(t + T_s) - v_{up}(t + T_s) \right) + i_z(t) \tag{6.40}$$

6.4 Model Predictive Control

6.4.1 MPC Multiobjective Problem

According to the mathematical model of the MMC, an MPC strategy is proposed in this section. The proposed MPC strategy seeks the best switching sequences of u_i to control ac-side current, capacitor voltage, and circulating current simultaneously.

Three objectives have been defined for MMC control in the literature[57]:

i to track the ac-side current (i) of all phases to their reference values (i_{ref})

ii to mitigate the circulating current i_z flowing between the converter legs, and

iii to regulate all the capacitor voltages on their nominal value (V_{dc}/n)

Assuming that the capacitor voltages are kept very close to their nominal value (V_{dc}/n), one constraint on total number of switched-on submodules is defined. Indeed, half of the submodules on each phase must be switched on and the other half must be off, all the time. The molti-objective optimization problem is illustrated as below,

$$\min \quad |i_{ref} - i(t + T_s)|$$

$$\min \quad |i_z(t + T_s)|$$

$$\min \quad \left| V_{C_i}(t + T_s) - \frac{V_{dc}}{n} \right|$$

$$\text{over: } \{u_1, u_2, ..., u_n\}$$

$$\text{s.t. } (6.35) - (6.40)$$

$$\sum_{i=1}^{2n} u_i = n \tag{6.41}$$

6.4.2 Optimization Alternative 1

6.4.2.1 Problem Reformulation

Let us define $(\cdot)^*(t + T_s)$ to be the ideal value of corresponding variable for the next time step. By replacing the variables in (6.35) by their ideal values implying *exact AC current tracking*,

$$i^*(t + T_s) = i_{ref} = \frac{1}{K'} \left(\frac{v^*_{low}(t + T_s) - v^*_{up}(t + T_s)}{2} - v_s(t + T_s) + \frac{L'}{T_s} i(t) \right) \tag{6.42}$$

which leads to the following relation between v^*_{low} and v^*_{up}:

$$v^*_{low}(t + T_s) - v^*_{up}(t + T_s) = 2K' i_{ref}(t + T_s) + 2v_s(t) - \frac{2L'}{T_s} i(t) \tag{6.43}$$

Likewise, for zero circulating current in the bridges, replacing the ideal value of i_z in (6.40) leads to

$$i^*_z(t + T_s) = \frac{T_s}{2l} \left(V_{dc} - v^*_{low}(t + T_s) - v^*_{up}(t + T_s) \right) + i_z(t) = 0 \tag{6.44}$$

which determines another relation between $Vlow*$ and $Vup*$ which is proposed below:

$$v^*_{low}(t + T_s) + v^*_{up}(t + T_s) = V_{dc} + \frac{2l}{T_s} i_z(t) \tag{6.45}$$

The variables $v^*_{low}(t + T_s)$ and $v^*_{up}(t + T_s)$ are derived from (6.43) and (6.45) as follows:

$$v^*_{low}(t + T_s) = \left(\frac{V_{dc}}{2} + \frac{l}{T_s} i_z(t) \right) + \left(K' i_{ref}(t + T_s) + v_s(t) - \frac{L'}{T_s} i(t) \right) \tag{6.46}$$

$$v^*_{up}(t + T_s) = \left(\frac{V_{dc}}{2} + \frac{l}{T_s} i_z(t) \right) - \left(K' i_{ref}(t + T_s) + v_s(t) - \frac{L'}{T_s} i(t) \right) \tag{6.47}$$

where V_{dc} is assumed to be constant.

Let the variables Δv_{low}, Δv_{up}, and Δi denote the deviation of the corresponding variables from their ideal values, defined as below:

$$\Delta v_{low} = v_{low}^* - v_{low} \tag{6.48}$$

$$\Delta v_{up} = v_{up}^* - v_{up} \tag{6.49}$$

$$\Delta i = i_{ref} - i(t + T_s) \tag{6.50}$$

Subtraction of (6.35) from (6.42) gives an explanation of the first objective function (ac current deviation) in terms of v_{up}^* and v_{low}^*, as follows:

$$\Delta i = \frac{1}{2K'} \left(\Delta v_{low}(t + T_s) - \Delta v_{up}(t + T_s) \right) \tag{6.51}$$

The explanation of the second objective function (circulating current) in terms of v_{up}^* and v_{low}^* is also derived by subtracting (6.44) from (6.40):

$$i_z(t + T_s) = \frac{T_s}{2l} \left(\Delta v_{low}(t + T_s) + \Delta v_{up}(t + T_s) \right) \tag{6.52}$$

Hence, (6.51) and (6.52) can be applied to (6.41).

$$\min_{U} \quad f_1(U) = \frac{1}{2K'} |\Delta v_{low}(t + T_s) - \Delta v_{up}(t + T_s)|$$

$$\min_{U} \quad f_2(U) = \frac{T_s}{2l} |\Delta v_{low}(t + T_s) + \Delta v_{up}(t + T_s)|$$

$$\min_{U} \quad f_3(U) = \sum_{i=1}^{2n} |V_{C_i}(t + T_s) - \frac{V_{dc}}{n}| \tag{6.53}$$

$$\text{s.t.} \quad (6.35) - (6.40), (6.46) - (6.49)$$

$$\sum_{i=1}^{2n} u_i = n \tag{6.54}$$

$$U = [u_1, u_2, ..., u_{2n}] : u_k \in \{0, 1\} \ \forall k \in [1, 2n]$$

Applying weighted sum method to the optimization problem (6.41) leads to the following formulation, which is called P_1 hereafter:

$$\min_{U} \quad f_4(U) = \frac{\lambda}{2K'} \left| \Delta v_{low}(t+T_s) - \Delta v_{up}(t+T_s) \right| + \frac{\lambda_z T_s}{2l} \left| \Delta v_{low}(t+T_s) + \Delta v_{up}(t+T_s) \right| \quad (6.55)$$

$$\min_{U} \quad f_3(U) = \sum_{i=1}^{2n} \left| V_{C_i}(t+T_s) - \frac{V_{dc}}{n} \right| \quad (6.56)$$

$$\text{s.t.} \quad (6.35) - (6.40), (6.46) - (6.49)$$

$$\sum_{i=1}^{2n} u_i = n \quad (6.57)$$

$$U = [u_1, u_2, ..., u_{2n}] : u_k \in \{0, 1\} \ \forall k \in [1, 2n]$$

where the first objective is derived by applying the weighted sum method to the objective functions $f_1(U)$ and $f_2(U)$ with coefficients λ and λ_z, respectively. The weighted sum method with equal coefficient is also employed to merge the third objective function to a single objective function for capacitor voltage deviation.

6.4.2.2 Solution Algorithm 1

The approach proposed here to solve the multi-objective optimization problem P_1 includes three steps. First, the function corresponding to the capacitor voltage deviation (6.56) sorts the submodules to be switched on. Next, the priorities defined are used to form the feasible solution sets considering the constraint (6.57). Finally, the objective function (6.55) determines the best switching pattern based on the feasible solution sets determined previously. Following is a detailed description of these steps. In the first step, the second objective function (6.56) is minimized by sorting the submodules on both the upper and lower arm. According to (6.38), the direction of i_{up} defines whether the capacitor voltages of the upper-arm submodules are subjected to increase or decrease. Since the capacitor of a switched-on submodule gets charged when $i_{up} > 0$, the algorithm prefers to select the submodules with least capacitor voltages. Thus they are sorted in the ascending order. Likewise, the submodules are sorted in the descending order if $i_{up} < 0$. Let

the vector $V_{C_{up}}^{sort} = [V_{C_1}^{sort}, ..., V_{C_n}^{sort}]$ denote the submodule voltages on the upper-arm after sorting. The algorithm applies the same logic to sort the submodules on the lower-arm to define the vector $V_{C_{low}}^{sort} = [V_{C_{n+1}}^{sort}, ..., V_{C_{2n}}^{sort}]$.

In the second step, having the submodules sorted based on their capacitor voltages, the algorithm calculates the cumulative sum vectors of the components of $V_{C_{up}}^{sort}$ and $V_{C_{low}}^{sort}$. The sets of cumulative sum values are denoted as $V_{C_{up}}^{sum}$ and $V_{C_{low}}^{sum}$ are defined as below:

$$V_{C_{up}}^{sum} = \{\alpha_k : k = 0, 1, ..., n\} \tag{6.58}$$

$$V_{C_{low}}^{sum} = \{\beta_k : k = 0, 1, ..., n\} \tag{6.59}$$

where

$$\alpha_0 = \beta_0 = 0$$

$$\alpha_k = \sum_{i=1}^{k} V_{C_i}^{sort} \quad \forall k \in [1, n]$$

$$\beta_k = \sum_{i=n+1}^{n+k} V_{C_i}^{sort} \quad \forall k \in [1, n]$$

To make sure that the number of the submodules that switched on is n, the sum of the subscripts of α and β should add up to n. Fig. 6.6-a describes all n feasible solutions $U \in S$ where each $\leftrightarrow$ represents one feasible solution.
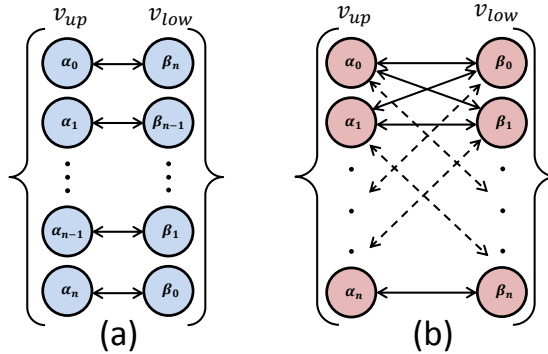

Figure 6.6. Feasible solution sets through both algorithms. a) algorithm 1, b) algorithm 2.

In the third step, size of feasible set is remarkably lower than that introduced in [57]. The algorithm then compares the objective function (6.55) for all feasible solutions to find the optimal solution $U^* = \text{argmin } f_4(U) : U \in S$. If more than one $U \in S$ minimizes the function f_4, the one returning less value for f_3 is the final solution.

6.4.3 Optimization Alternative 2

6.4.3.1 A Relaxation to the Problem P_1

The simulation results of the algorithm and optimization problem P_1 illustrates that the constraint (6.57) has an adverse impact on the circulating current. The constraint, in fact, restricts the algorithm from selecting the most appropriate solution to mitigate the circulating current.

In this section, a modified version of the optimization problem P_1 is solved to overcome this problem. The first modification is to eliminate the constraint (6.57) from the optimization problem. Therefore, the algorithm is able to switch on as many submodules as required to reach v_{up}^* and v_{low}^*. Second, the weighting factors λ and λ_z are set on the values $2K'$ and $\frac{2l}{T_s}$ respectively. Having the first and second modifications applied to P_1, it is changed to the following format which will be called P_2 hereafter:

$$\min_{U} \quad f_5(U) = |\Delta v_{low}(t + T_s) - \Delta v_{up}(t + T_s)| + |\Delta v_{low}(t + T_s) + \Delta v_{up}(t + T_s)| \quad (6.60)$$

$$\min_{U} \quad f_3(U) = \sum_{i=1}^{2n} \left| V_{C_i}(t + T_s) - \frac{V_{dc}}{n} \right| \quad (6.61)$$

$$\text{s.t.} \quad (6.35) - (6.40), (6.46) - (6.49)$$

$$U = [u_1, u_2, ..., u_{2n}] : u_k \in \{0, 1\} \, \forall_{k \in [1, 2n]}$$

6.4.3.2 Solution Algorithm 2

Similar to the previous algorithm, Solution Algorithm 2 solves the multiobjective problem P_2 in three steps.

The first step is to sort the submodules according to their capacitor voltages and the sign of upper-arm and lower-arm currents, which is described in the first step of the algorithm 1. $V_{C_{low}}^{sort}$ and $V_{C_{low}}^{sort}$ are the outputs of step 1.

In the second step, having the submodules sorted, sets of $V_{C_{up}}^{sum}$ and $V_{C_{low}}^{sum}$ are defined using (6.58)-(6.59). The feasible solution set S includes the switching sequences associated with any $(\alpha_i, \beta_j) \in V_{C_{up}}^{sum} \times V_{C_{up}}$. Fig. 6.6-b represents the combinations of v_{up} and v_{low} which form feasible solutions of the optimization problem P_2, where each $\leftrightarrow$ represents one feasible solution. The total number of the feasible sets are n^2. Although the searching space is significantly reduced compared to the number of the sets examined in [57], it still needs significant computational efforts to compare the resulting objective f_5 for each feasible set and find the optimal set, especially for the converters with large number of submodules $e.g.$ $n = 400$. The reasoning provided in the next step makes the solution much more efficient.

In the third step, it is desired in this step to show that the optimal solution of P_2 cannot lie on any feasible solution other than $(\alpha_i, \beta_j),(\alpha_{i+1}, \beta_j),(\alpha_i, \beta_{j+1})$, and $(\alpha_{i+1}, \beta_{j+1})$ if $v_{up}^* \in [\alpha_i, \alpha_{i+1})$ and $v_{low}^* \in [\beta_j, \beta_{j+1})$.

Let us define $V_C^{sum} = V_{C_{up}}^{sum} \times V_{C_{low}}^{sum}$ and the function $O : V_C^{sum} \rightarrow \mathbf{U}$ mapping any $(\alpha_i, \beta_j) \in V_C^{sum}$ to its corresponding switching $U_{i,j} \in \mathbf{U}$ such that $U_{i,j} = O(\alpha_i, \beta_j)$. Fig. 6.7 illustrates a geometric representation of the feasible set S assuming that $v_{up}^* \in [\alpha_i, \alpha_{i+1})$ and $v_{low}^* \in [\beta_j, \beta_{j+1})$. The subset $S' \subset S$ is also defined as

$$S' = \{O(\alpha_i, \beta_j), O(\alpha_{i+1}, \beta_j), O(\alpha_i, \beta_{j+1}), O(\alpha_{i+1}, \beta_{j+1})\}$$

which includes the switching sequences corresponding to the points 1-4 shown in Fig. 6.7.

It is claimed here that the optimal solution in feasible set S certainly belongs to the subset S', that is, $\{\min f_5(U) : U \in S'\} = \{\min f_5(U) : U \in S\}$.

To prove the cliam above, for any feasible solution $U_{k,l} = O(\alpha_k, \beta_l)$, the objective function (6.60) equals to

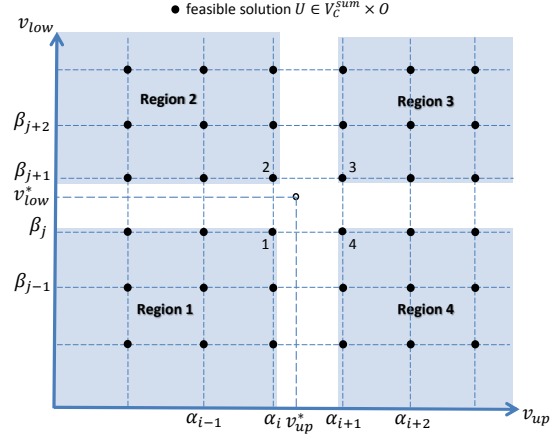$$f_5(U_{k,l}) = 2 \times \max \left\{ |\alpha_k - v_{up}^*|, |\beta_l - v_{low}^*| \right\} \tag{6.62}$$

Figure 6.7. Different regions for the feasible solution set $S = V_C^{sum} \times O$.

Having the *Region 1* in Fig. 6.7 defined as $R_1 = \{(k,l)|k \leq i, l \leq j\}$ spanning the feasible solution subset $S_1 = \{U_{k,l}|k \leq i, l \leq j\}$, we have

$$\left|\alpha_i - v_{up}^*\right| \leq \left|\alpha_k - v_{up}^*\right|$$
$$\left|\beta_j - v_{low}^*\right| \leq \left|\beta_l - v_{low}^*\right|$$

for any $(k,l) \in R_1$, which leads to

$$\min\{f_5(U) : U \in S_1\} = f_5(U_{i,j}) \tag{6.63}$$

regarding (6.62). Similar justifications for the subsets S_2, S_3, and S_4 in Fig. 6.7 illustrates that

$$\min\{f_5(U) : U \in S_2\} = f_5(U_{i,j+1}) \tag{6.64}$$

$$\min\{f_5(U) : U \in S_3\} = f_5(U_{i+1,j+1}) \tag{6.65}$$

$$\min\{f_5(U) : U \in S_4\} = f_5(U_{i+1,j}) \tag{6.66}$$

According to (6.63)-(6.66), the optimal solution definitely lies on one of the solutions belonging to the subset S', and the claim is proved.

According to the mathematical proof stated above, if $v_{up}^* \in [\alpha_i, \alpha_{i+1})$ and $v_{low}^* \in [\beta_j, \beta_{j+1})$, the objective function f_5 is needed to be calculated for just four (v_{up}, v_{low}) combinations belonging to

$$\{(\alpha_i, \beta_j), (\alpha_{i+1}, \beta_j), (\alpha_i, \beta_{j+1}), (\alpha_{i+1}, \beta_{j+1})\}$$

to determine the optimal switching pattern. In case more than one $U \in S'$ minimizes the function $f_5(U)$, the one returning lower value for $f_3(U)$ is the final solution.

Although removing the constraint (6.57) may result in ripples in dc link voltage, it remarkably mitigates the circulating current. Simulation results show that the total number of switched-on submodules on upper and lower arms $(\sum_{i=1}^n u_i)$ is equal to either n, most of the time. The incidents where less than n submodules are activated mostly happens when both i_{up} and i_{low} are negative and the submodules with highest capacitor voltages are selected. The cases with higher number of switched-on submodules than n mostly happen if i_{up} and i_{low} are both positive. In all these cases, given the circulating current being mitigated at the current time step t, the algorithm exactly selects as many submodules to switch on as required in order to provide the nominal voltage of the dc link.

6.5 Case Study

6.5.1 Study System

This section evaluates the performance of an MMC system of Fig. 6.1. We apply both MPC strategies proposed in this chapter (Algorithm 1 and Algorithm 2) on this system to compare the performance. In practice, an MMC-HVDC can have a large number of submodules in each arm. In order to simplify the simulation study without loss of generality, a 7-level MMC is considered and simulated in MATLAB/Simpowersystem environment. The system parameters are given in Table 6.2. The ac-side voltage is expected to be 52 kV (line-to-line, peak value), and the reference of the ac-side current is 300 A in phase with the ac voltage.

Table 6.2. MMC parameters for case study.

Nominal DC voltage V_{dc}	60 kV
Submodule capacitance C_{sm}	2500 μF
Carrier signal frequency f	2.5 kHz
Output current reference I_{ref}	300 A
R	0.03 Ω
L	5 mH
l	3 mH
Sampling period T_s	25 μs

6.5.2 Simulation Result

Figs. 6.8 and 6.9 present the comparison of N_{up}, N_{low} and the total number of switched-on submodules for both cases. The switching scheme based on Algorithm 1 results in total six submodules to be switched on at all time. However, for Algorithm 2, due to the relaxation, the total number of submodules to be switched on can also be 7 or 5.
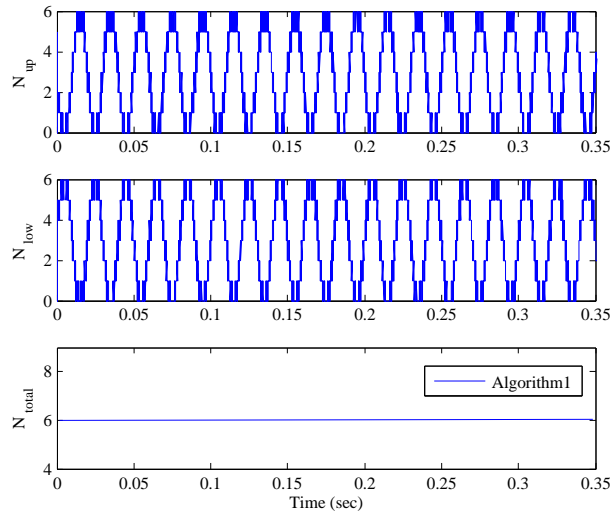
Figure 6.8. Number of active submodules for Algorithm 1. a) upper arm, b) lower arm, c) entire bridge.

However, according to the percentage of the total number of switched-on submodules for Algorithm 2 based on the simulation results which is illdtrated in Fig. 6.10, in 75% percent of the switching sequences the total number of the submodules turned on is equal to 6. This value is equal to 5 and 7 in 11% of the incidents, each.
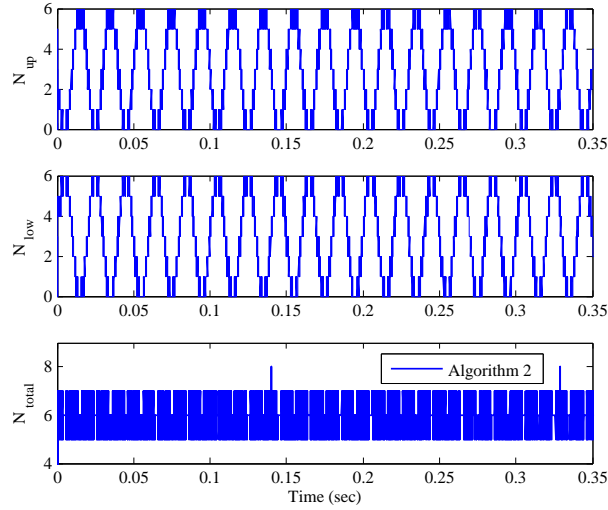
Figure 6.9. Number of active submodules for Algorithm 2. a) upper arm, b) lower arm, c) entire bridge.

Fig. 6.11 presents the circulating current in phase a. In Algorithm 1, the circulating current is not well mitigated due to the constraint on total number of switched-on submodules. In contrary, the algorithm 2 has more freedom to seek the best solution for circulation current suppression. As shown in Fig. 6.11, the algorithm 2 suppresses the circulating current down to 0.1 pu while this value reaches 2.5 pu in algorithm 1. The results of the algorithm 2 show similar performance demonstrated by the results presented in [70], where a PWM technique equipped with circulating current suppressing control (CCSC) is developed. In this reference, the CCSC-equipped PWM has reduced the circulating current from 2 pu down to 0.1 pu.
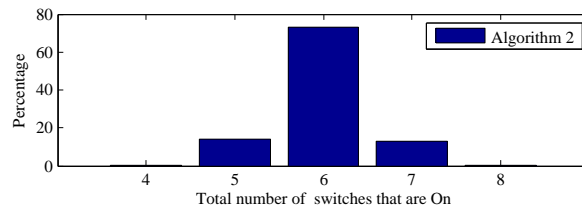

Figure 6.10. The percentage of submodules switched on for Algorithm 2.

Fig. 6.12 presents the ac currents for the three cases. Both algorithms lead to an appropriate switching scheme from current tracking point of view. The ac current waveforms completely follow the sinusoidal current reference with correct amplitude and phase.
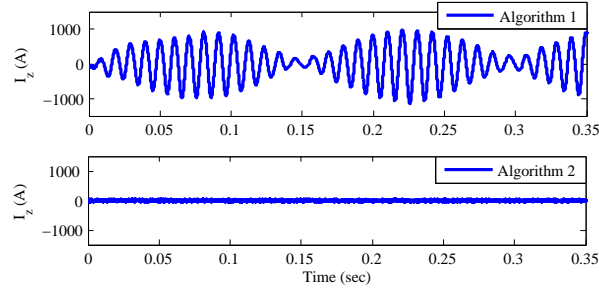
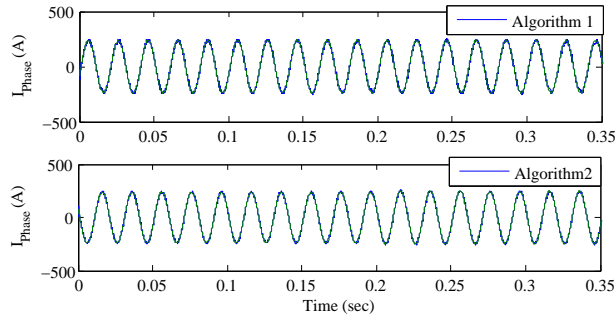Figure 6.11. Circulating current in different switching methods.

Figure 6.12. Output phase current in different switching methods.

As shown in Fig. 6.13, where the first submodule's capacitor voltage is depicted for both algorithms, Algorithm 1 results in a $\pm 10\%$ ripple on capacitor voltage mostly because of its unsuccessful mitigation of the circulating current. In contrast, the capacitor voltage of the case simulated by Algorithm 2 has just $\pm 1\%$ ripple which proves the efficiency of this algorithm for this objective as well. The algorithm 2 demonstrates slightly better results in capacitor voltage control compared to the control method proposed in [70], where the capacitor voltage ripple is about $\pm 1.5\%$.
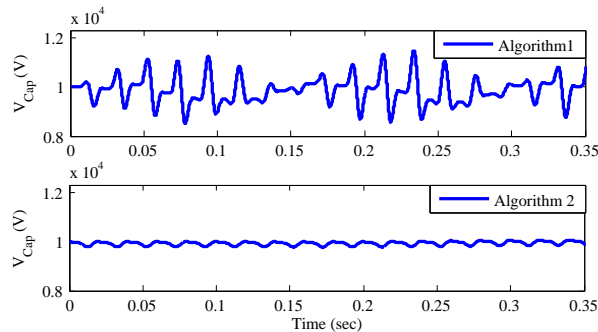

Figure 6.13. Capacitor voltage in different switching methods.

CHAPTER 7

CONCLUSIONS AND FUTURE WORK

7.1 Conclusions

This dissertation can be concluded in four parts as follows.

First, a distributed DC-OPF solution has proposed chapter 3 based on partial Primal-Dual algorithm. Each bus in the power system is identified as a distinct agent. The algorithm is developed by applying partial Primal-Dual algorithm to economic dispatch problem. The algorithm is finally studied against a radial power network for both congested and non-congested conditions.

Second, chapter 4 presents multi-agent control based demand response programs. Based on two different information exchange structures, two distributed algorithms are proposed to facilitate communities and utility interactions to achieve a global cost minimization objective. Each community and the utility behave as an autonomous agent to minimize their own cost. The two algorithms are developed based on Lagrangian relaxation and duality. Our contribution is three-fold: 1) Unlike many demand response papers in the literature where the network model is simplified, ac OPF problems is formulated in this work, considering network constraints. 2) Robust distributed algorithms are proposed and tested for multi-agent control of community and utility. 3) Mathematics are presented along with physical meaning of demand response to shed insights on distributed algorithms and optimization decomposition.

Third, the utility-community interaction problem proposed in the chapter 4 is extended to tackle the problem in presence of storage and renewable systems. Therefore, in chapter 5, reserve-constrained Multi-Horizon Optimal Power Flow has been decomposed between utility and communities to develop two iterative distributed algorithms. Such decomposition scheme reduces the complicatedness of the original multi-horizon nonconvex problem by introducing several single-

136

horizon nonconvex for utility and several multi-horizon convex problems for communities. An update process then trajects the solution to reach the global optimal solution through an iterative procedure. An analytical approach to evaluate sensitivity of optimal system and market parameters (power generation, reserve availability and energy/reserve prices) versus battery sizing has been also proposed in this chapter. The efficiency of the iterative algorithms as well as validity of the sensitivity analysis are tested against several case studies.

Finally, binary integer programming based MPC strategies with significantly less computing effort has been proposed in the chapter 6 to control the ac currents, keep the capacitor voltages nominal, and mitigate the circulating currents. The algorithm also determines which submodules to be switched on/off for the next time step according to the corresponding upper/lower current. The proposed algorithms use sorting to find the feasible solution sets. These feasible solution sets are then compared for their objective values. The performance of the proposed methods are evaluated via simulation in Matlab SimPowerSystems. The proposed MPC schemed are compared for their control effort and performance. It is found that MPC based schemes are capable to achieve better ac current tracking and circulating current elimination.

7.2   Future Work

The future work of this dissertation can be suggested in the following categories.

First, the convergence issue involved with distributed unit commitment is still one of challenges of this problem. The problem becomes more challenging when the network congestion is considered, which makes the problem more interesting to do research on. It is suggested to use the knowledge of distributed DC-OPF problem and conduct research on development of multi-agent solution for network-constrained unit commitment problem. The conver

Second, several achievements have been reported in convexifying the AC-OPF problem through semidefinite relaxations[33, 96]. Although the results obtained by these methods is guaranteed to be the global optimal solution, They do not guarantee that they will converge to a feasible solution. Therefore, these algorithms cannot replace MATPOWER, as a robust and sufficiently accurate OPF solver, in subgradient and LUBS methods because they are not robust enough to be

137

used in an iterative algorithm. It is also suggested to conduct research on improving the robustness of these convex models of OPF problem to obtain global optimal solution of the multi-agent and moving-horizon OPF problem.

REFERENCES

[1] Y. Gu, X. Xiang, W. Li, and X. He, "Mode-adaptive decentralized control for renewable dc microgrid with enhanced reliability and flexibility," *Power Electronics, IEEE Transactions on*, to appear.

[2] M. Babazadeh and H. Karimi, "Robust decentralized control for islanded operation of a microgrid," in *Power and Energy Society General Meeting, 2011 IEEE*, 2011, pp. 1–8.

[3] M. Hamzeh, H. Mokhtari, and H. Karimi, "A decentralized self-adjusting control strategy for reactive power management in an islanded multi-bus mv microgrid," *Electrical and Computer Engineering, Canadian Journal of*, vol. 36, no. 1, pp. 18–25, 2013.

[4] N. Cai and J. Mitra, "A decentralized control architecture for a microgrid with power electronic interfaces," in *North American Power Symposium (NAPS), 2010*, 2010, pp. 1–8.

[5] "California iso day-ahead market overview," http://content.caiso.com/training/Day-Ahead_Market_Overview/index.html, accessed: 2015-06-01.

[6] "California iso real-time market overview," http://www.caiso.com/CBT/Real-TimeMarketOverview_CBT/presentation.html, accessed: 2015-06-01.

[7] "California iso energy impulse market," http://www.caiso.com/documents/energyimbalancemarket-draftfinalproposal092313.pdf, accessed: 2015-06-01.

[8] X. Guan, P. B. Luh, H. Yan, and J. Amalfi, "An optimization-based method for unit commitment," *International Journal of Electrical Power & Energy Systems*, vol. 14, no. 1, pp. 9–17, 1992.

[9] A. Kargarian, Y.-S. Fu, and Z. Li, "Distributed security-constrained unit commitment for large-scale power systems," *Power Systems, IEEE Transactions on*, pp. 1–12, 2015.

[10] J. Yu, J. Zhou, W. Wu, J. Yang, and W. Yu, "Solution of the profit-based unit commitment problem by using multi-agent system," in *Intelligent Control and Automation, 2004. WCICA 2004. Fifth World Congress on*, vol. 6.   IEEE, 2004, pp. 5079–5083.

[11] T. Nagata, M. Ohono, J. Kubokawa, H. Sasaki, and H. Fujita, "A multi-agent approach to unit commitment problems," in *Power Engineering Society Winter Meeting, 2002. IEEE*, vol. 1.   IEEE, 2002, pp. 64–69.

[12] D. P. Bertsekas and J. N. Tsitsiklis, *Parallel and distributed computation: numerical methods.* Prentice-Hall, Inc., 1989.

[13] S. Boyd, L. Xiao, A. Mutapcic, and J. Mattingley, "Notes on decomposition methods," *Notes for EE364B, Stanford University*, pp. 1–36, 2007.

[14] G. Gordon and R. Tibshirani, "Subgradient method," http://www.cs.cmu.edu/afs/cs.cmu.edu/user/ggordon/www/10725-F12/slides/06-sg-method.pdf, accessed: 2015-06-03.

[15] V. R. Disfani, L. Fan, L. Piyasinghe, and Z. Miao, "Multi-agent control of community and utility using lagrangian relaxation based dual decomposition," *Electric Power Systems Research*, vol. 110, pp. 45–54, 2014.

[16] V. Disfani, Z. Miao, L. Fan, B. Zeng *et al.*, "Dual decomposition-based privacy-preserving multi-horizon utility-community decision making paradigms," *arXiv preprint arXiv:1503.09087*, pp. 1–8, 2015.

[17] V. Disfani, L. Fan, and Z. Miao, "Distributed dc optimal power flow for radial networks through partial primal dual algorithm," in *Power and Energy Society General Meeting (PES), 2015 IEEE*, July 2015, pp. 1–5.

[18] D. Yuan, S. Xu, and H. Zhao, "Distributed primal–dual subgradient method for multiagent optimization via consensus algorithms," *Systems, Man, and Cybernetics, Part B: Cybernetics, IEEE Transactions on*, vol. 41, no. 6, pp. 1715–1724, 2011.

[19] S. J. Wright, *Primal-dual interior-point methods*. Siam, 1997.

[20] S. Mehrotra, "On the implementation of a primal-dual interior point method," *SIAM Journal on optimization*, vol. 2, no. 4, pp. 575–601, 1992.

[21] Y. Nesterov, A. Nemirovskii, and Y. Ye, *Interior-point polynomial algorithms in convex programming*. SIAM, 1994, vol. 13.

[22] S. Boyd, N. Parikh, E. Chu, B. Peleato, and J. Eckstein, "Distributed optimization and statistical learning via the alternating direction method of multipliers," *Foundations and Trends® in Machine Learning*, vol. 3, no. 1, pp. 1–122, 2011.

[23] T. Erseghe, "A distributed and scalable processing method based upon admm," *Signal Processing Letters, IEEE*, vol. 19, no. 9, pp. 563–566, 2012.

[24] A. M. Geoffrion, "Generalized benders decomposition," *Journal of optimization theory and applications*, vol. 10, no. 4, pp. 237–260, 1972.

[25] A. Grothey, S. Leyffer, and K. McKinnon, "A note on feasibility in benders decomposition," *University of Dundee Numerical Analysis Report NA-188*, pp. 1–13, 1999.

[26] M. Shahidehopour and Y. Fu, "Benders decomposition: applying benders decomposition to power systems," *Power and Energy Magazine, IEEE*, vol. 3, no. 2, pp. 20–21, 2005.

[27] N. Alguacil and A. Conejo, "Multiperiod optimal power flow using benders decomposition," *Power Systems, IEEE Transactions on*, vol. 15, no. 1, pp. 196–201, 2000.

[28] S. Kar, G. Hug, J. Mohammadi, and J. Moura, "Distributed state estimation and energy management in smart grids: A consensus+ innovations approach," *Selected Topics in Signal Processing, IEEE Journal of*, vol. 8, no. 6, pp. 1022–1038, Dec 2014.

[29] W. Zhang, W. Liu, X. Wang, L. Liu, and F. Ferrese, "Online optimal generation control based on constrained distributed gradient algorithm," *Power Systems, IEEE Transactions on*, to appear.

[30] B. H. Kim and R. Baldick, "Coarse-grained distributed optimal power flow," *IEEE Transactions on Power Systems*, vol. 12, no. 2, pp. 932–939, 1997.

[31] ——, "A comparison of distributed optimal power flow algorithms," *Power Systems, IEEE Transactions on*, vol. 15, no. 2, pp. 599–604, 2000.

[32] E. Dall'Anese, H. Zhu, and G. B. Giannakis, "Distributed optimal power flow for smart microgrids," *Smart Grid, IEEE Transactions on*, vol. 4, no. 3, pp. 1464–1475, 2013.

[33] J. Lavaei and S. H. Low, "Zero duality gap in optimal power flow problem," *Power Systems, IEEE Transactions on*, vol. 27, no. 1, pp. 92–107, 2012.

[34] L. Xiao and S. Boyd, "Optimal scaling of a gradient method for distributed resource allocation," *Journal of optimization theory and applications*, vol. 129, no. 3, pp. 469–488, 2006.

[35] A. J. Conejo and J. A. Aguado, "Multi-area coordinated decentralized dc optimal power flow," *Power Systems, IEEE Transactions on*, vol. 13, no. 4, pp. 1272–1278, 1998.

[36] A. G. Bakirtzis and P. N. Biskas, "A decentralized solution to the dc-opf of interconnected power systems," *Power Systems, IEEE Transactions on*, vol. 18, no. 3, pp. 1007–1013, 2003.

[37] P. N. Biskas, A. G. Bakirtzis, N. I. Macheras, and N. K. Pasialis, "A decentralized implementation of dc optimal power flow on a network of computers," *Power Systems, IEEE Transactions on*, vol. 20, no. 1, pp. 25–33, 2005.

[38] C. Zhao, U. Topcu, and S. Low, "Swing dynamics as primal-dual algorithm for optimal load control," in *Smart Grid Communications (SmartGridComm), 2012 IEEE Third International Conference on*. IEEE, 2012, pp. 570–575.

[39] C. Zhao, U. Topcu, N. Li, and S. Low, "Design and stability of load-side primary frequency control in power systems," *Automatic Control, IEEE Transactions on*, vol. 59, no. 5, pp. 1177–1189, May 2014.

[40] L. Chen, N. Li, S. H. Low, and J. C. Doyle, "Two market models for demand response in power networks," in *Smart Grid Communications (SmartGridComm), 2010 First IEEE International Conference on*. IEEE, 2010, pp. 397–402.

[41] N. Li, L. Chen, and S. H. Low, "Optimal demand response based on utility maximization in power networks," in *IEEE Power and Energy Society General Meeting*. IEEE, 2011, pp. 1–8.

[42] A. Mohsenian-Rad, V. W. Wong, J. Jatskevich, R. Schober, and A. Leon-Garcia, "Autonomous demand-side management based on game-theoretic energy consumption scheduling for the future smart grid," *IEEE Transactions on Smart Grid*, vol. 1, no. 3, pp. 320–331, 2010.

[43] W. Saad, Z. Han, H. Poor, and T. Basar, "Game-theoretic methods for the smart grid: an overview of microgrid systems, demand-side management, and smart grid communications," *Signal Processing Magazine, IEEE*, vol. 29, no. 5, pp. 86–105, 2012.

[44] D. P. Palomar and M. Chiang, "A tutorial on decomposition methods for network utility maximization," *Selected Areas in Communications, IEEE Journal on*, vol. 24, no. 8, pp. 1439–1451, 2006.

[45] R. Hermans, M. Almassalkhi, and I. Hiskens, "Incentive-based coordinated charging control of plug-in electric vehicles at the distribution-transformer level," in *American Control Conference (ACC), 2012*. IEEE, 2012, pp. 264–269.

[46] A. G. Beccuti, T. H. Demiray, G. Andersson, and M. Morari, "A lagrangian decomposition algorithm for optimal emergency voltage control," *Power Systems, IEEE Transactions on*, vol. 25, no. 4, pp. 1769–1779, 2010.

[47] P. B. Luh and D. J. Hoitomt, "Scheduling of manufacturing systems using the lagrangian relaxation technique," *Automatic Control, IEEE Transactions on*, vol. 38, no. 7, pp. 1066–1079, 1993.

[48] N. Li and J. R. Marden, "Designing games for distributed optimization," in *Decision and Control and European Control Conference (CDC-ECC), 2011 50th IEEE Conference on*. IEEE, 2011, pp. 2434–2440.

[49] K. M. Chandy, S. H. Low, U. Topcu, and H. Xu, "A simple optimal power flow model with energy storage," in *Decision and Control (CDC), 2010 49th IEEE Conference on*. IEEE, 2010, pp. 1051–1057.

[50] D. Gayme and U. Topcu, "Optimal power flow with large-scale storage integration," *Power Systems, IEEE Transactions on*, vol. 28, no. 2, pp. 709–717, 2013.

[51] A. Gabash and P. Li, "Active-reactive optimal power flow in distribution networks with embedded generation and battery storage," *Power Systems, IEEE Transactions on*, vol. 27, no. 4, pp. 2026–2035, 2012.

[52] D. Chattopadhyay and R. Baldick, "Unit commitment with probabilistic reserve," in *Power Engineering Society Winter Meeting, 2002. IEEE*, vol. 1. IEEE, 2002, pp. 280–285.

[53] J. Condren, T. W. Gedra, and P. Damrongkulkamjorn, "Optimal power flow with expected security costs," *Power Systems, IEEE Transactions on*, vol. 21, no. 2, pp. 541–547, 2006.

[54] R. D. Zimmerman, C. E. Murillo-Sánchez, and R. J. Thomas, "Matpower's extensible optimal power flow architecture," in *Power & Energy Society General Meeting, 2009. PES'09. IEEE*. IEEE, 2009, pp. 1–7.

[55] E. Sortomme and M. El-Sharkawi, "Optimal power flow for a system of microgrids with controllable loads and battery storage," in *Power Systems Conference and Exposition, 2009. PSCE'09. IEEE/PES.* IEEE, 2009, pp. 1–5.

[56] Y. Wen, C. Guo, D. S. Kirschen, and S. Dong, "Enhanced security-constrained opf with distributed battery energy storage," *Power Systems, IEEE Transactions on*, vol. 30, no. 1, pp. 98–108, 2015.

[57] J. Qin and M. Saeedifard, "Predictive control of a modular multilevel converter for a back-to-back hvdc system," *Power Delivery, IEEE Transactions on*, vol. 27, no. 3, pp. 1538–1547, 2012.

[58] M. Saeedifard and R. Iravani, "Dynamic performance of a modular multilevel back-to-back hvdc system," *Power Delivery, IEEE Transactions on*, vol. 25, no. 4, pp. 2903–2912, 2010.

[59] A. Lesnicar and R. Marquardt, "An innovative modular multilevel converter topology suitable for a wide power range," in *Power Tech Conference Proceedings, 2003 IEEE Bologna*, vol. 3, 2003, p. 6.

[60] G. Ding, G. Tang, Z. He, and M. Ding, "New technologies of voltage source converter (vsc) for hvdc transmission system based on vsc," in *Power and Energy Society General Meeting - Conversion and Delivery of Electrical Energy in the 21st Century, 2008 IEEE*, 2008, pp. 1–8.

[61] T. M. Iversen, S. S. Gjerde, and T. Undeland, "Multilevel converters for a 10 mw, 100 kv transformer-less offshore wind generator system," in *Power Electronics and Applications (EPE), 2013 15th European Conference on*, 2013, pp. 1–10.

[62] M. Hagiwara and H. Akagi, "Control and experiment of pulsewidth-modulated modular multilevel converters," *Power Electronics, IEEE Transactions on*, vol. 24, no. 7, pp. 1737–1746, 2009.

[63] ——, "Experiment and simulation of a modular push-pull pwm converter for a battery energy storage system," pp. 1–1, 2013.

[64] A. Gupta and A. Khambadkone, "A space vector pwm scheme for multilevel inverters based on two-level space vector pwm," *Industrial Electronics, IEEE Transactions on*, vol. 53, no. 5, pp. 1631–1639, 2006.

[65] W. Lau, B. Zhou, and H.-H. Chung, "Compact analytical solutions for determining the spectral characteristics of multicarrier-based multilevel pwm," *Circuits and Systems I: Regular Papers, IEEE Transactions on*, vol. 51, no. 8, pp. 1577–1585, 2004.

[66] N. Nho and M. J. Youn, "Comprehensive study on space-vector-pwm and carrier-based-pwm correlation in multilevel invertors," *Electric Power Applications, IEE Proceedings*, vol. 153, no. 1, pp. 149–158, 2006.

[67] B. McGrath and D. Holmes, "Sinusoidal pwm of multilevel inverters in the overmodulation region," in *Power Electronics Specialists Conference, 2002. pesc 02. 2002 IEEE 33rd Annual*, vol. 2, 2002, pp. 485–490.

[68] Q. Tu, Z. Xu, and L. Xu, "Reduced switching-frequency modulation and circulating current suppression for modular multilevel converters," *Power Delivery, IEEE Transactions on*, vol. 26, no. 3, pp. 2009–2017, 2011.

[69] X. She, A. Huang, X. Ni, and R. Burgos, "Ac circulating currents suppression in modular multilevel converter," in *IECON 2012-38th Annual Conference on IEEE Industrial Electronics Society*. IEEE, 2012, pp. 191–196.

[70] Y. Ma, L. Fan, and Z. Miao, "Integrated control and switching strategy for a grid-connected modular multilevel converter," in *Power and Energy Society General Meeting (PES), 2015 IEEE*, July 2015, pp. 1–5.

[71] K. Ilves, L. Harnefors, S. Norrga, and H.-P. Nee, "Analysis and operation of modular multilevel converters with phase-shifted carrier pwm," *Power Electronics, IEEE Transactions on*, vol. 30, no. 1, pp. 268–283, 2015.

[72] B. Li, R. Yang, D. Xu, G. Wang, W. Wang, and D. Xu, "Analysis of the phase-shifted carrier modulation for modular multilevel converters," *Power Electronics, IEEE Transactions on*, vol. 30, no. 1, pp. 297–310, 2015.

[73] R. Naderi and A. Rahmati, "Phase-shifted carrier pwm technique for general cascaded inverters," *Power Electronics, IEEE Transactions on*, vol. 23, no. 3, pp. 1257–1269, 2008.

[74] J. Mei, K. Shen, B. Xiao, L. M. Tolbert, and J. Zheng, "A new selective loop bias mapping phase disposition pwm with dynamic voltage balance capability for modular multilevel converter," *Industrial Electronics, IEEE Transactions on*, vol. 61, no. 2, pp. 798–807, 2014.

[75] A. Antonopoulos, L. Ängquist, and H.-P. Nee, "On dynamics and voltage control of the modular multilevel converter," in *Power Electronics and Applications, 2009. EPE'09. 13th European Conference on*. IEEE, 2009, pp. 1–10.

[76] Q. Tu, Z. Xu, H. Huang, and J. Zhang, "Parameter design principle of the arm inductor in modular multilevel converter based hvdc," in *Power System Technology (POWERCON), 2010 International Conference on*. IEEE, 2010, pp. 1–6.

[77] Y. Ma, Z. Miao, V. Disfani, and L. Fan, "A one-step model predictive control for modular multilevel converters," in *Power and Energy Society General Meeting (PES), 2014 IEEE*, July 2014, pp. 1–5.

[78] Y. Wan, S. Liu, and J. Jiang, "Generalised analytical methods and current-energy control design for modular multilevel cascade converter," *IET Power Electronics*, vol. 6, no. 3, pp. 495–504, 2013.

[79] Y. Fu and M. Shahidehpour, "Fast scuc for large-scale power systems," *Power Systems, IEEE Transactions on*, vol. 22, no. 4, pp. 2144–2151, 2007.

[80] D. Streiffert, R. Philbrick, and A. Ott, "A mixed integer programming solution for market clearing and reliability analysis," in *Power Engineering Society General Meeting, 2005. IEEE*. IEEE, 2005, pp. 2724–2731.

144

[81] J. Peralta, H. Saad, S. Dennetière, J. Mahseredjian, and S. Nguefeu, "Detailed and averaged models for a 401-level mmc–hvdc system," *Power Delivery, IEEE Transactions on*, vol. 27, no. 3, pp. 1501–1508, 2012.

[82] H. Saad, J. Peralta, S. Dennetiere, J. Mahseredjian, J. Jatskevich, J. Martinez, A. Davoudi, M. Saeedifard, V. Sood, X. Wang *et al.*, "Dynamic averaged and simplified models for mmc-based hvdc transmission systems," *Power Delivery, IEEE Transactions on*, vol. 28, no. 3, pp. 1723–1730, 2013.

[83] U. N. Gnanarathna, A. M. Gole, and R. P. Jayasinghe, "Efficient modeling of modular multilevel hvdc converters (mmc) on electromagnetic transient simulation programs," *Power Delivery, IEEE Transactions on*, vol. 26, no. 1, pp. 316–324, 2011.

[84] M. Guan and Z. Xu, "Modeling and control of a modular multilevel converter-based hvdc system under unbalanced grid conditions," *Power Electronics, IEEE Transactions on*, vol. 27, no. 12, pp. 4858–4867, 2012.

[85] Q. Song, W. Liu, X. Li, H. Rao, S. Xu, and L. Li, "A steady-state analysis method for a modular multilevel converter," *Power Electronics, IEEE Transactions on*, vol. 28, no. 8, pp. 3702–3713, 2013.

[86] X. Li, Q. Song, W. Liu, H. Rao, S. Xu, and L. Li, "Protection of nonpermanent faults on dc overhead lines in mmc-based hvdc systems," *Power Delivery, IEEE Transactions on*, vol. 28, no. 1, pp. 483–490, 2013.

[87] Q. Tu, Z. Xu, Y. Chang, and L. Guan, "Suppressing dc voltage ripples of mmc-hvdc under unbalanced grid conditions," *Power Delivery, IEEE Transactions on*, vol. 27, no. 3, pp. 1332–1338, 2012.

[88] A. Chambolle and T. Pock, "A first-order primal-dual algorithm for convex problems with applications to imaging," *Journal of Mathematical Imaging and Vision*, vol. 40, no. 1, pp. 120–145, 2011.

[89] R. D. Zimmerman, C. E. Murillo-Sánchez, and R. J. Thomas, "Matpower: Steady-state operations, planning, and analysis tools for power systems research and education," *Power Systems, IEEE Transactions on*, vol. 26, no. 1, pp. 12–19, 2011.

[90] G. L. Nemhauser and L. A. Wolsey, *Integer and combinatorial optimization*. Wiley New York, 1988, vol. 18.

[91] S. Boyd and L. Vandenberghe, *Convex optimization*. Cambridge university press, 2004.

[92] D. K. Molzahn, B. C. Lesieutre, and C. L. DeMarco, "A sufficient condition for global optimality of solutions to the optimal power flow problem," *Power Systems, IEEE Transactions on*, vol. 29, no. 2, pp. 978–979, 2014.

[93] S. Bose, S. H. Low, T. Teeraratkul, and B. Hassibi, "Equivalent relaxations of optimal power flow," *Automatic Control, IEEE Transactions on*, vol. 60, no. 3, pp. 729–742, 2015.

[94] Y. Weng, Q. Li, R. Negi, and M. Ilic, "Semidefinite programming for power system state estimation," in *Power and Energy Society General Meeting, 2012 IEEE.* IEEE, 2012, pp. 1–8.

[95] V. R. Disfani, M. C. Bozchalui, and R. Sharma, "Sdp-based state estimation of multi-phase active distribution networks using micro-pmus," *arXiv preprint arXiv:1504.03547*, 2015.

[96] B. Kocuk, S. S. Dey, and X. A. Sun, "Inexactness of sdp relaxation and valid inequalities for optimal power flow," *Power Systems, IEEE Transactions on*, pp. 1–12, 2015.

[97] "Ieee recommended practice for industrial and commercial power system analysis," *IEEE Std 399-1990*, pp. 1–384, 1990.

[98] F. Li and R. Bo, "Small test systems for power system economic studies," in *Power and Energy Society General Meeting, 2010 IEEE*, 2010, pp. 1–4.

[99] R. D. Zimmerman, C. E. Murillo-Sánchez, and R. J. Thomas, "Matpower: Steady-state operations, planning, and analysis tools for power systems research and education," *Power Systems, IEEE Transactions on*, vol. 26, no. 1, pp. 12–19, 2011.

[100] Z. Miao, L. Xu, V. R. Disfani, and L. Fan, "An soc-based battery management system for microgrids," *Smart Grid, IEEE Transactions on*, vol. 5, no. 2, pp. 966–973, 2014.

[101] M. Hagiwara and H. Akagi, "Control and experiment of pulsewidth-modulated modular multilevel converters," *Power Electronics, IEEE Transactions on*, vol. 24, no. 7, pp. 1737–1746, 2009.

[102] M. Saeedifard, R. Iravani, and J. Pou, "Analysis and control of dc-capacitor-voltage-drift phenomenon of a passive front-end five-level converter," *Industrial Electronics, IEEE Transactions on*, vol. 54, no. 6, pp. 3255–3266, 2007.

APPENDIX A

LIST OF ABBREVIATIONS
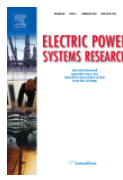
μG	Micro-Grid
AC	Alternative Current
ADMM	Alternating Direction Method of multipliers
CAISO	California Independent System Operator
DC	Direct Current
DER	Distributed Energy Resources
DG	Distributed Generation
DMS	Distribution Management System
DR	Demand Resonse
ED	Economic Dispatch
EPRI	Electric Power Reseach Institute
ESS	Energy Storage Susyem
IEEE	Institute of Electrical and Electronics Engineers
IT	Information Technology
KKT	KarushKuhnTucker
LUBS	Lower-Upper Bound Switching
MGCC	Micro-Grid Control Center
MHOPF	Multi-Horizon Optimal Power Flow
MMC	Modular Multilevel Converter
MPC	Model Predictive Control
OPF	Optimal Power Flow
PHEV	Plug-in Hybrid Electric Vehicle
PUC	Price Update Unit
PWM	Pulse Width Modulation
SDP	Semi-Definite Programming
SG	Sub-Gradient
SPWM	Sinusoidal Pulse Width Modulation
VSC	Voltage Source Converter

APPENDIX B

REUSE PERMISSIONS OF PUBLISHED PAPERS FOR CHAPTER 4

ABOUT THE AUTHOR

Vahid Rasouli Disfani was born in 1983 in Tehran, Iran. He obtained his Bachelor's degree and master's degree both in Electrical Engineering from Amirkabir University of Technology in 2006 and Sharif University of Technology in 2008, respectively. He received his Ph.D. degree in Electrical Engineering from the University of South Florida, Tampa, FL in August 2015. He has worked as power market analyst at Iran Grid Management Company (Iran ISO), Tehran, Iran from 2008 to 2012 and as power system research intern at NEC Laboratories America, Cupertino, CA during summer 2014. His research interests include power system analysis, modeling, and optimization as well as distributed optimization and control in smart grids.